DOCTORAL THESIS 2020

RNA Helicases in 60S Ribosomal Subunit Biogenesis in *Saccharomyces cerevisiae*

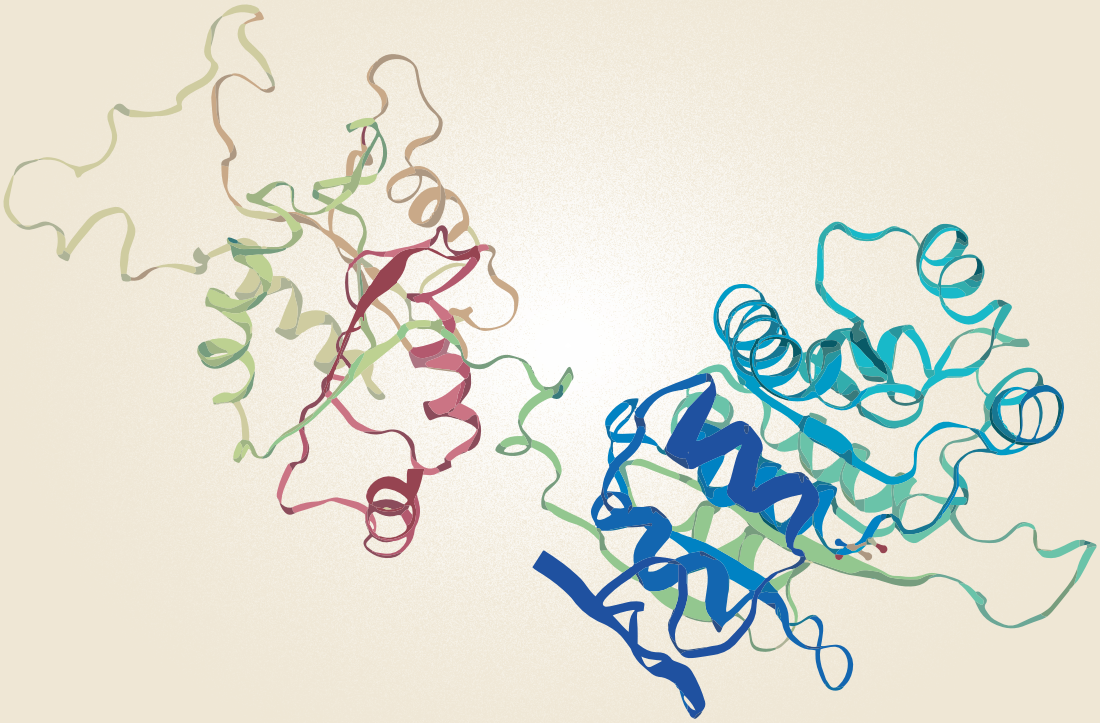

Julia Mª Contreras Fernández

Universidad de Sevilla

Departamento de Genética
Universidad de Sevilla

RNA Helicases in 60S Ribosomal Subunit Biogenesis in *Saccharomyces cerevisiae*

Memoria presentada para aspirar al grado de
Doctora en Biología

V.o B.o: El director de la Tesis 1

Eduardo Villalobo Polo

V.o B.o: El director de la Tesis 2

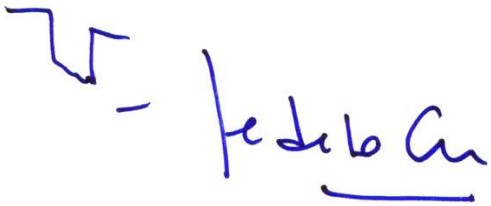

Jesús de la Cruz Díaz

La doctoranda

Julia Mª Contreras Fernández

This work was funded by a contract associated to the grant BFU2013-42958-P and a fellowship from the University of Seville (PPI2015-II.2). A short-term fellowships from the University of Seville (VIPPIT-2017-II.2 and VIPPIT-2018-EBRV) is also acknowledges.

Un científico en su laboratorio no es sólo un técnico: es también un niño colocado ante fenómenos naturales que le impresionan como un cuento de hadas.

Marie Curie

A mis padres,

siempre.

INDEX

1.SUMMARY

ABSTRACT

1.-SUMMARY

The ribosomes are the cellular organelles responsible for translating messenger RNA (mRNA) to proteins. In eukaryotic organisms, the ribosomes are composed by two subunits: the large subunit and the small subunit that come together to make a complete ribosome. The biogenesis of eukaryotic cytoplasmic ribosomes is a very complex process. The eukaryotic organism where this process has been best studied is the budding yeast *Saccharomyces cerevisiae*. This microorganism is considered a model organism of study due to its low complexity, rapid growth and dispersion of its cells. In *S. cerevisiae*, the large subunit or 60S is composed by three rRNAs called 25S, 5.8S and 5S and about 46 ribosomal proteins; the small subunit or 40S is composed by only one rRNA called 18S and about 33 ribosomal proteins. The ribosome biogenesis process is not only complex, but it is also compartmentalized. The precursors of rRNA (pre-rRNA) are transcribed in the nucleolus by the RNA polymerase I (25S, 5.8S y 18S) and by the RNA polymerase III (5S). Along the processing of the pre-rRNAs take place accurate endo- and exonucleolytic reactions, at the same time that some molecular building blocks of pre-rRNA are modified by methylases enzymes or by small nucleolar RNA complexes (snoRNPs). The processing and modification of the pre-rRNAs do not occur in naked RNAs, conversely, these reactions take place in pre-ribosomal particles, which are complexes where the ribosomal proteins are assembling hierarchically. The restructuration of the pre-ribosomal particles and its subsequent maturation to ribosomal subunits needs a large number of protein factors, more than 300, which are known as assembly factors or *trans*-acting factors. These factors are not present in the mature ribosomal particles. One part of these reactions occurs in the nucleoplasm or even in the cytoplasm.

The ribosomal synthesis process has not only academic, but also biomedical interest, because a set of hereditary diseases with bad prognostic, called ribosomopathies are associated to loss of function mutation in some ribosomal proteins and/or assembly factors. Moreover, this process has been related with autoimmune pathologies and in a direct manner with large number of cancers and viral infections.

ABSTRACT

The RNA dependent RNA helicases are among the assembly factors that facilitate the biogenesis of ribosomes. In a biochemical sense, these enzymes unwind RNA duplexes using the energy released by ATP hydrolysis. The RNA helicases are classified according to their sequence and structural properties in superfamilies (SF1-SF5). The superfamilies are formed at the same time by several subfamilies. Of special interest for our work are the RNA helicases belonging to the so-called *DEAD-box* protein subfamily, named as such due to the presence of the amino acids aspartic, glutamic, alanine and aspartic, in this order, in a specific place of its sequences. These amino acids are involved in ATP binding and hydrolysis. The *DEAD-box* proteins are composed by two structural domains, each one similar to the bacterial RecA protein, that contain a set of highly conserved sequence motifs. These motifs are involved in ATP binding and hydrolysis, nucleic acid binding, duplex unwinding or in the coordination between those reactions.

Today, up to 19 helicases from the *DEAD-box* protein subfamily have been identified to be involved in the biogenesis of cytoplasmic ribosomes. However, the precise role of these enzymes in that process is clearly not fully understood. Therefore, the objective of this work has consisted in the biochemical and functional characterization of two functionally-related helicases during the biogenesis of the 60S ribosomal subunit. These helicases are Dbp7 and Dbp9. Both proteins are necessary for the 60S subunits biogenesis due to their roles during the processing of the early 27SA pre-rRNAs and therefore for the accumulation of the mature 25S and 5.8S rRNAs. However, the exact role of Dbp7 and Dbp9 in this process is still unknown.

To accomplish these objectives, we have carried out a functional characterization of Dbp7 protein *in vivo*. The conserved motifs of this protein, and its two longs N- and C-terminal extensions were identified in the amino acid sequence. In the N-terminal extension, we could identify a putative nuclear localization signal (NLS). Several mutants were constructed for the study. The results of growth analysis and polysome profiles in point mutants in the motifs I and VI, involved in ATP binding and hydrolysis, demonstrated that these motifs play an important role in Dbp7 function, since they showed a delay in growth, possibly due to a decrease in the levels of 60S subunits.

Similar results were obtained in mutants with deletions of specific regions in the N- and C- terminal extensions of the protein. The observed defects were not due to a delocalization of Dbp7, since in all the mutants with deletions in the N- and C-extensions, the protein was still associated to hight molecular weight complexes, probably pre-60S ribosomal particles. Moreover, by epifluorescence, we have checked that the putative NLS localized in the N-terminal end of Dbp7 is a *bona fide* nuclear localization signal. A *dbp7* mutant lacking the NLS grew as an isogenic wild-type strain and the protein was able to reach the nucleus; therefore, Dbp7 must contain others redundant NLS not recognizable in a sequence analysis or is imported into the nucleus through binding to another protein that transfers it to that location.

It has been demonstrated that Dbp7 is functionally associated to a protein complex called Npa1 complex and it is formed by the proteins Dbp6, Nop8, Rsa3, Npa1 and Npa2. Npa1 binds to specific positions in rRNA in the domains I and VI of rRNA 25S, so it has been proposed that the Npa1 complex is involved in the restructuration of these domains during the early nucleolar maturation of 60S subunits. This process involves the assembly of the ribosomal protein uL3. Dbp7 is genetically associated to this complex. Some snoRNAs participate in these restructuring reactions, among them snR190, whose target sequences of RNA are neighboring the region where Npa1 binds. Npa1 also binds directly to snR190. Our group has been identified mutations in the 25S rRNA that interfere with the binding of snR190 to the rRNA and partially suppress the growth defects of a *dbp7* null mutant. In this work, we have generated a double *dbp7Δ snR190* mutant strain, whose growth is improved compared to that of a single *dbp7Δ* mutant. Consistent with this result, snR190, among other snoRNAs, is retained in pre-ribosomal particles in the absence of Dbp7. This phenomenon does not occur in an isogenic wild-type strain. Thus, our work suggests that Dbp7, probably carrying out its function as a RNA helicase enzyme, participates in the releasing of the at least snR190 from the early 60S ribosomal particles in progression to maturation.

In the second part of this Thesis work, we have studied the enzymatic characteristic of Dbp7 *in vitro*, more specifically its possible activities ATPase, binding to RNA and

helicase. Making use of colorimetric enzymatic and radioactive assays, we have demonstrated that a recombinant protein of Dbp7 that was expressed and purified from *Escherichia coli* extracts presents an ATPase activity dependent of RNA and specific DNA oligonucleotides (i.e. poly dT of 30 nucleotides length). Simultaneously, we have demonstrated that Dbp7 binds to RNA and shows helicase activity *in vitro*. Dbp7 is able to unwind RNA duplexes in 5´-3´and 3´-5 directions. This activity is only dependent of ATP hydrolysis. Likewise, we have studied the previous activities in the Dbp7 point mutants in domains involved in the ATP binding and hydrolysis (Dbp7[K197A] and Dbp7[R553A]). However, surprisingly, both mutants maintain the activities of the wild-type protein. These results are discussed in the context of the functional and structural domains of Dbp7. Finally, in this work, we have started the preliminary characterization of the biochemical activities of the RNA helicase Dbp9. In a similar approach to that done with Dbp7, we have expressed and purified the recombinant Dbp9 protein from *E. coli* extracts and we have started it biochemical characterization. Our first assays suggest that the recombinant protein has ATPase activity dependent of an DNA oligonucleotide, but it neither has the ability to bind RNA nor helicase activity under the conditions tested.

ABSTRACT

1.-RESUMEN

Los ribosomas son los orgánulos celulares encargados de traducir el RNA mensajero (mRNA) a proteínas. En organismos eucariotas, los ribosomas se componen de dos subunidades: la subunidad grande y la subunidad pequeña que se unen para dar lugar a un ribosoma completo. La biosíntesis de ribosomas citoplásmicos eucarióticos es un proceso profundamente complejo. El organismo eucariota donde mejor se ha estudiado este proceso es la levadura de gemación *Saccharomyces cerevisiae*. Este microrganismo es considerado un organismo modelo de estudio debido a su baja complejidad, rápido crecimiento y dispersión de sus células. En *S. cerevisiae,* la subunidad grande o 60S está compuesta por tres RNAs ribosómicos (rRNAs) denominados 25S, 5.8S y 5S y unas 46 proteínas ribosómicas; la subunidad pequeña o 40S se compone de un único rRNA denominado 18S y unas 33 proteínas ribosómicas. El proceso de biogénesis de ribosomas citoplásmicos no es sólo complejo, sino que además está compartimentalizado. Los precursores de rRNA (pre-rRNAs) son transcritos en el nucléolo por la RNA polimerasa I (25S, 5.8S y 18S) y la RNA polimerasa III (5S). Durante el procesamiento de los pre-rRNAs se producen reacciones precisas endo y exonucleolíticas, a la vez que algunos sillares de los pre-rRNAs son modificados bien por la acción de enzimas metilasas o por complejos de RNAs pequeños nucleolares (snoRNPs). El procesamiento y modificación de los pre-rRNAs no ocurre en los RNAs desnudos, por el contrario, estas reacciones suceden en partículas pre-ribosómicas, complejos donde las proteínas ribosómicas van jerárquicamente ensamblándose. La reestructuración de las partículas pre-ribosómicas y su ulterior maduración a subunidades ribosómicas necesita igualmente de un amplio número de factores proteicos, más de 300, conocidos como factores de ensamblaje o de actuación en *trans,* dado que no son componentes de las subunidades ribosómicas maduras. Parte de estas reacciones suceden en el nucleoplasma o incluso en el citoplasma.

El proceso de síntesis de ribosomas no sólo tiene interés académico, sino que también lo tiene biomédico, dado que un conjunto de enfermedades hereditarias de mal pronóstico, denominadas ribosomopatías, están ligadas a mutaciones de pérdida de

función de algunas proteínas ribosómicas y/o factores de ensamblaje. También, este proceso ha sido relacionado con patologías autoinmunes y de modo directo con numerosos tipos de cáncer e infecciones víricas.

Las helicasas de RNA dependientes de ATP están entre los factores de ensamblaje que favorecen el proceso de biogénesis de ribosomas. En sentido bioquímico, estas enzimas llevan a cabo el desenrollamiento de dúplices de RNA utilizando para ello la energía liberada por la hidrólisis de ATP. Las helicasas de RNA se clasifican atendiendo a su secuencia y propiedades estructurales en superfamilias (SF1-SF5) y éstas a su vez en subfamilias. De especial interés para nuestro trabajo son las helicasas de RNA pertenecientes a la subfamilia denominada de las helicasas *DEAD-box*, llamadas así por la presencia de los aminoácidos aspártico, glutámico, alanina y aspártico, en ese orden, en un lugar específico de sus secuencias, los cuales se involucran en la unión e hidrólisis de ATP. Las helicasas *DEAD-box* están formadas por dos dominios estructurales, cada uno similar a la proteína RecA que, a su vez, contienen una serie de motivos de secuencia altamente conservados. Estos motivos se encuentran implicados en la unión e hidrólisis de ATP, en la unión y desenrollamiento de los ácidos nucleicos o en la coordinación entre ambas reacciones. A día de hoy, se han identificado hasta 19 helicasas de la subfamilia *DEAD-box* implicadas en la biogénesis de ribosomas citoplásmicos. Sin embargo, la función exacta que desempeña la mayoría de estas enzimas en el proceso no se conoce con claridad.

Por ello, el objetivo de este trabajo ha consistido en la caracterización bioquímica y funcional de dos helicasas relacionadas funcionalmente con la biogénesis de subunidades ribosómicas 60S, las llamadas Dbp7 y Dbp9. Ambas proteínas son necesarias para la biogénesis de subunidades 60S debido a su papel durante el procesamiento de los pre-rRNAs tempranos 27SA y, por tanto, para la acumulación de los rRNAs maduros 25S y 5.8S. Sin embargo, su función concreta en este proceso es aún desconocida.

Para cumplir estos objetivos hemos acometido una caracterización funcional de la proteína Dbp7 *in vivo*. Los motivos conservados de esta proteína, así como sus dos largas

extensiones N- and C- terminales se identificaron en su secuencia aminoacídica. En la extensión N-terminal se identificó una posible señal de localización nuclear (NLS). Se realizaron distintos mutantes para el estudio. Los resultados de los análisis de crecimiento y perfiles de polisomas en mutantes puntuales en los motivos I y VI, implicados en unión e hidrólisis de ATP, demostraron que estos motivos cumplen un papel importante en la función de Dbp7, puesto que mostraron un retraso en el crecimiento debido, posiblemente, a una disminución en los niveles de subunidades 60S. Resultados similares fueron obtenidos en mutantes de deleción de regiones concretas de las extensiones N- and C-terminales de la proteína. Los defectos observados no se debieron a una deslocalización de Dbp7, puesto que en todos los mutantes con deleciones en los extremos N- and C- terminales, la proteína se encontraba asociada a complejos de alto peso molecular, probablemente partículas ribosómicas pre-60S.

Por otra parte, mediante epifluorescencia hemos comprobado que la posible NLS localizada en el extremo N-terminal de Dbp7 es realmente una secuencia de localización nuclear verdadera; no obstante, el mutante carente de esta NLS crece de manera similar a como lo hace una estirpe silvestre, siendo la proteína capaz aún de alcanzar el núcleo; por tanto, Dbp7 debe presentar otras NLS redundantes no identificables en un análisis de secuencia o importarse al núcleo a través de la unión a otra proteína que la transfiera a esa localización.

Se ha demostrado que Dbp7 está asociada funcionalmente a un complejo proteico denominado complejo Npa1 y que está formado por las proteínas Dbp6, Nop8, Rsa3, Npa1 y Npa2. Npa1 se une a posiciones específicas de rRNA en los dominios I y VI del rRNA 25S por lo que se ha propuesto que el complejo Npa1 participa en la restructuración de estos dominios durante la maduración temprana nucleolar de subunidades 60S, proceso que implica el ensamblaje de la proteína ribosómica uL3. Dbp7 se encuentra genéticamente asociada a este complejo. En estas reacciones de reestructuración participan algunos snoRNAs, entre ellos snR190, cuyas secuencias dianas de rRNA son vecinas a la región donde Npa1 se une, y al que Npa1 también se une directamente. Nuestro grupo ha identificado que mutaciones en el rRNA 25S que

interfieren con la unión de snR190 suprimen parcialmente los defectos de crecimiento de un mutante *dbp7* nulo. En este trabajo, hemos generado una estirpe doble mutante *dbp7Δ snR190* que recapitula la supresión del defecto de crecimiento de la mutación *dbp7Δ.* En consonancia con este resultado, snR190, entre otros snoRNAs, queda retenido en partículas pre-ribosómicas en ausencia de Dbp7, fenómeno que no ocurre en una estirpe silvestre isogénica. Así, nuestro trabajo sugiere que Dbp7, probablemente ejerciendo su función como helicasa de RNA, participa en la liberación de al menos snR190 de las partículas pre-ribosómicas 60S tempranas en progresión de su maduración.

En una segunda parte de esta Tesis, hemos estudiado las características enzimáticas de Dbp7 *in vitro*, más concretamente de sus posibles actividades ATPasa, de unión a RNA y helicasa. Haciendo uso de ensayos enzimáticos colorimétricos y radiactivos, hemos demostrado que una proteína Dbp7 recombinante expresada y purificada a partir de extractos de *Escherichia coli* presenta actividad ATPasa dependiente de RNA y de oligonucleótidos específicos de DNA (ej. poly dT de 30 nucleótidos de largo). Simultáneamente, hemos demostrado que Dbp7 se une a RNA y que presenta capacidad helicasa *in vitro*, pudiendo desenrollar dúplices de RNA tanto en la dirección 5´-3´como en la dirección 3´-5´. Esta actividad es dependiente de la hidrólisis de ATP. Hemos estudiado igualmente las actividades anteriores en mutantes de Dbp7 puntuales en dominios implicados en la unión e hidrólisis de ATP (Dbp7[K197A], Dbp7[R553A]). Sin embargo, ambos mutantes sorprendentemente mantiene las actividades de la proteína silvestre. Estos resultados se discuten en el contexto de los dominios estructurales y funcionales de Dbp7.

Finalmente, en este trabajo, hemos iniciado la caracterización preliminar de las actividades bioquímicas de la helicasa de RNA Dbp9. De manera similar al trabajo realizado con Dbp7, hemos expresado y purificado la proteína Dbp9 recombinante a partir de extractos de *E. coli* e iniciado su caracterización bioquímica. Nuestros primeros ensayos sugieren que la proteína recombinante tiene actividad ATPasa dependiente de

un oligonucleótido de DNA, pero ni tiene la capacidad de unirse a RNA ni actividad helicasa en las condiciones ensayadas.

2.INTRODUCTION

2.- INTRODUCTION

Ribosomes are the macromolecular machines, made out of proteins and RNAs, that translate the mRNAs into proteins in all living beings. Structurally, all ribosomes are composed by two subunits (r-subunits), separable from each other, the so-called large and small subunit (LSU and SSU, respectively); these names are given by the difference in sedimentation coefficient, in sucrose density gradient, of each subunit. The size of each r-subunit is higher in eukaryotes than in prokaryotes since, on the one hand, the number of ribosomal proteins (r-proteins) is greater in eukaryotes and, on the other hand, the length of each ribosomal RNA (rRNA) is bigger in eukaryotes. The synthesis and assembly (biogenesis) of ribosome subunits take place for each subunit during a complex and tightly regulated process. Once each subunit is fully assembled, they bind to each other to yield a fully competent-to-translate ribosome (1). In a functional ribosome, the LSU catalyses the formation of the peptide bond between the peptidyl-tRNA and the nascent aminoacyl chain, while the SSU mediates the mRNA codon and tRNA anticodon pairing (1, 25, 69).

The study of the ribosome biogenesis pathway has been performed in several eukaryotic organisms but so far, most of the information concerning this process comes from the budding yeast *Saccharomyces cerevisiae*. *S. cerevisiae* is a low complexity eukaryotic system. Its growth and cells dispersion are fast, and mutant isolation is easy. Besides all this, the genome of *S. cerevisiae* has been completely sequenced, and its biology is in constant revision. For all these advantages, *S. cerevisiae* was the eukaryotic organism selected to perform this work.

2.1.-Ribosomes in *Saccharomyces cerevisiae*

In *S. cerevisiae*, the LSU and the SSU have sedimentation coefficients of 60S and 40S, respectively. These r-subunits build up an 80S ribosome. The LSU possesses three different rRNA species (25S, 5.8S and 5S) and 46 different ribosomal proteins (r-proteins). The SSU possesses a single rRNA species (18S) and 33 different r-proteins (1). In addition to rRNAs and r-proteins, accessory proteins or trans-acting factors (from now

on factors), and small nucleolar RNAs (snoRNAs) bind to the ribosomal subunits transiently. The function of these factors could be involved in stablish or dissociate snoRNA-pre-rRNA base pairings, prepare the rRNA for an efficient nuclease attack or participate in specific modulations of rRNA, rRNA-protein or protein-protein interactions (71). Most snoRNAs participates in rRNA modifications that generally stabilize the ribosome structure, while other serve as RNA chaperones for rRNA folding (82).

The 18S rRNA of the SSU is 1869 nucleotides long and is folded in four conserved domains, which constitute the secondary structure of the rRNA. These conserved domains are the 5´, central, 3´ major, and 3´ minor domains (**Figure 1A**). At the same time, the domains fold and together with the r-proteins form the tertiary structures of the SSU: the head (containing for example: uS2, uS3, uS7, uS9, eS10, uS15, uS17 and eS19) and the body, which has the shoulder (eS30), the platform (for example: eS6, eS8, uS17, uS19, and uS13), the foot (uS10) the decoding centre cleft (for example: uS3, eS4, uS7,eS7 and eS12) and the beak (eS31, eS12 and eS10) (76, 90) (75) (**Figure 1B**). These tertiary structures function as scaffold to which accessory factors bind and release until giving rise the ribosomal 40S particles (44). In the case of the LSU, the 25S rRNA is 3396 nucleotides long and is folded giving rise to six conserved domains (I-VI), each beginning by a root helix (37) (**Figure 1C**). The 5.8S rRNA (156 nucleotides) is bound by base pairing with the 25S rRNA in the domain I. As occurring for SSU, these domains fold and with the binding of the r-proteins yield the remarkable functional sites of the LSU: the central protuberance (CP) (containing for example: uL18 and uL5), where is localized the 5S rRNA (121 nucleotides) (91), the P-stalk (P0, P1 and P2), involved in recruitment and activation of translation factors, the L1 stalk (uL1) implicated in tRNA movements during translocation through the ribosome (83, 86), the peptidyl transferase centre (PTC) (containing for example: uL2, uL3, eL6, eL14, uL16, eL40, eL41 and eL43), which is responsible for peptide bond formation, and the polypeptide exit tunnel (PET) (for example: uL4, eL22, uL14, eL29, eL31 and eL39) (6, 59), from where the nascent growing polypeptide chain leaves the ribosome (**Figure 1D**) (40, 89).

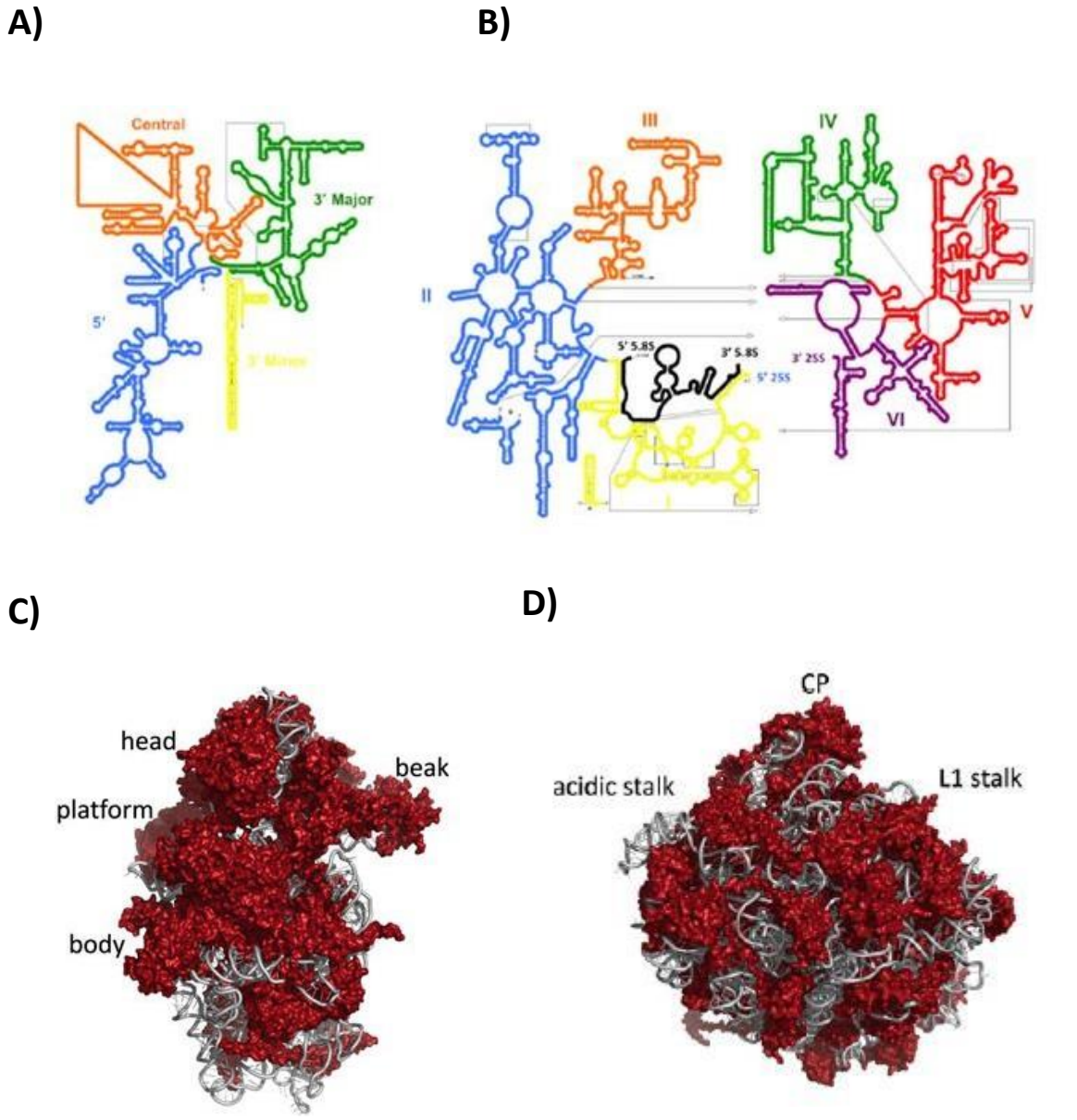

Figure 1. Secondary and tertiary structures of the SSU and LSU. (**A**) Secondary structure of 18S rRNA and (**B**) 25S and 5.8S rRNAs from *S. cerevisiae*. The four domains of 18S rRNA and the six domains of 25S rRNA are showed in different colours. The 5.8S rRNA is showed in black and is bound by base pairing with the domain I of 25S rRNA. The 5S rRNA is not represented. (**C**) Crystal structure of the SSU and (**D**) LSU of the ribosome from *S. cerevisiae*. In the SSU, the head, platform, body and beak are indicated. In the LSU, the central protuberance (CP) the L1 and P-stalks and are indicated. The peptidyl transferase centre (PTC) and the polypeptide exit tunnel (PET) are not highlighted (89).

2.2.-Ribosome biogenesis in *S. cerevisiae*

The ribosome biogenesis pathway is an integrated process, in which we can highlight three principal steps: pre-rRNA synthesis and processing, pre-rRNA modifications, and r-subunits synthesis and assembly. The rRNA is transcribed in the nucleolus and concomitantly, it undergoes process of folding and nucleotide modification. The spacer sequences are removed, and r-proteins are bound to rRNA. Then, the rRNA travel to the nucleoplasm, where different factors and r-proteins bind to rRNA and the ribosome pre-particles are assembled. The pre-ribosomal particles do not contain the same r-proteins and conformation as the mature ribosomal subunits. When the pre-ribosomal particles are competent for the export, they travel to the cytoplasm where the pre-ribosomal particles mature with the acquisition of its definitive conformation, the binding of the last r-proteins and the elimination of remaining factors (89).

2.2.1.-Pre-ribosomal RNA synthesis and processing

The rDNA containing the information to yield the different rRNA species is comprised in the chromosome XII and it is composed by approximately 150 rDNA repetitions in tandem localized in the nucleolus (**Figure 2**) (60). A single-copy rDNA is a fragment of 9.1 kb that codes for the 35S and the 5S pre-rRNA. The 35S pre-rRNA is the largest detectable rRNA precursor and contains the 18S, 25S, and 5.8S rRNAs. The 35S precursor also contains two internal transcribed spacers (ITS1 and ITS2) separating the three rRNA species, and two external transcribed spacers (5´ETS and 3´ETS). Within the spacer regions are located different cleavage sites, which are the target of distinct endo and exonucleases to generate the rRNA intermediates. Two non-transcribed regions, called NTS1 and NTS2 separate the 35S and 5S transcriptional units. Several elements acting in *cis*, such as the origin of DNA replication and the replication fork block site, are present in the NTS regions.

The 35S and the 5S are transcribed by the RNA polymerase I (RNAP I) and RNA polymerase III (RNAP III), respectively. In fast growing *S. cerevisiae* cells, the nascent rRNA transcripts are processed co-transcriptionally (43). However, a less common post-

transcriptional pathway also exists (43, 64). With the purpose of simplify the explanation, only the post-transcriptionally pathway will be explained here.

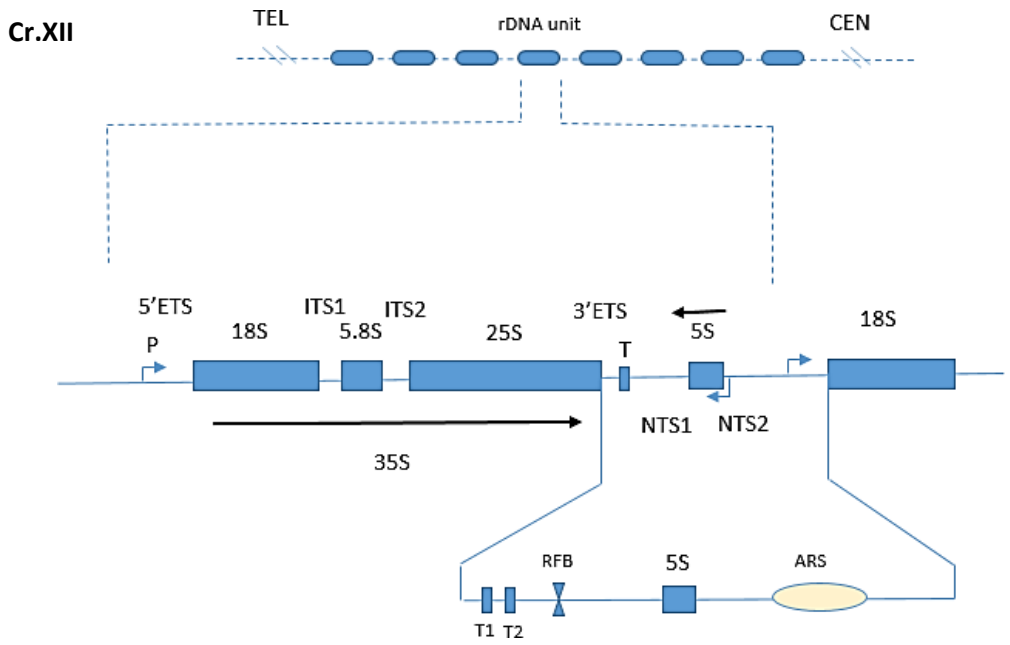

Figure 2. Structure of the rDNA region in *S. cerevisiae*. A 9.1 kb repetition unit is expanded to show the disposition of the 35S rRNA and the 5S rRNA coding regions and the non-transcribed spacers, NTS1 and NTS2. The transcription and processing of the 35S pre-rRNA give rise to the mature 18S, 5.8S and 5S rRNAs. The 35S rRNA precursor is flanked by two external spacer sequences (5'ETS and 3' ETS) and contains two internal spacer sequences (ITS1 and ITS2). The 35S rRNA and 5S rRNA pre-RNAs are separated by the non-transcribed spacers, NTS1 and NTS2. The NTS region is amplified and positions of terminators 1 and 2 (T1 and T2), RFB (replication fork blocking) and ARS (autonomous replication sequence) are indicated. P and T indicate the promoter and terminator of the transcript. Modified from 60.

During pre-rRNA transcription, the endonucleolytic cleavage by Rnt1 of the nascent pre-rRNA in the 3'ETS at site B_0 generates the 35S pre-rRNA (24). The nascent 35S pre-rRNA is cleaved at the A_0 and A_1 sites by the Utp24 nuclease (64, 88), giving rise to the 33S and to 32S pre-rRNA intermediaries, respectively. The 32S intermediary is further cleaved in the A_2 site by the endonuclease Rcl1 (41). This latter cleavage generates the 20S and the $27SA_2$ intermediaries (85). The 20S pre-rRNA intermediary is processed in the D site of the 3' end by the Nob1 endonuclease (23, 47). In this step, the mature 18S rRNA is directly generated. During the ulterior processing of the $27SA_2$ intermediary, two different

pathways (major and minor) occur depending on the processing of the internal ITS1 region. The major pathway is the preponderant. Again, only the most common pathway will be explained. The $27SA_2$ intermediary is subjected to a 3'-5' exonucleolytic digestion at the 3' end from B_0 to B_2 site by Rnt1 and Rex1. Subsequently, the $27SA_2$ is digested in the A_3 site by the endonuclease RNase MRP, while the $27SA_3$ intermediary rRNA is formed. The $27SA_3$ pre-rRNA is then digested, until reaching the B_{1S} site, by the exonucleases Xrn1, Rat1, and Rrp17. These latter cleavages generate the $27SB_S$ species. The $27SB_S$ intermediary is cleaved in the C_2 site, located in the ITS2, by the endonuclease Las1, which originates the 7S and 25.5S species (26, 41). The 25.5S precursor is rapidly processed to mature 25S rRNA by the 5'-3' exonucleases Xrn1, Rat1 and Rrp17 (89). The 7S precursor is 3'-5' digested by the exosome to give rise an immature form called 6S. Finally, the 6S intermediate yields to the mature 5.8S rRNA by the exonucleases Rex 1-3 and Ngl2 (**Figure 3**) (31, 82, 84).

The transcription of the 5S rRNA is carried out independently by the RNAP III, which transcribes this rRNA as a precursor with a short 3' extension (**Figure 3**). The exonuclease Rex1 remove this extension leading to the mature 5S rRNA (14, 84).

2.2.2.-Pre-ribosomal RNA modification

Approximately 2% of rRNA nucleotides undergo chemical modifications (42). Most modifications take place co-transcriptionally and/or briefly after transcription, but in some cases, modifications can occur late during rRNA processing (71). The rRNA modifications increase the topological properties of RNA, both stabilizing its structure and improving their interaction with ligands (79). The distribution of rRNA chemical modifications is not random, since most of them cluster in conserved regions of the rRNA or in functionally important regions of the r-subunit (71). The following are the rRNA modifications identified so far: base methylation, 2´-O-methylation of the ribose (Nm), isomerisation of uridine to pseudouridine (Ψ) and acetylation (only in SSU) (79). So far, 55 Nm sites and 45 Ψ sites have been characterized in the *S. cerevisiae* rRNA (80).

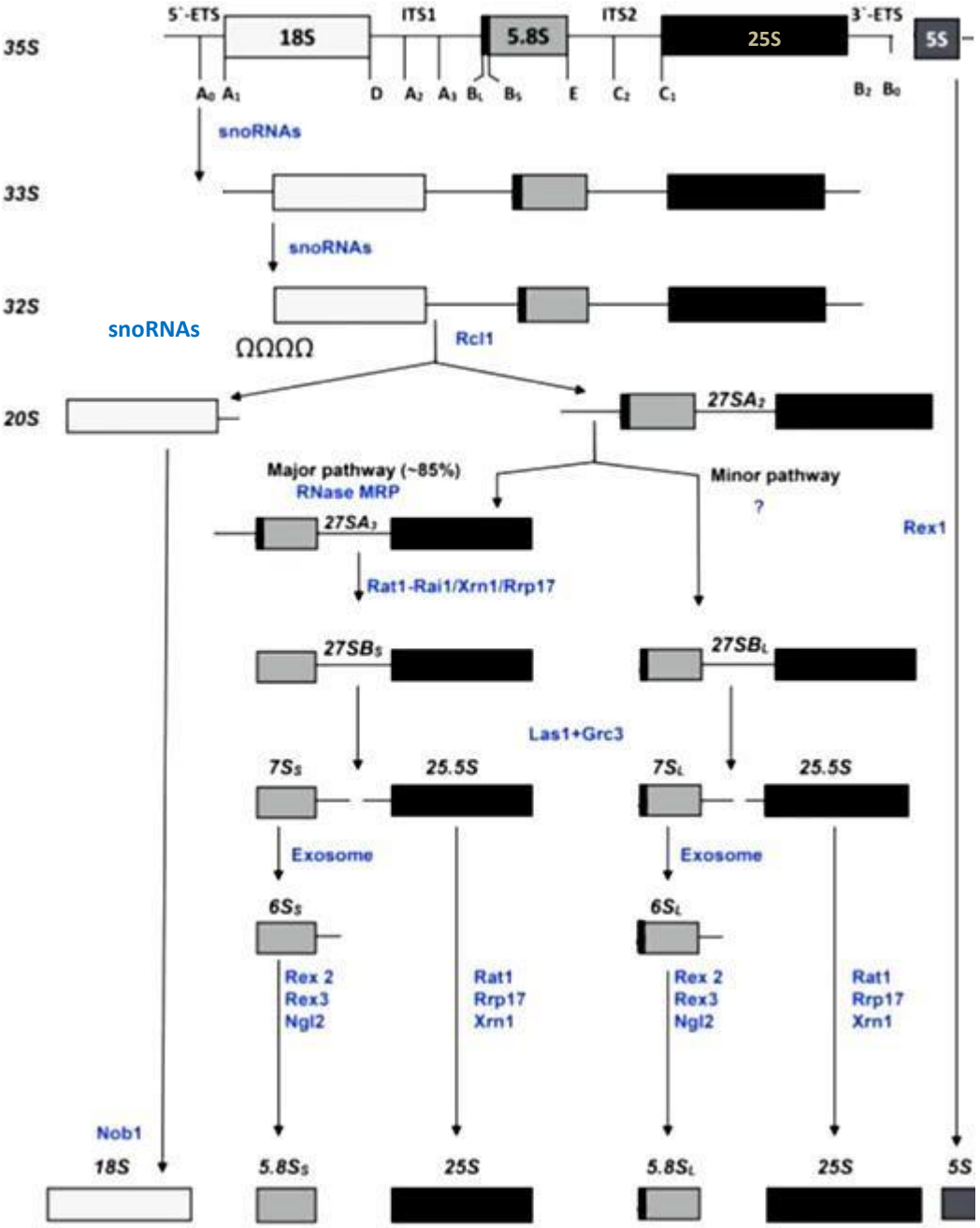

Figure 3. Pre-rRNA processing in *S. cerevisiae*. On the top the transcript of the first precursor, 35S is showed. The transcript contains the rRNAs 18S, 5.8S and 25S, the external (5' ETS and 3' ETS) and internal (ITS1 and ITS2) non-transcribed spacers. The cleave sites are indicates by letters. At right, the transcript of the 5S precursor is showed. The snoRNAs and exo and endonucleolitic enzymes that are involved in each step in the processing and maturation of each pre-rRNA are indicated in blue. The unknown enzymes are denoted by an interrogation symbol. Modified from 41.

2.2.3.-Assembly of ribosomal particles

The r-protein composition of the pre-ribosomal particles varies depending of its maturation stage. During the maturation process, the pre-ribosomal particles travel from the nucleus to the cytoplasm, where they reach the mature conformation. The necessary binding and dissociation of r-proteins to pre-ribosomal particles is carried out by assembly factors (AFs). AFs bind to pre-ribosomal particles in an apparent ordered manner and are essential to the formation of functional ribosomes particles.

Ribosome assembly begins with RNAP I, which carry out the transcription of the rDNA repeats in the nucleolus to produce the 35S precursor. The emerging 35S pre-rRNA associates with the snoRNA U3 and several other small nucleolar RNAs (snoRNAs), 40S-specific r-proteins and AFs to form the 90S pre-ribosome particle or SSU processome (precursor of 40S ribosomal particle). Co-transcriptional cleavage at site A_2 then separates the nuclear pre-40S particle from the emerging pre-60S particle, both of which undergo independent maturation pathways (64).

- *Assembly of the pre-40S r-particles*

Formation of 90S particle occurs co-transcriptionally and in a modular fashion by combination of several autonomous subcomplexes (12, 40, 64, 68). First, the subcomplex UTP-A or t-UTP joins to the emerging 5' ETS and prepares it to the subsequently recruitment of U3 snoRNP and UTP-B subcomplexes (11, 12, 32, 92). In this way, UTP-A and UTP-B subcomplexes function as RNA chaperones to start eukaryotic ribosome assembly (33). Simultaneously, the UTP-C subcomplex is recruited into the structure through the protein Rrp5 (66). UTP- C seems to act as a chaperone allowing that the emerging 5' domain of 18S rRNA enables the recruitment of several 40S r-proteins (63). Afterwards, several AFs such as Bms1 and Rcl1 form the central body of the 90S pre-ribosomal particle. Bms1 binds to Rcl1 forming a complex that could be involved in the cleavage at the A_2 site (65). This cleavage releases the first pre-40S r-particle containing the 20S rRNA intermediary. It has been proposed that the cleavage at the A_0 and A_1 sites allows the release of the 5´ETS from the pre-40S r-particle.

The release of the 5´ETS, as well as some major conformational remodeling, provokes the exit of several AFs. All these events give as result the separation of the pre- 40S ribosomal particle from the SSU processome (64). Processing of SSU pre-rRNA can also takes place post-transcriptionally in the site A_3 by the RNAse MRP. In this case, a 23S pre-rRNA specie is generated, whose function is not totally known (40) (**Figure 4**).

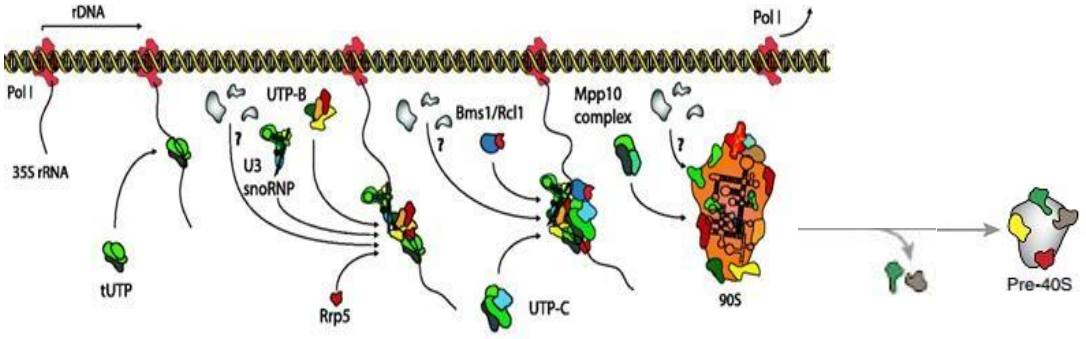

Figure 4. Model for the assembly of the 90S pre-ribosomal particle. UTP-A or t-UTP serves as a platform for the hierarchical recruitment of the following components. UTP-B subcomplex and U3 snoRNP are essential for 18S pre-rRNA incorporation into the 90S pre-ribosomal particle. Bms1/Rcl1 complex facilitates the incorporation of the Mpp10 complex and other factors that form the body of the 90S particle. Separately, the recruitment of UTP-C subcomplex by Rrp5 is a required step for 40S ribosomal proteins binding. Bms1 binds to Rcl1 forming a complex that could be involved in the cleavage at the A_2 site. The 90S pre-ribosomal particle is released from the 35S precursor. Finally, the release of the 5´ETS and few AFs generates the separation of the first pre-40S ribosomal particle from the 90S pre-ribosomal particle. Adapted from 27 and 63.

The pre-40S r-particle released from the 90S pre-particle contains the 20S pre-rRNA and several AFs (Enp1, Dim1, Pno1, Tsr1, Rio2, Ltv1, Hrr25 and Nob1) (10, 56, 64, 74). Some of these AFs are responsible of pre-40S r-particle export to the cytoplasm. An important step during the pre-40S ribosomal particle assembly takes place before the export to the cytoplasm. This step is the formation of the beak, a structural landmark in the head domain of the 40S mature subunit. The transport to the cytoplasm is RanGTP-dependent and Crm1-dependent. The protein Rrp12 is also a protein essential for the transport to the cytoplasm (41, 64).

The AFs remaining in pre-40S ribosomal particles block premature translation initiation. The remove of the remaining AFs allows the entrance of the mature SSU in the translating pool. Before the AFs removing, the pre-40S r- particles are subjected to a proofreading step that involves a translation-like cycle (81). During this step the mature LSUs transitory join to pre-40S r-particles forming non-productive 80S-like particles (81). This proofreading step is promoted by eIF5B/Fun12 and the ATPase Fap7 (10). The exit of few AFs like Rio2 promotes the disassembly of the 80S-like particles. Finally, the entrance of the 40S mature particles in the translating pool take place when the remaining AFs are removed and the last r-proteins like eS26 bind to the 40S subunits (**Figure 5)**.

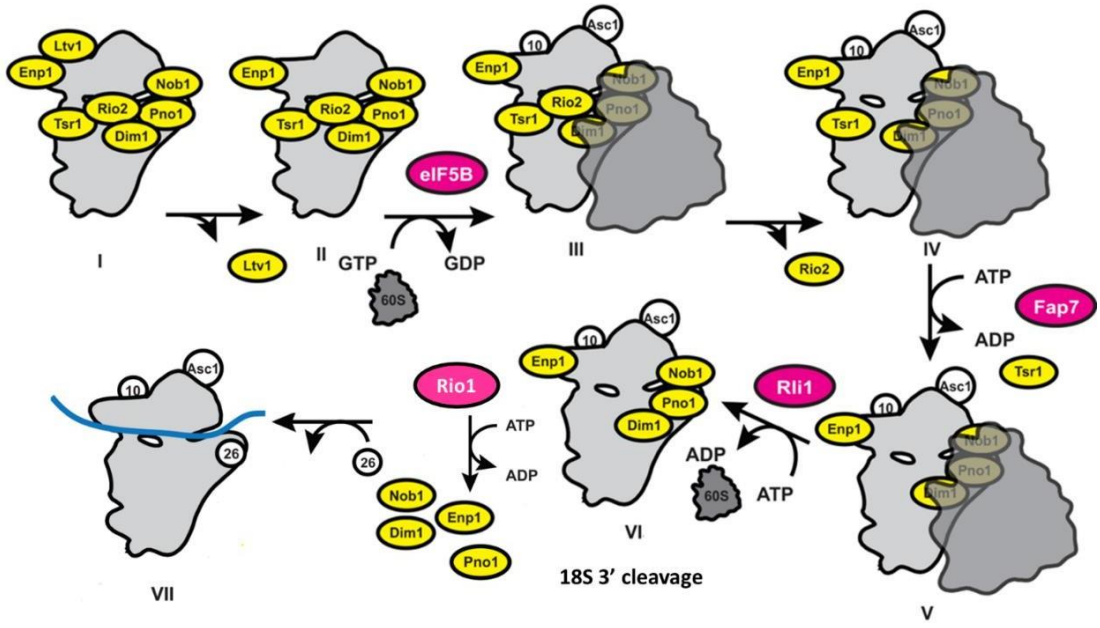

Figure 5. Late pre-40S r-subunit maturation model. Numbers indicates the progressive steps during pre- 40S r-subunit late maturation. Assembly factors that bind stably to these particles are indicated in yellow. Assembly factors that bind transiently to pre-40S r-subunit and its function is depending of energy are indicated in pink. Pre-40S r-particles and 60S ribosomal subunits are indicated in light and dark grey respectively. Ribosomal proteins are indicated in white and the mRNA in blue. Adapted from 81.

- *Assembly of the pre-60S r-particle*

The formation of LSUs is more complex than that of SSUs. During the first step of this process, in the nucleolus, several AFs facilitates the forming of the rigid scaffolds to stabilize the rRNA folding. Among these factors are present Dbp6, Npa1, Npa2, Rsa3 and Nop8. Six RNA helicases (Dbp2, Dbp3, Dbp7, Dbp9, Mak5 and Prp43) are also required in this very early stage to remodel RNA or RNPs. However, the binding site or the target of these helicases have not been yet properly identified (40). An important step during LSU assembly is the clustering of the six domains that compose the 25S rRNA. A set of AFs and r-proteins are responsible to build bridges between these domains. Some of these AFs form the complex Erb1-Ytm1-Nop7 (38, 40). Simultaneously, to the domains clustering the PET formation is accomplished. The rim around the exit of the PET is assembled by release of AFs (Ssf1-Rrp15 and Rrp14) and by stable association of some r-proteins such as eL19, uL23 and eL31 (40). The outer, wider portion of the PET is formed by the exit of Rpf1. The pre-ribosomes exit to the nucleoplasm and the other functional centers of the LSU (such as the CP and PTC) commence to emerge (89). An important step is the insertion of the carboxyl-terminal extension of Nog1 into the PET. This fact promotes the maturation of the walls of the tunnel. In the case of the CP, the chaperone Syo1 facilitates assembly of 5S rRNA together with the r-proteins uL18 and uL5 (46). The maturation of the CP allows the Nog2 association, which may influence in the construction of PTC. To reach mature conformation, the CP experiments a dramatic 180^{o} rotation mediated by the exit of Rpf2 and Rrp1 and the entrance of the AAA ATPase Rea1 (**Figure 6**) (4, 48, 57, 91). Rea1 also facilitates the binding of the essential nuclear export factor Nmd3 (41). It is possible that the binding of Nmd3 indicates the final nuclear step of pre-60S particles assembly. Maybe Nmd3 develops a structural proofreading role before nuclear export (**Figure 8**) (53). The late maturation steps of pre-60S r-particles take place in the cytoplasm. Pre-60S r-particles after nuclear export contain few AFs (53). All these factors are removed in a modular way. Finally, the incorporation of the last nine r-proteins, between them, uL16 allows the release of Nmd3. It is assumed that the

binding of uL16 is a rate-limiting step for cytoplasmic pre-60S ribosomal particles maturation (**Figure 7**) (53).

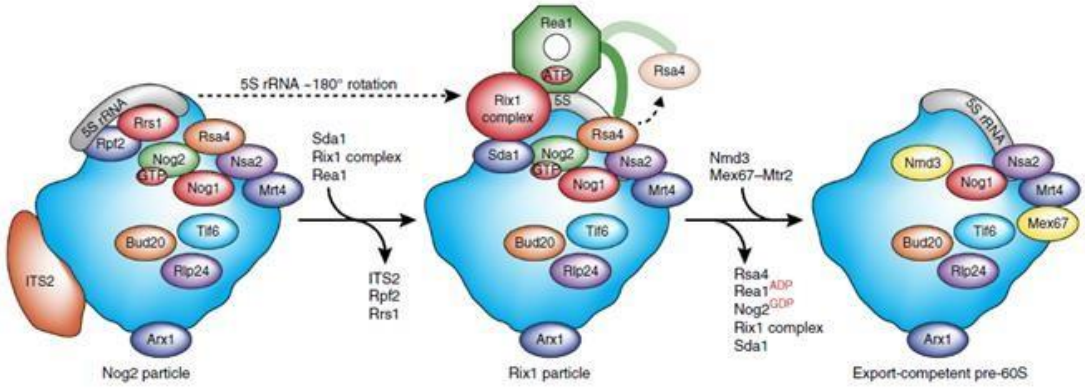

Figure 6. Nuclear pre-60S r-subunit maturation model including the AFs. The particles containing Nog2 and Rix1 are intermediate pre-60S particles. In the Nog2 particle the ITS2 spacer is present still and the 5S rRNA, that will form the CP, is in the premature conformation. In the Rix particle the ITS2 spacer is removed. The exit of Rpf2 and Rrs1 and the entrance of Rea1 promote the 5S rRNA rotation into the mature conformation. During this step the binding of the export factor Nmd3 takes place. Nmd3 recruitment makes the pre-60S particle competent for the export to the cytoplasm. Once in the cytoplasm Nmd3 and the remaining AFs are removed (64).

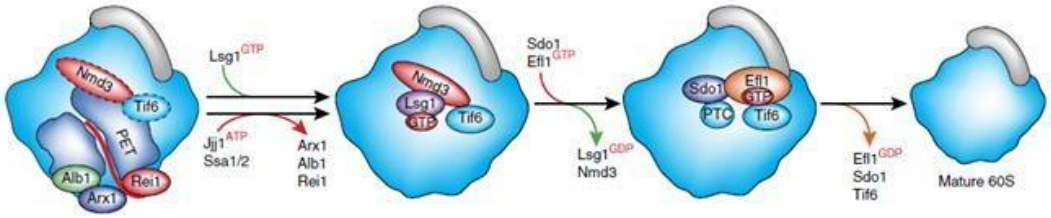

Figure 7. Cytoplasmic pre-60S r-subunit maturation model. The last quality control steps take place in the cytoplasm. The remaining AFs in the pre-60S r- particles are removed in a modular way. The exit of these AFs gives rise to the mature LSU (64).

At this point, it has been clear the importance of the AFs in the ribosome biogenesis process. Into the AFs group, RNA helicases are a group of important proteins involved in ribosome biogenesis. To date, it is known that 19 RNA helicases participate in yeast

ribosome biogenesis, most of them harbouring counterparts in higher eukaryotes (71). However, many of them remain poorly characterized.

2.3.-RNA helicases

In the literature, the RNA helicases are defined as enzymes that catalyse ATP-dependent unwinding of RNA duplexes (dsRNA). Today, it is known that besides to open dsRNA, the RNA helicases are involved in others biochemical process, such as RNA clamping, dsRNA destabilization, protein displacement from RNA and strand annealing (50, 71). For this reason, the term RNA helicases could be incomplete to define this category of enzymes.

2.3.1.-RNA helicases classification

RNA helicases are ubiquitous enzymes present in all forms of cellular life. Even many viruses can codify for these enzymes (22).

RNA helicases can be classified in different superfamilies (SFs), according to the pioneering sequence analysis of Gorbalenya and Kooning (1993) (29), and to more recent structural and functional analysis of Jankowsky and co-workers (22). So far, five superfamilies (SFs) of RNA helicases have been proposed (from SF1 to SF5) (**Figure 8**). RNA helicases belonging to SF1 and SF2 seems to be active as monomers or dimers. Conversely, SF3, SF4 and SF5 are active as oligomers (mostly hexamers) enzymes. The SF3, SF4 and SF5 are encoded principally in genomes of viruses and bacteria (49).

Helicases from the SF1 and SF2 superfamilies all contain a central core composed by two RecA-like identical domains (49). These domains resemble the structure of the bacterial recombination protein recombinase A (Rec A). The RecA-like domains are characterized by the presence of a few conserved motifs. SF1 and SF2 superfamilies are very similar with respect to the conserved motifs (15).

The SF2 is formed by five different sub-families: DEAD-box helicases, DEAH-RHA helicases, RIG-I like, Ski2-like and NS3/NPH-II proteins.

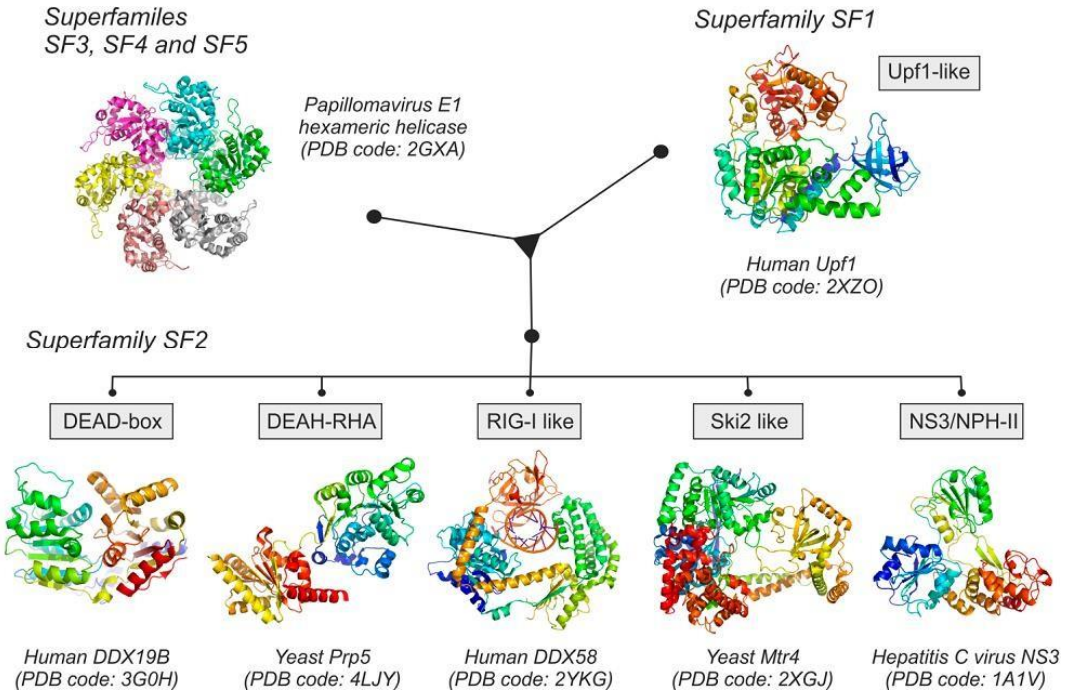

Figure 8. Structural classification of RNA helicases families. In each group, a structure of a representative protein from Protein Data Bank (PDB) is showed. SF1 and SF2 are formed by monomeric proteins. SF2 is very varied in its composition, and the only common characteristics in all the sub-families is the presence of a central core formed by two RecA-like domains. SF3, SF4 and SF5 are composed by hexameric proteins, basically of viral origin (49).

However, according to their action mechanism and catalytic properties, the SF2 can be further classified as processive and non-processive RNA helicases. Processive RNA helicases can perform multiple rounds of catalysis before substrate dissociation. Processive RNA helicases are able to unwind RNA duplexes by binding to a single-stranded region of the RNA and translocating along the dsRNA molecule using the ATP hydrolysis energy to open the structure (**Figure 9A**). After substrate release and ATP hydrolysis, the enzyme adopts an open conformation and the RecA2 domain form new contacts with the RNA substrate further downstream of the direction of translocation. The DEAH-box family is mostly composed by processive helicases. However, non-processive RNA helicases only use one substrate molecule by catalysis round (**Figure 9B**). DEAD-box proteins are non-processive enzymes that join to the RNA and open the duplexes by local strand separation. Thus, in the case of DEAH-box RNA helicases the

ATP hydrolysis drives the unwinding; however, in the DEAD-box helicases conversion of ATP to ADP generates the substrate release but not strand separation (8, 51).

A)

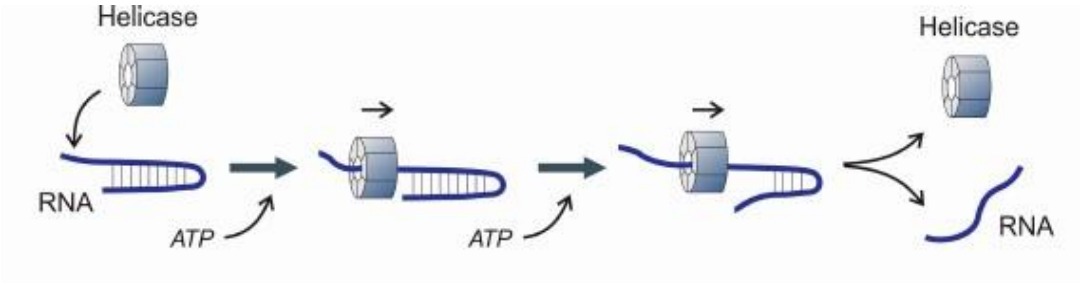

B)

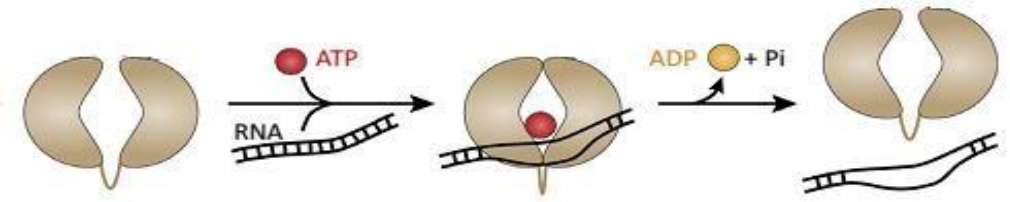

Figure 9. Schematic representation of the possible action mechanisms of RNA helicases from the SF2 superfamily. (**A**) Processive helicase, which can bind to a single-stranded region of the RNA and unwind the double RNA strand by translocation through it. In this case, the ATP hydrolysis is used to open the structure. (**B**) Non-processive helicase, which can bind to the double strand RNA molecule and unwind it by local strand separation. In this case the ATP hydrolysis is used to recycle the inorganic phosphate and to return to the original conformation. ATP is showed as a red circle and ADP is showed as a yellow circle. (49 and modified from 81)

2.3.2.-DEAD-box helicases

The DEAD-box helicases have the Rec A-like domains connected by a flexible short linker. In eukaryotes, the RecA-like domains are composed by a set of conserved motifs with invariable consensus sequences. These conserved motifs are involved in ATP-binding and hydrolysis, nucleic acid binding, and coordination between both activities. In most of the cases, the RecA-like domains are flanked by both a N- and a C- terminal

extensions. It is generally thought that these extensions interact with other proteins or with RNA targets (**Figure 10**) (15, 49, 50, 71).

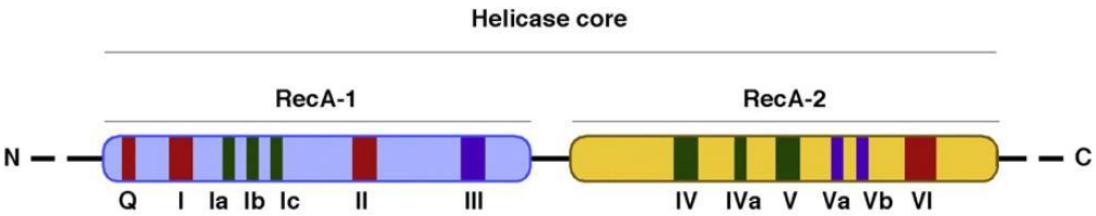

Figure 10. General structural organization of DEAD-box RNA helicases. The central core of the DEAD-box helicases is formed by the RecA-like 1 and RecA like 2 domains. These domains are connected by a flexible short linker. The central core harbours a set of conserved motifs. The motifs are showed in different colours depending of its biochemical function: In red; involved in ATP binding and hydrolysis, in green; involved in nucleic acid binding and in blue involved in coordination between ATP and nucleic acid binding. The central core can be flanked by N- and C- terminal extensions of variable length (71).

The conserved motifs are distributed in the two RecA-like domains forming an RNA substrate tunnel and a catalytic binding pocket for ATP. The ATP binding pocket contains also a divalent ion (e.g. Mg^{2+}) and a water molecule (84). The N-terminal RecA-like domain or domain 1 contains the ATP binding motifs F, Q, I, and II, the ATP hydrolysis motif III, and the RNA binding motifs Ia and Ib. The C-terminal RecA-like domain or domain 2 bears the RNA binding motifs IV and V and the motif VI that is able to coordinate ATPase and unwinding activities (15).

The motifs are mentioned from the N- to the C-terminal end of a general RNA helicase (7, 15, 80).

- Motif F: It is a highly conserved phenylalanine. It is present in the 88% of the DEAD-box RNA helicases. This phenylalanine is localized generally 16 amino acids upstream of the Q motif. It seems to function as a molecular switch to regulate ATP binding and hydrolysis.
- Motif Q: **GaccPoh1Q** (a, aromatic residue, c, charged amino acid, h, hydrophobic amino acid, o, alcohol and 1 aliphatic residue). The motif contains an invariant

glutamine residue that is present in the 99% of the DEAD-box RNA helicases. It is localized generally 16 amino acids upstream of motif I. This glutamine establishes direct interaction with the bound nucleotide and it is necessary for adenine recognition and binding.

- Motif I (Walker A): **AxTGoGKT** (x, any amino acid). It is involved in ATP binding and hydrolysis by forming hydrogen bonds with the pyrophosphates of the nucleotide and by interacting with the coordinated Mg^{2+} ion.
- Motif Ia: **PTRELA.** It participates in the structural rearrangements that occur upon ATP binding and hydrolysis. It is mainly involved in RNA binding.
- Motif Ib: **TPGRI.** It is involved in RNA binding.
- GG doublet: **GG**. It is proposed to participate in protein-protein interactions.
- Motif II (Walker B): **DEAD.** It gives the name to the family. This motif is involved in ATP binding and hydrolysis through the coordination of the ion Mg^{2+} by the first aspartate and the water molecule by the glutamate.
- Motif III. **SAT.** It establishes a communication between ATP-and RNA-binding sites via interaction with the γ-phosphate of the ATP.
- Motif IV: **1IFhxT+cx**. (+, positively charged amino acid). It contributes to substrate binding through interactions with the RNA.
- Motif V: **TDVuARGID**. (u: A, G). It regulates the hydrolysis of ATP. This motif is also involved in RNA binding.
- Motif Va: **QxxR.** It establishes a communication between ATP-and RNA-binding sites.
- Motif VI. **HRIGRTGR.** It is involved in ATP binding and hydrolysis. Contains two important arginine residues (first and second) that could bind the γ-phosphate of the ATP.

The DEAD-box helicases function in all processes that involve RNA: transcription, pre-mRNA splicing, RNA editing, RNA interference, RNA nucleo-cytoplasmic export, translation initiation and termination, RNA degradation, RNA quality control and in ribosome biogenesis, among them (50, 71, 78).

The conformational ATP-dependent changes of DEAD-box RNA helicases during its catalytic cycle is possible due to the linker that bind both RecA-like domains. This flexible short linker allows the change of orientation of one domain respect to the other. In this way, the RecA-like domains can adopt two different conformations. One of them is the closed active conformation, in which both motifs are in contact forming a cleft in the middle of motifs. To reach this conformation is necessary that both substrates join to the RecA-like domains 1 and 2. This conformation allows the formation of the ATP binding pocket and the RNA binding site. The ATP and RNA binding sites are arranged in perpendicular position in the cleft formed by the two RecA-like motifs (68). However, in the opened inactive conformation both RecA-like domains are separated, and this fact impairs the ATP and RNA sites assembly.

The DEAD-box RNA helicases interaction with the RNA is always sequence independent as the protein bind to the phosphate backbone of the RNA molecule (19). The catalytic activity responds to a model in which the double strand RNA separation is completed before ATP hydrolysis and depending of the length and stability of the RNA duplex (35). The unwinding process is limited to short RNA duplexes (10-15 bp) and it is accomplished in a single cycle of ATP-dependent conformational changes (19, 28, 36).

The binding of ATP and dsRNA causes the closure step and the formation of the functional ATP and RNA binding sites. Then, the dsRNA is unwound; one of the strands remains bound to the enzyme while the other is released from the complex. After that, the ATP is hydrolysed to ADP and inorganic phosphate (Pi). This fact promotes the recycling of the enzyme and the release of the second bound RNA strand (**Figure 11**) (3, 28, 49).

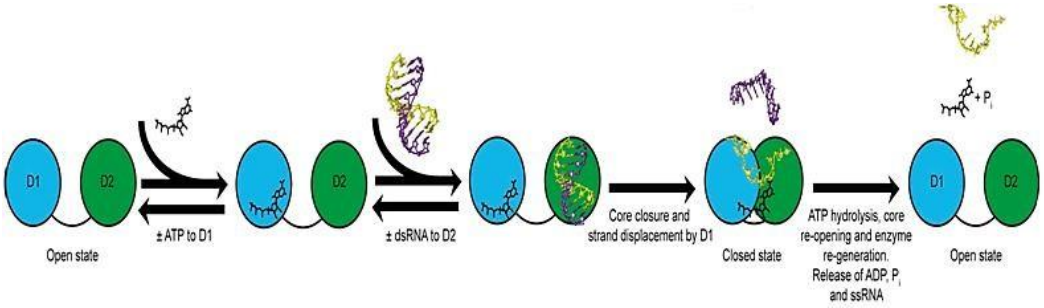

Figure 11. Structural changes in DEAD-box helicases during dsRNA unwinding. In the inactive or open conformation both domains are separated. The binding of ATP to the domain 1 and the dsRNA to the domain 2 promote the joining of both domains and induce the active or closed conformation. One of the dsRNA strands is released from the complex while the other remains bound to the enzyme. The ATP hydrolysis promotes the release of the second RNA strand and the return of the enzyme to the open conformation (54).

2.3.3.-3D structure of DEAD-BOX RNA helicases

The detailed understanding of how the RNA helicases convert chemical energy into RNA remodelling need the knowledge about the structure of both domains in active or closed conformation and in inactive or opened conformation. Today, crystal structures of tandem domains are available for several DEAD-box helicases (eIF4AI, eIF4AII, Dbp4, Rok1, etc…). A comparative analysis of these structures showed not only the specific features of the isoforms but also nucleotide specific positioning of flexible elements that are common to several proteins. Considering the DEAD-box RNA helicase model eIF4A, the tertiary structure of these proteins can be defined by a ‘‘dumbbell’’ molecule with two globular domains connected by an extended (and in all probability, flexible) linker (**Figure 12**) (9). The superposition of the crystal structures revealed the location of others flexible regions. In general, regions of high sequence conservation (the conserved motifs) contribute to the binding sites for nucleotide and for RNA, and these sites coincide with the highest structural similarity. Concerning to the surface charge distribution of the DEAD-domain structure, there is a conserved patch that forms the nucleotide binding site and part of the RNA binding site. This conserved patch is negatively charged and formed a channel that extends from the α-helices 8-10 to the Mg^{2+} binding site. However, the RNA binding cleft is positively charged in all DEAD domains. Referring to ATP binding site, the P-loop (motif I) and motif II coordinate the nucleotide phosphates. Superposition of the DEAD-domains showed that the conformation of the P-loop (motif I) is determined by the nucleotide phosphates and longer phosphate tails result in a more open loop. Motifs Ia, Ib and II seem unaffected by the state of ATP hydrolysis, and their conformations remain unchanged even in the crystal structures in which the nucleotide binding site is not occupied.

The helicase domain is composed fundamentally, by the domains V and VI. Apparently, four side chains are of importance: The aspartate of motif V coordinates the *O3´* of the ribose. The second arginine side chain of motif VI interacts with the γ-phosphate. The third arginine, which is also the putative arginine finger during ATP hydrolysis, coordinates all three ATP phosphates. It is seeming that the unblocking of the RNA binding site is related with α helix 8. When the two RecA-like domains are separated, α helix 8 would block the RNA binding site. It is proposed that the ATP facilitates the RNA binding since it pushes α helix 8 out of the RNA site (78).

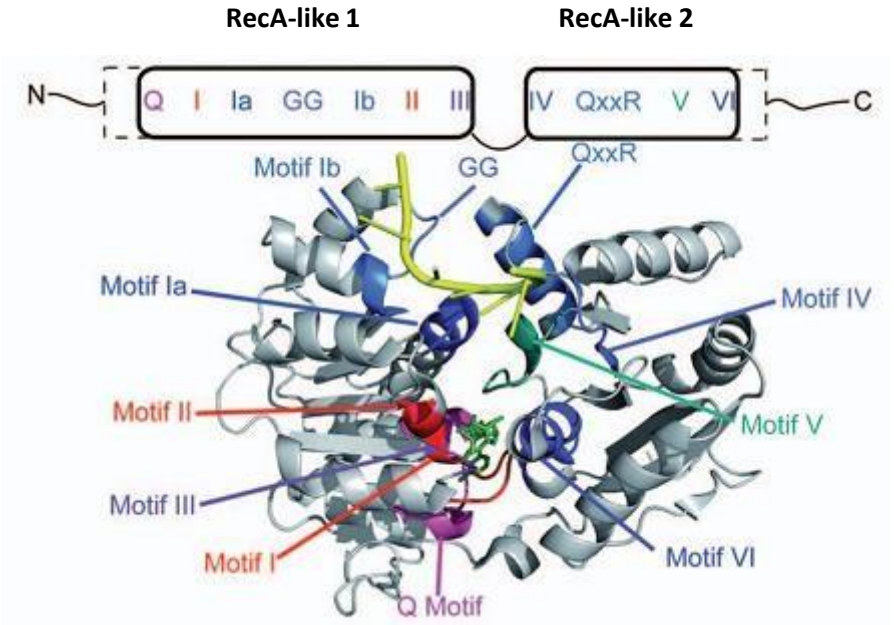

Figure 12. Structure of eIF4AIII in complex with single RNA (yellow) and ADPNP (green). The DEAD-box RNA helicases are formed by two RecA-like domains connected by a flexible short linker. Both domains bear conserved sequence motifs. In red are indicated motifs involved in ATP binding and hydrolysis, in blue are indicated motifs involved in RNA binding and in purple are indicated motifs involved in coupling ATP hydrolysis and duplex unwinding (2).

2.3.4.- Biochemical properties of DEAD-box RNA helicases

So far, several DEAD-box RNA helicases involved in ribosome biogenesis have showed RNA dependent ATPase activity and ATP dependent helicase activity. Study of these properties, construction of mutants in conserved motifs and analysis of its phenotypes have allowed determine the function of each conserved motif in the DEAD-box RNA helicases subfamily. Into the category of DEAD-box helicases biochemical data have

been found for Ded1, Has1, Rok1 and Dbp9. Ded1 are involved in translation initiation and could has a role in ribosome binding in *S. cerevisiae*. The ATPase activity of Ded1 is stimulated by natural RNAs, such as rRNA and polyadenylated mRNA *in vitro*. Concerning to the helicase activity, a high concentration of protein respects the template is necessary to open the dsRNA. The unwinding of RNA only is possible in presence of ATP; thus, ATP hydrolysis is necessary for driving the unwinding reaction. The mutant DAAD in the motif II of Ded1 is able to bind RNA as the wild-type, however, the ATPase activity is 60 times lower than in the wild-type and is deficient for the unwinding activity. Another important characteristic of Ded1 is that ATP binding and hydrolysis increase the relative affinities of Ded1 for ssRNA versus dsRNA. All the data obtained about Ded1 make it a good candidate to be involved in the unwinding of the cap-proximal secondary structures (35). Has1 are involved in SSU and LSU biogenesis. This protein has RNA dependent-ATPase activity *in vitro* and it can unwind DNA/RNA heteroduplexes in an ATP-dependent manner. Has1 is able to unwind heteroduplexes in 5´-3´or 3´-5´directions, showing preferences by the 5´-3´direction. Mutation in the motif I or motif VI decreases the ATPase activity of Has1. However, mutations in the motif III affect the unwinding activity of the protein (70). Rok1 is, as Has1, involved in ribosome biogenesis. The ATPase activity of Rok1 is independent of ssRNA. Mutations in the motif I had different phenotype depending of the changed residue. K172L and G166D showed a drastic defect in ATP hydrolysis, however, the mutation K172R hardly affects the ATPase activity of Rok1. Referring to the helicase activity Rok1 did not present the capacity to open dsRNA duplexes (61). Finally, Dbp9 is an RNA helicase involved in LSU biogenesis. In contrast to other members the ATPase activity of Dbp9 seems to be stimulated by DNA and inhibited by RNA *in vitro*. Concerning to the helicase activity, Dbp9 exhibits DNA-RNA and DNA-DNA helicase activity dependent of ATP, but also unwinds RNA in absence of an NTP. Mutants in the motif VI of Dbp9 did not present ATPase activity neither or helicase activity (39). When it was possible, the kinetics parameters of these RNA helicases were measured. The K_M values oscillate from 300-400 µM in all cases.

2.3.5.- Helicases in ribosome biogenesis

Currently, it is known that approximately, 19 RNA helicases are involved in ribosome biogenesis in yeast. Most of them belong to the superfamily 2. All the RNA helicases involved in ribosome biogenesis are essential for cell viability, except Dbp2, Dbp3 and Dbp7, where their genetic deletion causes a strong growth delay. The functions of RNA helicases in ribosome biogenesis can be envisaged in one of these activities:

- Annealing or unwinding of snoRNA-pre-rRNA base pairing : as an example of this function it can be reported the activity of Rok1, which is involved in the release of the snR30-containing snoRNP of 90S pre-ribosomal particles or Dbp4, which is required for release of U14 and snR41 also from these particles. Other RNA helicase essential for the release of a subset of snoRNAs is Prp43. Prp43 is one of the best studied DEAH-box helicases and its function implies also structural remodelling of pre-ribosomal particles to facilitate pre-rRNA processing at different stages of maturation (19, 71).
- Preparation of the pre-rRNA for an efficient nuclease attack: In this category it can be included, on one hand the RNA helicases Dbp4, Dbp8, Fal1, Dhr1, Dhr2, Rok1 and Rrp3 as their absence generates defects in pre-rRNA processing at sites A_0, A_1 and A_2. On the other hand, Dbp2, Dbp3, Dpb6, Dpb7, Dbp9, Dbp10, Drs1, Mak5, Mtr4/Dob1 and Spb4 that control the levels of $27SA_2$ pre-rRNA precursor or downstream precursors during the the pre-60S r-particle proccesing (56). From all these examples, it seems that Dbp3 and Mtr4 are more directly involved in this reaction as they likely target the $27SA_3$ and 7S pre-rRNAs to the RNase MRP and the exosome, respectively (71).
- Modulation of specific intra- and inter-molecular RNA, rRNA–protein or protein–protein interactions inside pre-ribosomal particles during the maturation of r-subunits. An example of this activity can be found in Prp43, which establishes base-pairing between 25S and 5.8S rRNAs or Dbp6, Dbp7 and Dbp9 that are involved in the efficient assembly of uL3 in early pre-60S r-particles (**Figure 13**) (71).

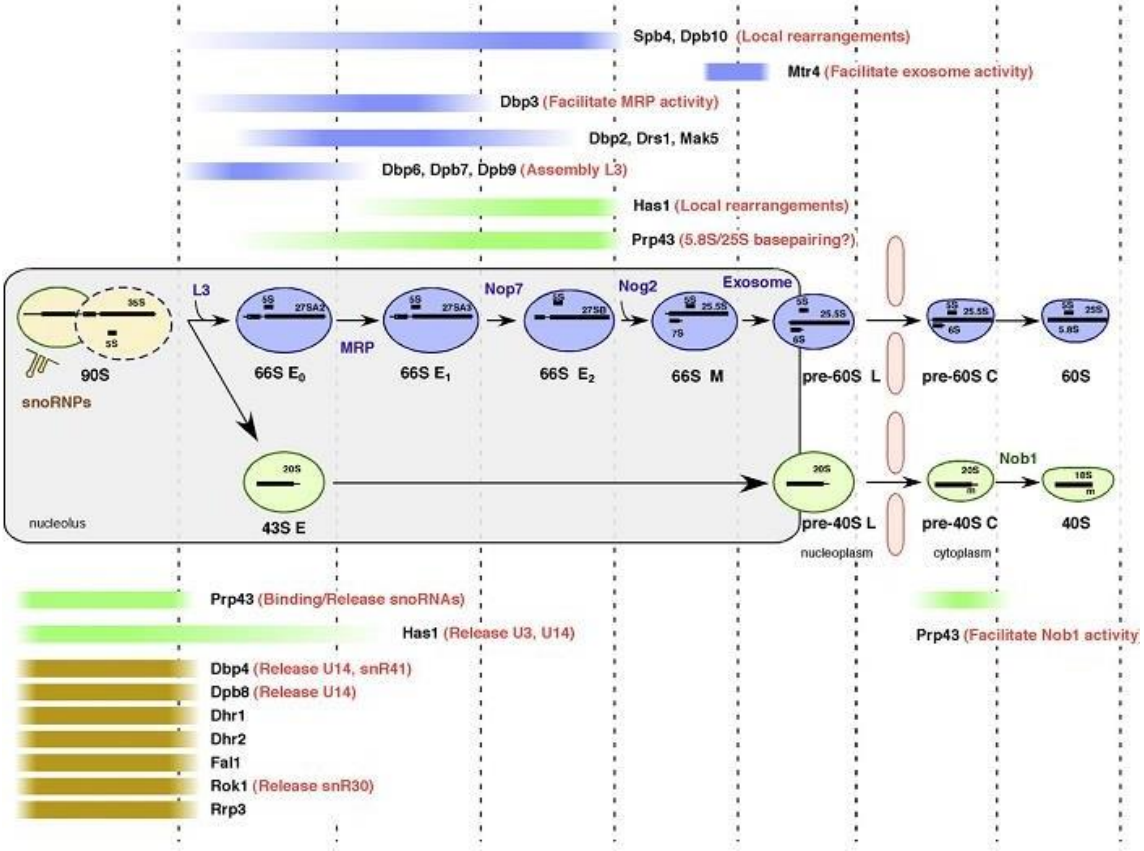

Figure 13. Function of RNA helicases in ribosome biogenesis and position of action of each enzyme. The formation, maturation and export of pre-ribosomal particles are indicated. The first pre-ribosomal particle detected is the 90S, which contains the 35S pre-rRNA and the precursor for the rRNA 5S. Cleavage in the A_2 site of the 35S pre-rRNA provokes the separation of pre-60S (66S) and pre-40S (43S) particles. The early 43S pre-ribosomal particle is rapidly exported to the cytoplasm, where the pre-rRNA 20S is processed to mature 18S rRNA by Nob1 and the mature SSU is formed. The maturation of the LSU takes place along a serial of steps. The 66S pre-ribosomal particle contains the $27SA_2$ pre-rRNA. The complexity of pre-60 r-particles decreases during the maturation, in which the 25S and the 5.8S pre-rRNA are being processed until generate the mature rRNA species inside of the mature LSU in the cytoplasm. The different intermediaries are called early (E), middle (M), late (L) and cytoplasmic (C). The colour bar next to each protein indicates the level of the process in which the protein is involved. The function or possible function of the protein is also indicated (71).

2.3.6.- Dbp6 and Dbp9 in ribosome biogenesis. Complex containing Dbp6, Dbp9, Nop8, Rsa3, Rsa1

Dbp6 and Dbp9 are DEAD-box RNA helicases essential for cell viability. Both enzymes are involved in LSU biogenesis (16, 45). In absence of Dbp6 or Dbp9, 35S pre-rRNA might not have been stable and as a consequence, less 27S pre-rRNA is formed. The formation of 18S rRNA is also affected since an aberrant 23S pre-rRNA appeared and less 20S rRNA is formed. However, Dbp6 and Dbp9 are more necessary for the normal formation of 25S and 5.8S rRNA. It has been determined that Dbp6 and Dbp9 genetically interact between each other. Dbp9 is a dosage suppressor of several temperature-sensitive *dbp6* mutants. Moreover, combination of dbp9 mutations with mild *dbp6* alleles led to a strong synthetic enhancement of the respective phenotypes. So, mutations in the genes that codify for RNA helicases Dbp6 and Dbp9 generate a synthetic enhancement of their mutant phenotypes (16). Another important evidence for the fact that Dbp6 and Dbp9 interact comes from the yeast two-hybrid assay, that show that both enzymes weakly but physically interact with themselves and with each to other. The RNA helicase Dbp7 has also been shown to genetically interact with Dbp6 and Dbp9 thus, a null *dbp7* allele enhances the mutant slow growth phenotype of distinct *dbp6* and *dbp9* alleles. In conclusion, there is a genetic and physic interaction between Dbp9 and Dbp6 and a genetic interaction between Dbp7 and Dbp9 and Dbp6. The functional environment of Dbp6 has been extended; thus, it has been discovered that exist a functionally interaction network between Dbp6, Dbp9, Nop8, Rsa3, Rsa1 and uL3 (**Figure 14**) (18). It has been concluded that all these factors may interplay to support a function during early pre-60S r-subunit assembly.

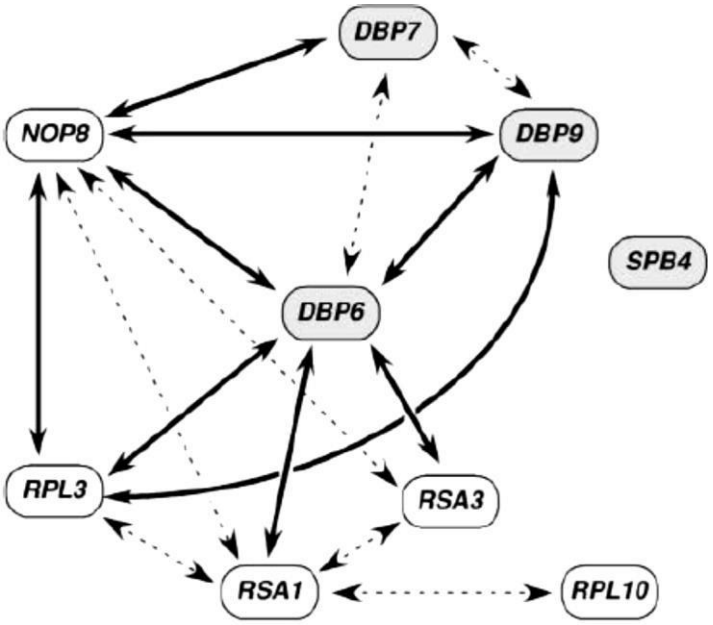

Figure 14. Synthetic enhancement interaction network of protein *trans*-acting factor and ribosomal protein encoding genes involved in the biogenesis of LSU. Solid arrows indicate synthetic lethal interactions and dashed arrows indicate synthetic enhancement. DEAD-box RNA helicases are indicated by grey ovals and r-proteins and others trans-acting factors are indicated by white ovals (18).

2.3.7.- Dbp6 and Dbp9 in ribosome biogenesis. Complex containing Npa1, Npa2, Dbp6, Dbp9, Nop8, Rsa3 and Rsa1

The functional network established between Dbp6, Dbp9, Nop8, Rsa3 and uL3 was extended with the identification of other two proteins that interact with the above-mentioned group. These two proteins are Npa1/Urb1 and Npa2/Urb2 (**Figure 15**) (20, 72, 73).

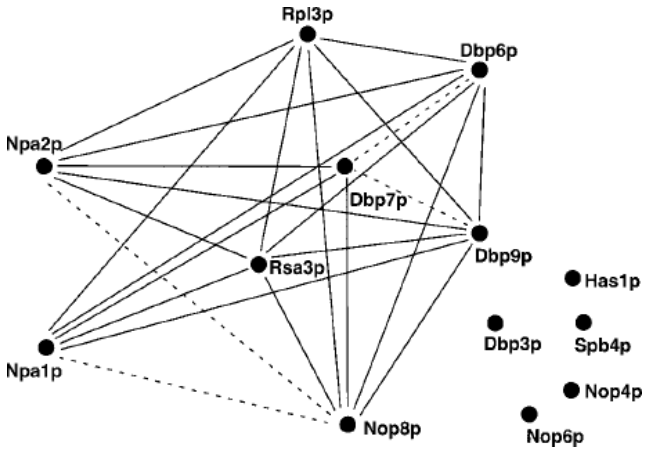

Figure 15. Synthetic interaction network between the members of the complex Dbp6, Nop8, Rsa3 and uL3 including Npa1and Npa2. Solid lines indicate synthetic lethality, and dashed lines indicate synthetic enhancement. The protein Dbp7 maintains a genetic interaction with some components of the complex. Any of the proteins Dbp3, Has1, Spb4, Nop4 and Nop6 do not form part of the interaction network, which support the specificity of the interactions (72).

The Npa1 and Npa2 proteins are involved in early assembly of pre- 60S r-particles. All the proteins of this functional complex, with exception of Rsa3, are essential for cell growth and all are necessary for the normal production of LSU. Rsa3 and Nop8 are proteins with coiled-coiled domains and may be implicated in protein-protein interaction. In the case of Nop8, also contains a putative RNA recognition motif that may allow the binding of Nop8 to pre-rRNA (37). Npa1 is the largest protein of the complex and seems that forms the backbone for physical interaction with few other components. Npa2 is essential for Npa1 and Dbp6 interaction. It has been shown that, on one hand Npa1 binds directly to Npa2, Nop8, Rsa3 and Dbp6 while on the other hand Npa2, Nop8 and Rsa3 do not interact directly in absence of Npa1, Dbp6 also binds to Npa2. Together, this physical complex has received the name of Npa1 complex (**Figure 16**).

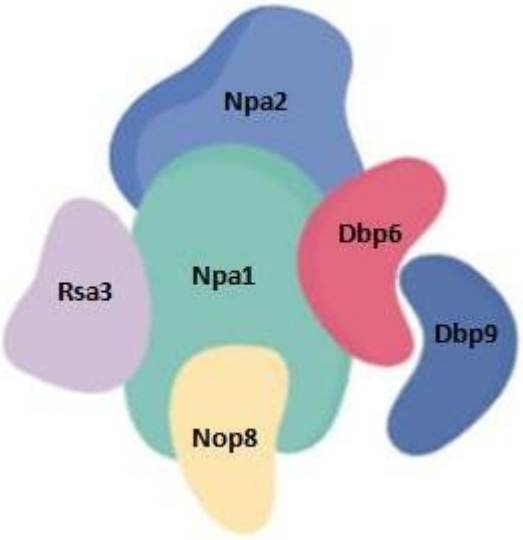

Figure 16. Model of protein-protein interaction in the Npa1 complex. Npa1 is the backbone of the complex. All the proteins are bound to Npa1. However, Npa2 is necessary for Npa1 and Dbp6 interaction. In the absence of Npa1; Npa2, Nop8 and Rsa3 do not interact. Dbp9 is bound to the complex through Dbp6. Adapted from 37.

Npa1 is also essential for the stable integration of the complex in the 90S pre-ribosomal particles. However, maybe Nop8 can strengthen the interaction of Npa1 complex to pre-ribosomal particles since Nop8 possesses the RNA binding domain. Finally, Dbp6 is the only enzymatic component of the complex, and might facilitate the complex integration into pre-ribosomal particles through local remodeling of these particles. It is important to highlight also the relation between Npa1 complex and the uL3 r-protein. This relation was established through synthetic lethal interaction between members of Npa1 complex and uL3 (18). It has been suggested that uL3 is a necessary protein in the folding of central core of 25S rRNA by binding to both the 3' end of 25S rRNA and the 5'end of 5.8S rRNA. UV cross-linking and analysis of cDNAs (CRAC) identified that Npa1 cross linking sites that are positioned in the immediate vicinity of rRNA sequences contacted by uL3 in the mature LSU. Thus, Npa1 complex may collaborate with the function of uL3 during the early steps in the LSU assembly. The CRAC analysis also revealed that Npa1 cross-linked to different snoRNAs that bind to the PTC (20, 37) or domain II of 25S rRNA.

The reads that mapped to snR190 are the most abundant by far, but other reads less abundant mapped to snR10, snR42, snR5 and snR61. Altogether, these data are concordant with the hypothesis that the Npa1 complex is involved in pre-rRNA folding events within the earliest pre-60S particle modulating interactions between snoRNAs and 25S rRNA into pre-60S particles (37).

2.3.8.-Dbp7 in ribosome biogenesis

Dbp7 (YKR024C) belong to the DEAD-box subfamily of RNA helicases and is involved in ribosome biogenesis; however, its precise function is still unknown (18).

Dbp7 is a nucleolar protein of 742 amino acids (pI: 9.33 and predicted mass 84 KDa). The gene that encodes for Dbp7 is located in the chromosome XI. All conserved amino acid motifs of the DEAD-box protein family are present in Dbp7 (**Figure 16**). Besides this, the RecA-like domains of Dbp7 are flanked by two longs N- and C- terminal extensions of approximately 200 amino acids each (18).

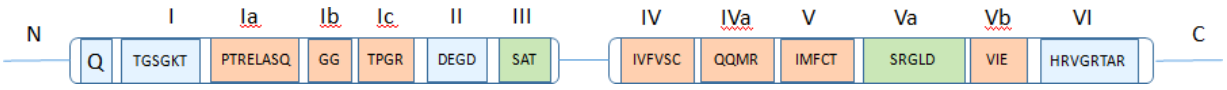

Figure 16. Representation of the RecA-like domains of Dbp7. The conserved motifs are shown. Each motif is indicated by a different color. In blue, motifs involved in ATP binding and hydrolysis, in red, motifs involved in nucleic acid binding and in green, motifs involved in the coordination between both functions. The sequence of each motif is showed inside rectangles. The name of each domain is showed over the rectangles. The N- and C-terminal extensions are indicated by a line with the letter N or C, respectively.

Dbp7 is a non-essential protein in *S. cerevisiae*. However, the deletion of *DBP7* generated a deficit of 60S ribosomal subunit observed due to a delay in the processing of 27SA and the derived precursors that lead the mature 25S and 5.8S rRNA. The involvement of Dbp7 in the 60S ribosomal subunit metabolism makes it necessary for optimal vegetative growth of the cells. As shown in this Thesis book, the understanding of the function of Dbp7 in ribosome biogenesis is the main objective of this work.

3.OBJECTIVES

3.- OBJECTIVES

Ribosome biogenesis is a very important cellular process in cells. In eukaryotic organisms, many proteins and factors are involved in this proccess. Among these factors, RNA helicases belonging to DEAD-box family are of special relevance. These enzymes catalyse ATP-dependent unwinding of RNA duplexes (dsRNA). Some members of the DEAD family have been characterized, but their specific role in the process of ribosome biogenesis is barely known. In this work, we have studied RNA helicases involved in 60S ribosomal subunit biogenesis in *S. cerevisiae* . For this purpose, we raised the following objectives:

- To study *in vitro* the catalytic properties of Dbp7 and Dbp9.
- To study the *in vivo* function of Dbp7, including the role of N- and C-terminal extensions.
- To dissect the functional environment of Dbp7 within pre-60S r-particles, including its relationship with selected snoRNPs.

4. MATERIALS AND METHODS

4.-MATERIALS AND METHODS

4.1.-Microorganisms and growth conditions

S. cerevisiae and *E. coli* strains used in this work are listed in the Table 1.

Table 1. Yeast and bacterial strains used in this study. The relevant characteristics of the strain genotypes and the references that describe them are indicated.

Strain	Relevant genotype	SOURCE
W303-1A	MAT**a**/**α** *ade 2-1/ade 2-1 his 3-11,15/his 3-11,15 leu 2-3, 112/ leu 2-3, 112 trp 1-1/trp 1-1 ura 3-1/ura 3-1*	Thomas and Rothstein, 1989
YKL500	As W303-1B but *NOP58*-yEmCherry::natNT2 *ade3*::kanMX4	Pillet *et al.*, 2015
JDY306	MAT**a**/**α** *dbp7*:: HIS3MX6 /DBP7	Our lab collection
snR190 cl 2	MAT**a**/**α** *ade 2-1/ade 2-1 his 3-11,15/his 3-11,15 leu 2-3, 112/ leu 2-3, 112 trp 1-1/trp 1-1 ura 3-1/ura 3-1, snR190*	Henras et al, 2018
E. coli XL-1-Blue	*endA1* gyrA96 (nal^R) *thi-1* recA1 relA1 lac glnV44 F'[:: Tn10 $proAB^+lacI^q$ Δ(lacZ)M15] *hsdR17* ($r_K^- m_K^+$)	Stratagene
E. coli BL21 Codon Plus (DE3) -RIPL	F^- ompT hsdS (rB – mB –) dcm+ Tetr gal λ(DE3) endA Hte [argU proL Camr] [argU ileY leuW Step/Specr]	Agilent

The *dbp7Δ*[YCplac22] strain was constructed by transformation of the *dbp7Δ*[YCplac33-DBP7] strain with the plasmid YCplac22 (*CEN, TRP1*); transformants were counter-selected on 5-FOA (5-fluoroorotic acid) containing plates (plasmid shuffling) to allow the growth of those clones that have lost the YCplac33-DBP7 plasmid. Some of the colonies

growing on this media were further transferred to SD-Trp plates. We also constructed a *dbp7Δ*[YCplac22-HADBP7] strain (from now on HA-*DBP7*), using the same strategy.

The Dbp7[K197A] or Dbp7[R553A] protein variants were performed by PCR of the ORF of *DBP7* (with the correspondent point mutation) using Ycplac22-HA-DBP7 as a template. The ORF of *DBP7* was expressed under the control of the cognate *DBP7* promoter followed by a HA epitope. The N-terminally HA-tagged constructs were transformed in the strain *dbp7Δ*[YCplac33-DBP7]. The transformants were selected on SD-Trp and then, the *URA3*-marked plasmid counter-selected on 5-FOA plates (plasmid shuffling). Some of the colonies growing on this media were further transferred to SD-Trp plates.

The *dbp7* truncated mutants were performed by PCR of the ORF of *DBP7* (lacking the correspondent codons in the N- or C- terminal extension) using Ycplac22-HA-DBP7 as a template. The ORF of DBP7 was expressed under the control of the cognate *DBP7* promoter followed by a HA epitope. The N-terminally HA-tagged constructs were transformed in the strain *dbp7Δ*[YCplac33-DBP7]. The transformants were selected on SD-Trp and then, the URA3-marked plasmid counter-selected on 5-FOA plates (plasmid shuffling). Some of the colonies growing on this media were further transferred to SD-Trp plates.

The Dbp7-N-terminal-EGFP strain was constructed by cloning the first 162 amino acids of Dbp7 (N-terminal extension), which contained the putative NLS in phase with three tandem GFP proteins, and expressed from the strong *ADH1* promoter on a *LEU2*-marked pADH111 centromeric plasmid. In addition, we cloned in the same plasmid a variant of the N-terminal of Dbp7 lacking the NLS to construct the *dbp7ΔNLS*-N-terminal-EGFP strain. As a positive control we used the NLS of the large T antigen of the SV40 virus, which was also cloned in pADH111 plasmid. Each plasmid was transformed into the

YKL500 strain, which harboured a genomic functional copy of the gene coding the nucleolar reporter Nop58 tagged with the red fluorescent mCherry protein.

For the HA-*dbp7ΔNLS* mutant, a PCR of the ORF of *DBP7* lacking the codons corresponding to the NLS was performed using Ycplac22-HA-DBP7 as a template. The ORF of *DBP7* was expressed under the control of the cognate *DBP7* promoter followed by a HA epitope. To use as a control, a full-length HA-Dbp7 protein was cloned into YCplac22. Upon transformation of these constructs into the *dpb7Δ*[YCplac33-DBP7] strain, cells were subjected to plasmid shuffling on 5-FOA plates. Some of the colonies growing on this media were further transferred to SD-Trp plates.

The proteins wild-type Dbp7-$(GA)_5$-3xyEGFP, Dbp7ΔNLS-$(GA)_5$-3xyEGFP and Dbp7ΔN162-$(GA)_5$-3xyEGFP were constructed by fusion of the Dbp7 protein in the C-terminus to three variant GFPs (3xyEGFP) in tandem. These constructs were expressed from the cognate *DBP7* promoter and cloned onto a YCplac111 plasmid. The plasmids, were transformed independently into the YKL500 strain.

The *snR190* strain was performed by the CRISPR-Cas9 system in the collaborative laboratory of Prof. Henry. This system included a couple of relevant nucleotides in the C box of snR190 that compromise its binding to rRNA. Thus, the sequence GGCCCUGAUGA corresponding to the first 11 nucleotides of snR190 were substituted by the sequence GGAACUAUUGA.

To obtain a double mutant containing the non-functional version of the snR190 and lacking Dbp7, we crossed the strain *snR190* with an isogenic *dbp7Δ*[YCplc33-DBP7]. Diploids were selected and sporulated. After tetrad dissection, we confirmed that, as expected, the His3-marker that deleted-disrupted the *DBP7* gene segregated 2^+:2^- in

complete tetrads. Then, we counter-selected the Ura3-marked YCplac33-DBP7 plasmid from different tetrads in plates containing 5-FOA. Finally, to accurately establish the genotypes of the spore-clones, we obtained total DNA for several complete tetrads and sequenced the genomic region comprising the coding sequence of the snR190.

Unless otherwise indicated, all strains of *S. cerevisiae* were grown at 30 ºC in rich YPD medium (1% yeast extract, 2% peptone) containing 2% glucose as carbon source or in synthetic minimal medium (SD) (0.15% yeast nitrogen base, 0.5% ammonium sulphate) supplemented with the appropriate nutritional requirements and containing 2% glucose as carbon source with or without 2% agar.

E. coli was grown at 37 ºC on LB broth medium (10 g/L tryptone, 5 g/L yeast extract, and 10 g/L NaCl) supplemented with 2% of agar and antibiotics when was required. The following antibiotics were used alone or in combination: ampicillin (100 μg/mL), tetracycline (20 μg/mL) and chloramphenicol (50 μg/mL).

For serial dilutions in solid medium, yeast cultures were grown until reaching an OD_{600} of 0.8. Subsequently, these cultures were diluted to an OD_{600} of 0.05, 1:5 serial dilutions were performed, and five microliters of each dilution was spotted onto the corresponding plates. The plates were incubated at the appropriate temperature.

Growth curves were obtained by measuring the OD_{600} of cellular cultures at different incubation times and representing this OD_{600} versus time. To do so, cultures were previously grown to reach an OD_{600} between 0.5 and 0.8. Subsequently, these cultures were diluted to an OD_{600} of 0.05 and incubated at the interest temperature and 180 rpm until they reach an OD_{600} of 1.0, approximately. The measures of the OD_{600} were

performed in a spectrophotometer (Genesys 20, Thermo Scientific) along the day; samples were taken every 90 minutes.

4.2-Yeast transformation

Cells were grown to an OD_{600} between 0.5 and 1. Then, they were harvested by centrifugation; the cellular pellet was resuspended in a mix containing 100 mM lithium acetate, 10 mM Tris-HCl, pH 8.0, and 0.5 mM EDTA (ethylenediaminetetraacetic acid) and mixed with 5 µL boiled single-stranded DNA from salmon sperm (10 mg/mL). After that, 0.5-2 µg of plasmid DNA was added into the mix. A solution containing 100 mM lithium acetate, 10 mM Tris-HCl, pH 8.0, 0.5 mM EDTA, and 40% PEG 3350 (polyethylene glycol-3350) was also added. This final mix was incubated in a microcentrifuge tube at 30 ºC and 180 rpm for 30 minutes. Next, cells were incubated in a water bath at 42 ºC for 15 minutes, and then for 10 minutes on ice. Pellets were obtained by centrifugation at 6500 rpm in a microcentrifuge and resuspended in 50 µL of water. Finally, for selecting yeast transformants, cells were streaked onto selective media plates, which were incubated for 2-4 days in a 30 ºC incubator.

4.3.-Preparation of bacterial competent cells

E. coli was grown at 22 ºC and 180 rpm in 50 mL of SOB medium (2% tryptone, 0.5% yeast extract, 10 mM NaCl, 2.5 mM KCl, 10 mM $MgCl_2$, and 10 mM $MgSO_4$) until an OD_{600} of 0.4. Cells were centrifuged at 4000 rpm for 10 minutes at 4 ºC in a Sorvall ST 16R centrifuge (Thermo Scientific, TX-200 swinging bucket rotor). Cellular pellets were resuspended in 15 mL of TB buffer (10 mM KOH-Pipes (piperazine-N, N'-bis (2-ethanesulfonic acid)) pH 6.7, 15 mM $CaCl_2$, 250 mM KCl, and 50 Mm $MgCl_2$ and incubated on ice for 10 minutes. After centrifugation at 4000 rpm during 10 minutes at 4 ºC, cells were frozen in a mix containing 5 mL of TB buffer and 98 µL of 8% DMSO (dimethylsulfoxyde) in liquid nitrogen. Before freezing, cells were distributed into 100 µL aliquots and store at -80 ºC.

Alternatively, competent cells were also prepared by the so-called TSS method. A culture of 5 mL of *E. coli* was grown at 37 ºC and 180 rpm to an OD_{600} of 0.35. 1 mL of cells were

centrifuged at 10000 rpm for 2 minutes in a microcentrifuge. The supernatant was discarded and the cells were resuspended in 75 µL cold LB broth. Next, cells were incubated on ice for 5 minutes and 75 µL of cold TSS medium (LB broth containing 10% PEG, 5% DMSO, and 50 mM Mg^{2+}, pH 6.5) was added to the mix and incubated for 5 minutes on ice.

4.4.-Bacterial transformation

Plasmid was added to 100 µL of thawed competent cells, the mix was incubated during 30 minutes on ice, then in a water bath at 42 ^{o}C for 90 seconds, and finally for 2 minutes on ice. Subsequently, 200 µL of LB broth was added into cells, which were incubated at 37 ^{o}C and 180 rpm for 60 minutes. Finally, cells were plated onto LB agar plates supplemented with those antibiotics suitable for plasmid selection and incubated overnight in a 37 ^{o}C incubator.

4.5.-NUCLEIC ACIDS MANIPULATIONS

4.5.1.-Plasmid DNA extraction from bacteria

- **Alkaline lysis.**

E. coli cellular pellets obtained from 3 mL of cells cultures grown overnight were resuspended in 100 µL of 50 mM glucose, 25 mM Tris-HCl, pH 8.0, and 10 mM EDTA. Cells were lysed on ice by addition of 200 µL of 0.2 N NaOH, and 1% SDS (Sodium dodecyl sulfate). Subsequently, 150 µL of 2 M potassium acetate, pH 6.7 was added to the cellular lysate. After centrifugation at 13000 rpm during 15 minutes at room temperature in a microcentrifuge, the supernatant was transferred to a fresh 1.5 mL tube. Then, plasmid DNA was precipitated with 1 mL of cold absolute ethanol. The precipitated DNA was washed twice with 500 µL of 70 % ethanol, centrifuged again at 13000 rpm for 2 minutes, the supernatant was discarded and the pellet air-dried. Finally, the plasmid DNA was resuspended in 25 µL of TER buffer (10 mM Tris-HCl, pH 8.0, 0.5 mM EDTA, and 0.1 mg/mL RNase A).

- **In-column extraction and purification**.

The plasmid DNA extraction was performed following the instructions provided in the Speed tools plasmid DNA purification kit from Biotools. The plasmid DNA was eluted in 50 µL of 10 mM Tris, pH 8.5.

4.5.2.-Genomic DNA extraction from yeast

Cells cultures of 10 mL were grown in YPD medium to an OD_{600} between 0.5 and 0.8. After that, cells were centrifuged at 5000 rpm for 5 minutes in a Sorvall ST 16R centrifuge (Thermo Scientific, TX-200 swinging bucket rotor). Pellets were resuspended in 1 mL of cold water, 320 µL of 0.9 M sorbitol and, 0.1 M EDTA, pH 8.0. A mix with 3.2 µL of β-mercaptoethanol (10 %), and 10 µL of zymolyase 20T (15 mg/mL) was added. The mix was incubated during 1 hour at 37 ^{o}C. The cellular pellets were obtained by centrifugation in a microcentrifuge at 5000 rpm for 5 minutes at room temperature and were resuspended in 370 µL of TE buffer. Subsequently, 16 µL of SDS (10%) was added to the pellets and these were incubated first 30 minutes on ice and then one hour on ice in the presence of 85 µL of 5 M potassium acetate. After 15 minutes of centrifugation at 13000 rpm, genomic DNA was precipitated overnight in 1 volume of cold absolute ethanol and 1/10 of the volume of 3 M sodium acetate. After that, genomic DNA was centrifuged 30 minutes at 13000 rpm and the pellets were washed twice with 70 % ethanol. Pellets were dried at room temperature and resuspended in TER buffer. Genomic DNA obtained was phenolized by addition of 1 volume of phenol-chloroform-isoamyl alcohol (25:24:1). The mix was centrifuged at 13000 rpm for 5 minutes at room temperature. The aqueous phase was recovered, and 1 volume of chloroform-isoamyl alcohol (24:1) was added. Again, the mix was centrifuged as above-mentioned, and the aqueous phase was recovered. Genomic DNA was precipitated with ethanol, as above stated and resuspended in TER buffer.

4.5.3.-RNA extraction from yeast

Cellular pellets obtained from 20 mL of cultures at an OD_{600} between 0.5-0.8 were obtained by centrifugation at 4500 rpm, for 5 minutes at 4 ºC in a Sorvall ST 16R centrifuge (Thermo Scientific, TX-200 swinging bucket rotor). After two washes with water, the pellets were frozen in liquid nitrogen at least 30 minutes and then slowly thawed on ice. Cells were lysed in 400 µL of 10 mM Tris-HCl pH 7.5, 10 mM EDTA, and 0.5% SDS. To the mixture was added 1 volume of acid phenol. The mix was centrifuged at 13000 rpm for 5 minutes at 4 ºC in a microcentrifuge and the aqueous phase recovered. The extraction with acid phenol was repeated once. Subsequently, one extraction in 1 volume of chloroform was performed. Again, the mix was centrifuged as above mentioned, and the aqueous phase was recovered. RNA was precipitated in 2 volumes of cold ethanol and 1/10 of the volume of 3 M sodium acetate overnight. After two washes in 70 % ethanol, the RNA was dried at room temperature and resuspended in 25 µL of RNase free water.

4.5.4.-Ribosome isolation in yeast

Cells (200 mL in YPD or SD medium) were grown to an OD_{600} between 0.5 and 0.7. Cells were incubated on ice for 10 minutes with 100 µg/mL of cycloheximide, and then harvested by centrifugation at 5000 rpm for 5 minutes at 4 ºC in a Beckman Coulter Allegra 25R centrifuge (Rotor TA-14-250). The pellet of each culture was resuspended in 20 mL of lysis buffer (50 mM Tris-HCl, pH 7.5, 100 mM NaCl, 30 mM $MgCl_2$, 100 µg/mL cycloheximide, 200 µg/mL heparin, and 0.2 µg/mL DTT (diethylpyrocarbonate)), centrifuged again, as above, and resuspended in 0.5 mL of lysis buffer. Glass beads and lysis buffer (0.9 mL in total) were added to the cells in a microfuge tube, which was vigorous vortexed for 8 minutes at 4 ºC. Beads were separated by filtration, and the supernatant was centrifuged at 13000 rpm for 10 minutes at 4ºC in a Sorvall ST 16R centrifuge (Thermo Scientific, F2402H rotor). About 10 A_{260} units of each extract was loaded onto 11.2 ml of 7 to 50% linear sucrose gradients (in 50 mM Tris-acetate pH 7.5, 50 mM NH_4Cl, 12 mM $MgCl_2$, and 1 mM DTT). The gradients were centrifuged at 39000 rpm in a Beckman Coulter ultracentrifuge, (SW41 rotor) for 2 hours and 45 min at 4 °C.

Polysomes were separated using an ISCO UA-6-system. Fractions of 0.5 mL were collected every 30 seconds at 4.5 mL/h. A similar procedure with minor modifications was used to analyse total r-subunits. In this case, 0.06 % NaN_3 was added to the cultures instead cycloheximide; the lysis buffer contained 50 mM Tris-HCl, pH 7.5, 50 mM NaCl and, 1 mM DTT. The gradients were centrifuged at 39000 rpm in a Beckman Coulter ultracentrifuge (SW41 rotor) for 4 hours and 30 minutes at 4 °C.

4.5.5.-Polymerase chain reaction

DNA amplifications were performed by PCR in 50 µL reaction volumes. Each reaction contained 25 pM of each forward and reverse primer (see Table 2), 200 µM dNTPs, 1 U Taq polymerase (Bioline) in 75 mM Tris-HCl pH 9.0, 50 mM KCl, 20 mM $(NH4)_2SO_4$, and 2 mM $MgCl_2$, and 20 ng template DNA (total yeast DNA or plasmid DNA). The conditions of PCR were 4 minutes of denaturation at 94 ^oC, hybridisation (see Table 2 for annealing temperatures) and 1 minute per kilobase of DNA to synthetize of polymerization at 72 ^oC. In all the cases, 35 cycles were used. A final extension cycle of 10 minutes at 72 ^oC was done.

4.5.6.-Site-directed mutagenesis

Point mutations and truncated mutants were done following different PCR strategies: inverse PCR, Phusion PCR, Q5® Site-Directed Mutagenesis Kit (NEB), or In-Fusion kit (Clontech) following the instructions provided by each manufacturer. The presence of the different mutations was confirmed by DNA sequencing.

Table 2. **PCR primers.** The name of each primer is followed by F or R, indicating a forward or a reverse position, respectively. For each primer, the annealing temperature used in PCRs is indicated.

Name	5'-3' sequence	Annealing temperature (°C)
pET21aDbp7SacF	AAGAGCTCATGAGCGATGAAGATTCTATG	53
pET21aDbp7NotR	AAGCGGCCGCGTAGTTAAACTCACTTGCTAT	51
pET21aDbp9BamF	AAGGATCCATGAGCTATGAGAAAAAGT	45
pET21aDbp9SacR	AAGAGCTCCATTTGAAGTTCTTCAACGGGT	57
Dbp7KAF	CCAAACAGGCTCAGGTGCGACTTTATCGTATCTTTTACCTAT	45
Dbp7KAR	GTAAAAGATACGATAAAGTCGCACCTGAGCCTGTTTGGGCG	45
Dbp9KAF	CGCTACAGGTTCCGGAGCAACTTTGGCATACCTCATTCCTGT	45
Dbp9KAR	GAATGAGGTATGCCAAAGTTGCTCCGGAACCTGTAGCGGCC	45
Dbp7RAF	TTTACATAGAGTTGGTGCTACAGCAAGGGCCGGTGAGAAGGG	45
Dbp7RAR	TCTCACCGGCCCTTGCTGTAGCACCAACTCTATGTAAATGG	45
M13 REVERSE	CAGGAAACAGCTATGAC	50
NarIR	GAAATACCGCACAGATGCGTA	50
NONLSF	TCCTATAGTTCTGAAGAGCAGGAA	50
NONLSR	TGTCTTGCCCTCAAGCTTCATTTT	50
ΔN1F	ACTACCAATGAGGACACTGCA	50
ΔNR	TGCATAGTCCGGGACGTCATA	50
ΔN3F	ATTAAAAAGCCTACGAGCATC	53
ΔCF	TAAATAGACAAGAACAAGCAT	49
ΔC1R	ACTTTTAGCTAAATGGCCTAG	53
ΔC2R	ATTGGTATCCCACTCATATTC	53
N-terminal BamF	TTGGATCCATGAGCGATGAAGATTCTAT	49
N-terminal BamR	TTGGATCCACGCATTTTTTGCT	53
Dbp7GFPXmaI	GGTACCCGGGGATCTTCAATGGAAAC	48
Dbp7GFPSphI	AGTTAAACTCGCATGCTATTTGCTTCT	48
K197AF	CTCAGGTGCGAGTTTATCGTATCTTTTACC	55
K197AR	AAAGTCGCACCTGAGCCTGTTTGGGCG	55
R553AF	CGAGCATCGAGAAGCAGGCCATACCTC	55
R553AR	GCTTCTCGATGCTCGTAGGCTTTTTAATACG	55
DBP7-DelNLSF	GCAAGACATCCTATGTTCTGAAGAGCAGGAA	55

DBP7-DelNLSR	TATAGGATGTCTTGCCCTCAAGCTTC	55
DBP7-DelNterF	CCAAGATTAAAAAGCCTACCGAGCATCCA	55
DBP7-DelNterR	TTTTAATCATCTTGGTGTTAAATTGCTGAAT	55

4.5.7.-DNA restrictions

DNA restrictions were performed in 40 µL of reaction containing 1 U of restriction enzyme (Roche), 500 ng of DNA, and the restriction buffer recommended in each case by the manufacturer. The reactions were incubated at 37ºC for 4 hours.

4.5.8.-DNA ligations

DNA ligations were performed at room temperature and overnight in 10 µL reactions containing 3 U T4 ligase (Promega), 30 mM Tris-HCl pH 7.8, 10 mM $MgCl_2$, 10 mM DTT, 1 mM ATP, 5 % de PEG, and the DNAs to be ligated (normally a vector to insert ratio of 1:4 was used; 100 ng of vector).

4.5.9.-Agarose gel electrophoresis

DNA electrophoresis were performed in 1% low electroendosmosis agarose gel in 100 mM Tris-base, 90 mM boric acid, and 1 mM EDTA, pH 8.3. Red safe (Intron Biotechnology) was added at final dilution of 1X respect to the commercial concentrate to stain the DNA. Gels were run at 110 V for 40-50 minutes. DNA was visualised by UV light, and pictures taken in a ChemiDoc XRS system (BioRad).

4.5.10.-DNA purification from agarose or solution

When DNA required, DNA fragments were purified using a silica matrix adsorption method by a High Pure PCR cleanup microkit (Roche), following the manufacturer's instructions.

4.6.-PROTEIN MANIPULATIONS

4.6.1.-Recombinant protein expression

The strain used was *E. coli* BL21 Codon Plus (DE3) RIPL, which was previously transformed with the expression plasmid of interest. A preculture grown overnight was used to prepare a culture of 100 mL or 1L in 2X YT medium (16 g/L tryptone, 10 g/L yeast extract, and 5 g/L NaCl). The culture was grown at 37 ºC and 180 rpm with 100 µg/mL of ampicillin and 50 µg/mL of chloramphenicol to an OD_{600} of 0.6. The production of the protein was induced by adding of 0.5 mM of IPTG (isopropyl β-D-1-thiogalactopyranoside) to the culture. The induction was performed in small volume cell cultures during 4 hours at 37 ºC and 180 rpm or overnight at 18 ºC and 180 rpm in large volume cultures. After that, cells of small volume cultures were harvested by centrifugation at 5000 rpm for 10 minutes at 4 ºC in a Sorvall ST 16R centrifuge (Thermo Scientific, TX-200 swinging bucket rotor). Cell harvest from large volume cultures was done as above but using a Beckman coulter Avanti J25 centrifuge (JLA 10.500 rotor). Pellets were frozen and stored at -80 ºC.

Frozen pellets were thawed on ice, resuspended in lysis buffer (50 mM Tris-HCl, pH 7.4, 500 mM NaCl, 10% glycerol, 1 mM DTT, 1X complete inhibitor EDTA-free cocktail (Roche), 0.5 mM PMSF (phenylmethylsulphonyl fluoride), and 150 µg/µL lysozyme) and incubated for 15 minutes on ice. The cells were sonicated in a sonicator BRANSON SONIFIER 250 for 4 cycles (30 seconds On, 1 minute Off, 1 minute On, 1 minute Off), duty cycle: 50-60 and output control: 3-4. After sonication, 0.1% Triton X100 was added to the sample. The lysate coming from small cultures was centrifuged at 5500 rpm for 20 minutes at 4 ºC in a Sorvall ST 16R centrifuge (Thermo Scientific, TX-200 swinging bucket rotor); lysates from large cultures were centrifuged at 22000 rpm for 20 minutes at 4 ºC in a Beckman coulter Avanti J25 centrifuge (JA 25.50 rotor). The supernatants were kept for further purification.

4.6.2.-Affinity purification

A Ni-NTA agarose resin (HIS select Nickel Affinity Gel, Sigma) was equilibrated by adding 750 µL of 50 mM Hepes, pH 7.5, and 500 mM NaCl to 150 µL of resin. The supernatant from small cultures (10 mL) was added to the resin and the mix was incubated for 1 hour and 30 minutes at 4 ^{o}C in a rotating mixer of 26 cm of diameter. The mix was centrifuged at 5000 rpm for 10 minutes at 4 ^{o}C in a Sorvall ST 16R centrifuge (Thermo Scientific, TX-200 swinging bucket rotor), in order to remove the unbound proteins. The supernatant was discarded and 1.5 mL of 50 mM Hepes, pH 7.5, 500 mM NaCl, 10% glycerol, 1 mM DTT, and 0.1% Triton X100 was added to the resin in order to eliminate undesired contaminant proteins. The mix was incubated for 5 min at 4 ^{o}C in the rotating mixer, and centrifuged as above-mentioned. This step was repeated three times. To elute bound proteins, 150 µL of 50 mM Hepes, pH 7.5, 500 mM NaCl, 10% glycerol, 1 mM DTT, 0.1% Triton X100, and 20 mM imidazole was added to the resin. After that, the resin was incubated during 10 min at 4 ^{o}C in the rotating mixer, and centrifuged as above-mentioned. The elution step was repeated five times.

In case of large volume cultures, a FPLC system AKTA Purifier (GE Healthcare) was used. The supernatant obtained after cell lysis (50 mL) was loaded on a 5ml HisTrap FF (GE Healthcare) column pre-equilibrated with 5 column volumes of 50 mM Tris-HCl, pH 7.4, 500 mM NaCl, 10% glycerol, 1 mM DTT, 0.5 mM PMSF, 0.1% SDS, and 10 mM imidazole. Then, the column was washed with the same buffer until the UV lecture was of zero units. Next, proteins were eluted with 20 column volumes of 50 mM Tris-HCl, pH 7.4, 500 mM NaCl, 10% glycerol, 1 mM DTT, 0.5 mM PMSF, 0.1% SDS, and 500 mM of imidazole. The obtained eluates were ready for further purification by gel filtration.

4.6.3.-Gel filtration

Proteins (2 mL of eluate in 50 mM Tris-HCl, pH 7.4, 500 mM NaCl, 10% glycerol, 1 mM DTT, 0.5 mM PMSF, 0.1% SDS, and 500 mM of imidazole) were loaded on a Superdex 200 HiLoad 16/60 column (GE Healthcare) pre-equilibrated with 20 mM Tris pH 8.0, 100 mM KCl, 10% glycerol, and 1mM DTT. Protein elution was performed using the same

buffer. The elution was followed by measuring the A_{280}. Fractions, which elution volumes corresponded with the size of the protein of the interest were saved. When it was necessary, the proteins were concentrated using an Amicon Ultra-0.5 mL centrifugal filters units (30K).

4.7.-Probe labeling

To label different RNA probes used in this study, 10 picomole of oligonucleotide (see Table 3) were 5' end labeled with 10 mCi/mL [γ ^{32}P]-ATP (Perkin Elmer, 6000 Ci/mmol) using T4 polynucleotide kinase (NEB) in 70 mM Tris-HCl, pH 7.6, 10 mM $MgCl_2$, and 5 mM DTT. The mix was incubated at 37 ^{o}C for 60 minutes and at 65 ^{o}C for 25 minutes. The reaction was stopped by adding 0.5 M ammonium acetate and water to complete 50 µL. Labeled probe was purified with a microspin G50 column (GE Healthcare) by centrifugation at 3000 rpm for 2 minutes at room temperature.

4.8.-ATPase assays

- **By colorimetry assay**:

The reactions took place in a final volume of 60 µL containing 1.5 µg of protein and the nucleic acid substrate (see Table 3). ATP was used at 0.5 mM in 20 mM Hepes pH 6.0, 50 mM potassium acetate, 2 mM $MgCl_2$, and 2 mM DTT. The reactions were incubated at 30 ^{o}C for 10 minutes. The ATPase activity was stopped by adding 10 % EDTA. Each reaction was sampled into a well of a microtiter plate. Then, 50 µL of reaction was added to a 200 µL green malachite mix (molybdate (5.72 % in 6N HCl)-malachite (0.08%)-water mix 1:1:1) and incubated 10 minutes at 30 ^{o}C. The Abs_{620} was measured in a Sinergy H1 microplate reader (Biotek). To calculate the phosphate released in each assay was used the linear regression obtained upon measuring the values given by different concentrations of NaH_2PO_4. The conditions mentioned in this method are the standards but can vary depending of the experiment. The differences can be observed in the Results section.

- **By radioactivity assay**:

Reactions were carried out in a final volume of 2.1 µL, containing 0.10 µg protein, 100 µM non-radioactive ATP, 3 µM of a single stranded RNA substrate (see Table 3), and 0.2 µM [α-^{32}P] ATP (3000 Ci/mmol, Perkin Elmer) in buffer containing 25 mM Tris acetate, pH 8, 10 mM magnesium acetate, 0.2 mM DTT, and 100 µg/µl BSA. The mixture was incubated at 30 ºC for 1 hour. One microliter of each reaction was spotted on a chromatography plate (Machery Nagel CEL300 PEI/UV254, Merck). The plate was introduced in 0.75M KH_2PO_4 until the buffer reached the top of the plate. Next, the plate was dried and exposed to an intensifying screen in a Fuji cassette and revealed in Typhoon Trio imaging system (GE Healthcare). The results were quantified by the MultiGauge V3.0 software (Fujifilm).

4.9.-Helicase assays

Reactions were performed in 10 µL of final volume containing 0.6 µg of protein, 1 mM ATP, 1 nm [γ-^{32}P] double stranded RNA substrate (see Table 3), 10 nM non-radioactive RNA oligonucleotide (ssDNA complementary to the displaced strand) in the same buffer as in the radioactive ATPase assays. Reactions were incubated at 30 ºC for 3 minutes. Reactions were quenched by adding 2 µL of stop solution (25% glycerol, 1% SDS, 10 mM Tris-HCl pH 8.0, 1 mg/mL proteinase K, 0.3 µM stop oligo (ssDNA complementary to the displaced strand), 0.05% bromophenol blue, and 0.05% xylene cyanole), and kept it on ice. Reactions were run in an acrylamide gel under non-denaturing conditions (see below)**.** The gel was dried and exposed to an intensifying screen in a Fuji cassette and revealed in a Typhoon Trio imaging system (GE Healthcare). The results were quantified by the MultiGauge V3.0 software (Fujifilm). The annealing reaction was carried out in 100 µL of final volume. Each reaction contained 10 nM of labeled oligonucleotide, 10 nM of non-labeled oligonucleotide in 50 mM Tris-HCl, pH 7.5, 50 mM NaCl, and 1 mM EDTA. The reaction was incubated at 80 ºC for 2 minutes and later it was cooled slowly at room temperature. Finally, the annealed oligonucleotide was stored at 4 ºC.

4.10.-RNA binding assays

The reactions were performed in 10 µL of final volume containing 1nM [γ-^{32}P] ssRNA (see Table 3) in 25 mM Tris acetate pH 8.0, 10 mM magnesium acetate, 0.2 mM DTT, 100 µg/µL BSA, and 1.2 U RNasin Ribonuclease Inhibitor, and several protein amounts. Reactions were performed at 30 ºC for 15 minutes and were stopped by adding 2 µL of loading buffer (0,01% xylene cyanole, 50% glycerol, and 1 mg/mL BSA). Next, they were run in an acrylamide gel under non-denaturing conditions. The gel was dried, exposed in an intensifying screen in a Fuji cassette and revealed in a Typhoon Trio imaging system (GE Healthcare).

Table 3. Oligonucleotides used in the enzymatic assays. The name and the size of each oligonucleotide is indicated.

Name	5'-3' sequence	Size (nt)
Poly dT16	TTTTTTTTTTTTTTTT	16
Poly dT17	TTTTTTTTTTTTTTTTT	17
Poly dT30	TTTTTTTTTTTTTTTTTTTTTTTTTTTTTT	30
Poly dA18	AAAAAAAAAAAAAAAAAA	18
Poly dC18	CCCCCCCCCCCCCCCCCC	18
Poly GC18	GCGCGCGCGCGCGCGCGC	18
ssRNA1	UCGACGAUCGAUUUGCACGUCAGAACCGCUACACUGAAAUGAUGAAUUCCGGUCUCCC	58
ssRNA3	AACCGCUAC	9
ssRNA4	GUAGCGGUUCUGACGUGCAAAUCGAUCGUC	30
ssRNA5	GGGAGACCGGAAUUGAUCAUUUCAGUGUAGCGGUUCUG	38
ssDNA comp	CAGAACCGCTACAC	15
Oligo stop	AATGATCAATTCCGGTCTCCC	21
5.8S	TTTCGCTGCGTTCTTCATC	19
5S	GGTCACCCACTACACTACTCGG	22
snR190	CGAGGAAAGAAGAGACACCATTATC	25
snR5	GTCTACTTCCAGCCATTTGC	20

snR10	CATGGGTCAAGAACGCCCCGGAGGGG	26
snR42	TCAAACAATAGGCTCCCTAAAGCATCACAA	30

Table 4. Characteristics of snoRNAs studied. In each case is indicated the identification number obtained from the *Saccharomyces* genome database, the length of the snoRNA and the binding domain in the 25S rRNA (SnoRNABase, LBME, version 3).

snoRNA	SGD ID	Length (nts)	25S domain
snR190	S000006509	190	V
snR5	S000007291	197	II
snR10	S000007499	245	V
snR42	S000006502	351	V

4.11.-Protein extractions

Total proteins were extracted from yeast cells grown to an OD_{600} of about 1. Cellular pellets were obtained by centrifugation at 5000 rpm for 10 minutes at room temperature in a Sorvall ST 16R centrifuge (Thermo Scientific, TX-200 swinging bucket rotor). Cells were lysed with 0.2 N NaOH during 5 minutes at room temperature. Cellular lysates were recovered by centrifugation and resuspended in 160 mM Tris-HCl pH 6.8, 20 % glycerol, and bromophenol blue. The supernatants were recovered while the pellet was discarded.

Proteins were also extracted from the fractions of sucrose gradients. To do this, proteins were precipitated in 20 % TCA (trichloroacetic acid), vortexed and incubated on ice for 10 minutes. After centrifugation at 13000 rpm for 10 minutes at 4 ^{o}C, 1 mL of cold acetone was added to the pellet of each fraction. Proteins were centrifuged and the pellets were washed again in 1 mL of cold acetone. A final centrifugation was performed, the pellets were dried at room temperature and resuspended in 160 mM Tris-HCl pH 6.8, 20 % glycerol and, bromophenol blue.

4.12.-Polyacrylamide gel electrophoresis for proteins

Protein electrophoresis was performed in denaturing acrylamide-bisacrylamide (29:1) gels. The stacking gel was composed by 0.125 M Tris-HCl, pH 6.8, 0.1 % SDS, 0.1 % APS (ammonium persulfate), 0.2% TEMED, and 4 % acrylamide-bisacrylamide (29:1). The running gel was composed by 0.375 M Tris-HCl, pH 8.8, 0.1 % of SDS, 0.1 %APS, 0.2 % TEMED, and 10% acrylamide-bisacrylamide (29:1). Gels were run at 160 V for 50 minutes in a buffer composed by 25 mM Tris, 192 mM glycine, and 10 % SDS.

Proteins were stained using a Coomassie blue solution (50% ethanol, 10% acetic acid, and 0.5 g/L Coomassie Brilliant Blue R-250).

Non-denaturing 8% acrylamide-bisacrylamide (19:1) or non-denaturing 6 % acrylamide-bisacrylamide (37.5:1) gels were also used depending of the assay. Proteins gels for helicase assays were composed by 100 mM Tris-base, 90 mM boric acid, 1 mM EDTA, pH 8.3, 0.16 % APS ,0.05% TEMED, and 8 % of acrylamide-bisacrylamide (19:1). Gels were run at 80 V for 40 minutes at 4 ^{o}C in a buffer consisting of 100 mM Tris-base, 90 mM boric acid, and 1 mM EDTA, pH 8.3. Proteins gels for RNA binding assays were composed by 100 mM Tris-base, 90 mM boric acid, 1 mM EDTA, pH 8.3, 0.16 % APS, 0.05 % TEMED, and 6 % acrylamide-bisacrylamide (37.5:1). Gels were run at 120 V for 35 minutes at 4 ^{o}C in 100 mM Tris-base, 90 mM boric acid, and 1 mM EDTA, pH 8.3.

4.13.-RNA gel electrophoresis

RNA gel electrophoresis was performed in denaturing 7 % polyacrylamide (19:1)-8 M urea gels. The RNA samples were heated at 65 ^{o}C in a solution containing 10 M urea, 2 mM EDTA, 0.025 % xylene cyanol, and 0.025 % bromophenol blue before loading. The gels were run at 350 V during 2 hours and 30 minutes in 100 mM Tris-base, 90 mM boric acid, and 1 mM EDTA, pH 8.3.

4.14.-Gel to membrane transfer

Proteins were transferred from gels to nitrocellulose membrane in sandwiches at 100 V for 30 minutes in 25 mM Tris, 192 mM glycine, 10 % SDS, and 20% ethanol. After transfer, proteins were visualised using a solution containing 0.1% red Ponceau and 5 % acetic acid. RNA was transferred from the gel onto a Hybond^{TM}-N nylon membrane overnight at 15 V and 4 ^{o}C in 50 mM Tris-base, 45 mM boric acid, and 0.5 mM EDTA. RNAs were fixed at 1200 X100 μJ/cm^2 on the membranes using an UV crosslinker (Spectrolinker XL-1000). After transfer, RNAs were visualized using a solution containing 0.02% methylene blue and 0.3 M sodium acetate at pH 5.5.

4.15.-Inmunodetection

Membranes were blocked in a solution containing 5% skimmed milk, 15 mM Tris-HCl pH 7.5, and 200 mM NaCl at room temperature for 30 minutes. Membranes were incubated with a primary antibody in 5 % skimmed milk or 3 % BSA (Bovin serum albumin), 15 mM Tris-HCl pH 7.5 and 200 mM NaCl. The secondary antibodies used were horseradish peroxidase-coupled antibodies. The incubations of the membrane with the secondary antibody were carried out in 15 mM Tris-HCl pH 7.5, and 200 mM NaCl. Washes of the membrane between the primary and the secondary antibodies and after the secondary antibody were performed in 15 mM Tris-HCl, pH 7.5, 200 mM NaCl, and 0.1% Tween 20. Chemiluminescence was produced by addition of luminol and hydrogen peroxide using a detection kit (Super Signal West Pico Plus, Thermo Scientific). Chemiluminescence was detected in an Odissey FC Dual Mode Imaging System (Li-Cor Biosciences).

4.16.-RNA-DNA hybridisation

Prehybridisation of the membranes were done with a solution containing 0.3 M Na_2HPO_4, 0.2 M $NaHPO_4$, 7 % SDS, 0.5 M EDTA, pH 8, and 10 mg/mL BSA at 42 ^{o}C for 30 minutes. The hybridisation of the membranes was done in the buffer aforementioned but adding 10 picomoles of the labelled probe at 42 ^{o}C, which were incubated overnight. Three washes of 5 minutes were performed with 2X SSC (0.3 M NaCl, and 0.03 M sodium citrate) and 0.5 % SDS, and three washes with 0.1X SSC (0.015 M NaCl, and 0.0015 M

sodium citrate) and 0.5% SDS at 38 ºC. Membranes were exposed to intensifying screen in Fuji cassettes and revealed in a Typhoon FLA 9000 imaging system (GE Healthcare).

4.17.-Fluorescence microscopy

Cell cultures of 5 mL were grown to reach an OD_{600} of about 1, centrifuged and resuspended in 50 µL of medium. Samples were examined with a Leica DMR fluorescence microscope equipped with a DC350F digital camera and its software. The excitation channel used for fluorescent eGFP and mCherry proteins were BP450-490 and BP 515-560 respectively. Adobe Photoshop CS2 (Adobe Systems Inc.) was used to process the images.

Table 5. Plasmids used in this study.

Name	Relevant information	Source
pGEMT-Easy	Amp^r	Promega
pET-21 b (+)	Amp^r,6x His tag	Novagen
YCplac33	*CEN, URA3*	Gietz and Sugino, 1988
YCplac22	*CEN, TRP1*	Gietz and Sugino, 1988
YCplac111	*CEN, LEU2*	Gietz and Sugino, 1988
pADH111(GA_5)-3X-yEGFP	C-terminal yeGFP tag, *CEN, LEU2*	Koch, 2012
pRS415	*CEN, LEU2*	Sikorski and Hieter, 1989
YCplac111-yGFP7/TCYC1	C-terminal yGFP tag, TCYC1, *LEU2*	Koch, 2012
pADH111-SV40NLS-(GA_5)3XyEGFP	*CEN, LEU2*	Koch, 2015

Table 6. Plasmids constructed in this work. The primers used to obtain each plasmid are indicated in the table. The template from which the construction was obtained is showed also shown.

Name	Primers used	Template
pET-21 b-DBP7-His	pET21aDbp7SacF pET21aDbp7NotR	Genomic DNA *S. cerevisiae*
pET-21 b-dbp7-His [K197A]	Dbp7KAF Dbp7KAF pET21aDbp7SacF pET21aDbp7NotR	pET-21 b-DBP7-His
pET-21 b-dbp7-His [R553A]	Dbp7RAF Dbp7RAR pET21aDbp7SacF pET21aDbp7NotR	pET-21 b-DBP7-His
pET-21 b-DBP9-His	pET21aDbp9BamF pET21aDbp9SacR	Genomic DNA *S. cerevisiae*
pET-21 b-dbp9-His [K68A]	Dbp9KAF Dbp9KAR pET21aDbp9BamF pET21aDbp9SacR	pET-21 b-DBP9-His
YCplac22-HA-DBP7	M13 REVERSE NarIR	YCplac33-HA-DBP7
YCplac22-HA-*dbp7*[K197A]	K197A_FW K197A_FW	YCplac22-HA-DBP7
YCplac22-HA-*dbp7*[R553A]	R553A_FW R553A_RV	YCplac22-HA-DBP7
YCplac22-HA-*dbp7ΔN10*	ΔN1F ΔNR	YCplac22-HA-DBP7
YCplac22-HA-*dbp7ΔN162*	ΔN3F ΔNR	YCplac22-HA-DBP7
YCplac22-HA-*dbp7ΔN693*	ΔCF ΔC1R	YCplac22-HA-DBP7
YCplac22-HA-*dbp7ΔN635*	ΔCF ΔC2R	YCplac22-HA-DBP7
YCplac22-HA-*dbp7ΔNLS*	NONLSF	YCplac22-HA-DBP7

	NONLSR	
pADH111-DBP7 N-terminal-(GA_5)3X-yEGFP	N-terminal BamF N-terminal BamR	YCplac22-HA-DBP7
pADH111-*dbp7ΔNLS*-N-terminal-(GA_5)3X-yEGFP	N-terminal BamF N-terminal BamR	YCplac22-HA-*dbp7ΔNLS*
YCplac111-yGFP7/TCYC1-DBP7-(GA_5)3X-yEGFP	Dbp7GFPXmaI Dbp7GFPSphI	Genomic DNA *S. cerevisiae*
YCplac111-yGFP7/TCYC1- *dbp7ΔNLS* -(GA_5)3XyEGFP	DBP7-DelNLS-FW DBP7-DelNLS-RV	YCplac111-yGFP7/TCYC1-DBP7-(GA_5)3XyEGFP
YCplac111-yGFP7/TCYC1- *dbp7ΔN162* -(GA_5)3XyEGFP	DBP7-DelNter-FW DBP7-DelNter-RV	YCplac111-yGFP7/TCYC1-DBP7-(GA_5)3XyEGFP

5.RESULTS

5.- RESULTS

The Dbp7 protein from *Saccharomyces cerevisiae* is defined, according to its deduced amino acid sequence, as a putative ATP-dependent RNA helicase. To get insight into the physiological function of Dbp7, Linder and co-workers constructed in 1998 a null haploid mutant strain lacking Dbp7, named *dbp7-1* (17). This strain showed a very reduced growth rate; thus, these authors concluded that Dpb7 is required for optimal vegetative growth. They also showed that the *dpb7-1* presented a strong deficit of LSUs. Their work demonstrated that this deficit was due to kinetically delayed formation of the mature 25S and 5.8S rRNAs, as the consequence of an active degradation of the 27SA pre-rRNA precursors. Furthermore, they determined that Dbp7 localize in the nucleolus. In light of the above, they concluded that Dbp7 is a nucleolar *trans*-acting factor involved in 60S ribosomal subunit biogenesis.

For this Thesis work, first of all, we re-examined some of the aforementioned statements, and searched for more insights into the function of Dbp7. To do so, we first constructed the *dbp7Δ*[YCplac22] strain, which is a W303-derived null *dpb7::HIS3MX6* strain harbouring an empty YCplac22 plasmid (from now on *dbp7Δ*). To obtain the strain, we transformed a *dbp7Δ*[YCplac33-DBP7] strain with the plasmid YCplac22 (*CEN TRP1*); then, transformants were counter-selected on 5-FOA-containing plates to allowing the growth of those clones that have lost the YCplac33-DBP7 plasmid (plasmid shuffling). Some of the colonies growing on this media were transferred to SD-Trp plates for further use. We also constructed a *dbp7Δ*[YCplac22-HA-DBP7] yeast strain (from now on HA-*DBP7*), using the same strategy. This strain was used for the immunodetection of Dbp7, since we lack specific antibodies against this protein.

As expected, the growth of the *dbp7Δ* strain was significantly reduced when compared with the growth of its isogenic HA-*DBP7* counterpart. When the *dbp7Δ* strain was complemented with a YCplac33-DBP7 plasmid (**data not shown**) or with a YCplac22-HA-*DBP7* one, the wild-type phenotype was restored (**Figure 17A and B**).

To get some quantitative insights on the growth phenotypes, we calculated the doubling times from growth curve experiments (**Figure 17C**). Doubling times were of about 220 and 80 minutes for the *dbp7Δ* and HA-*DBP7* strains, respectively (**Figure 17C**). A doubling time of approximately 90 minutes was calculated for the W303-1A strain (the isogenic wild-type strain, from which derivates all strains used in this work).

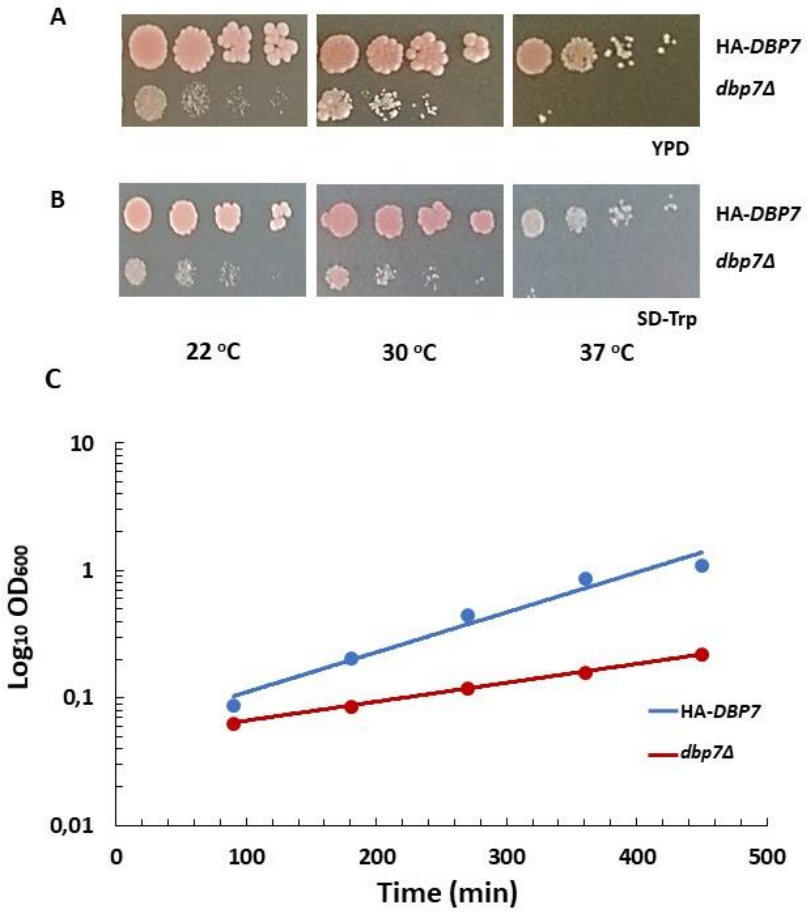

Figure 17. Growth features of the *dbp7Δ* strain. The growth phenotype was measured by serial dilutions in solid medium (**A**) YPD and (**B**) SD-Trp medium. (**C**) Growth curves of the HA-*DBP7* and *dbp7Δ* strains. Cultures were initiated in SD-Trp liquid medium and incubated at 30 °C. Three biological replicas were done for each strain. The curves of a representative experiment are shown. Note that only exponential growth phase is plotted.

The *dbp7-1* strain showed a deficit in LSUs (17). To study this phenotype in our strains, polysome profiles were obtained for *dbp7Δ*, HA-*DBP7* and the W303-1A strains. A conventional polysome profile (herein represented by the one obtained from the wild-type W303-1A strain) presents several peaks of absorbance at A_{254}. As show in **Figure 18**, these peaks, from left to right, correspond to free small and large r-subunits (40S and 60S, respectively), the monosome or the vacant 80S (80S), and polysomes. Note that most ribosomes are found as polysomes, indicating the translation capability of wild-type cells.

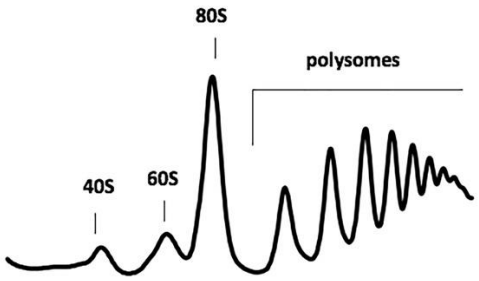

Figure 18. Standard polysome profile for a wild-type W303-1A strain. This strain was grown to exponential phase in liquid YPD medium at 30 ºC. Cell extracts were prepared, and 10 A_{260} units resolved on 7-50% sucrose gradients. The A_{254} was continuously measured. Sedimentation comes from left to right. The absorbance peaks of free 40S, 60S r-subunits, 80S vacant ribosomes/monosomes and polysomes are indicated.

For the HA-*DBP7* strain, the obtained polysome profile was indistinguishable to that of an isogenic wild type strain (**Figure 19A**). However, the polysome profile of the *dbp7Δ* strain showed a clear decrease in the levels of free 60S *versus* free 40S r-subunits. The 80S and the polysomal peaks were also reduced. Finally, half-mers (extra 43S ribosomal complex attached to the mRNAs) were present in both 80S and polysomal peaks (**Figure 19B**).

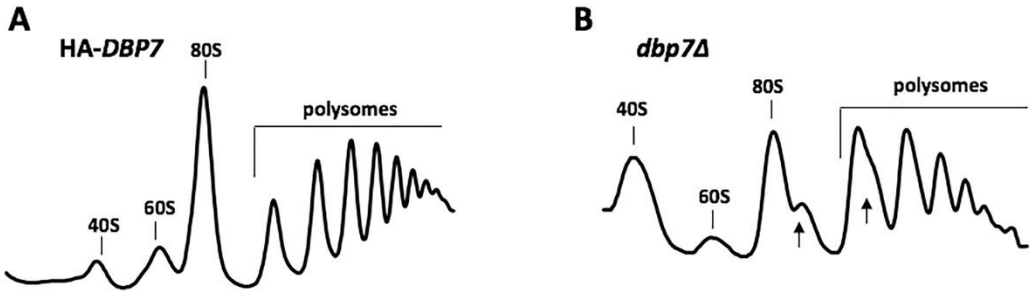

Figure 19. Polysome profile of (**A**) the HA-*DBP7* and (**B**) the *dbp7Δ* strains. These strains were grown to exponential phase in liquid SD-Trp medium at 30 ºC. Cell extracts were prepared, and 10 A_{260} units resolved on 7-50% sucrose gradients. The A_{254} was continuously measured. Sedimentation comes from left to right. The absorbance peaks of free 40S, 60S r-subunits, 80S vacant ribosomes/monosomes and polysomes are indicated, and the appearance of half-mers polysomes, pointed out by arrows.

5.1.- *In silico* analysis of Dbp7

Dbp7, as other DEAD-box proteins, contains two RecA-like domains. These domains are flanked by N- and C- terminal extensions. As mentioned in the Introduction section, each RecA-like domain comprises a set of conserved amino acid motifs involved in ATP binding and hydrolysis, nucleic acid binding, RNA unwinding, and coordination between ATP hydrolysis and unwinding activities. To uncover the importance of these conserved motifs in the ATPase or the helicase activities, we constructed a set of point mutants of Dbp7.

We extracted the conserved motifs of Dbp7 through the sequence alignment described by Jankowsky's laboratory (21). In that work, all the conserved motifs were identified in the amino acid sequence of Dbp7 (**Figure 20**, see also the Introduction section, pages 16-17). Additionally, we found a putative nuclear localization signal (NLS) of 31 amino acids in the N-terminal extension of Dbp7 (**Figure 20**).

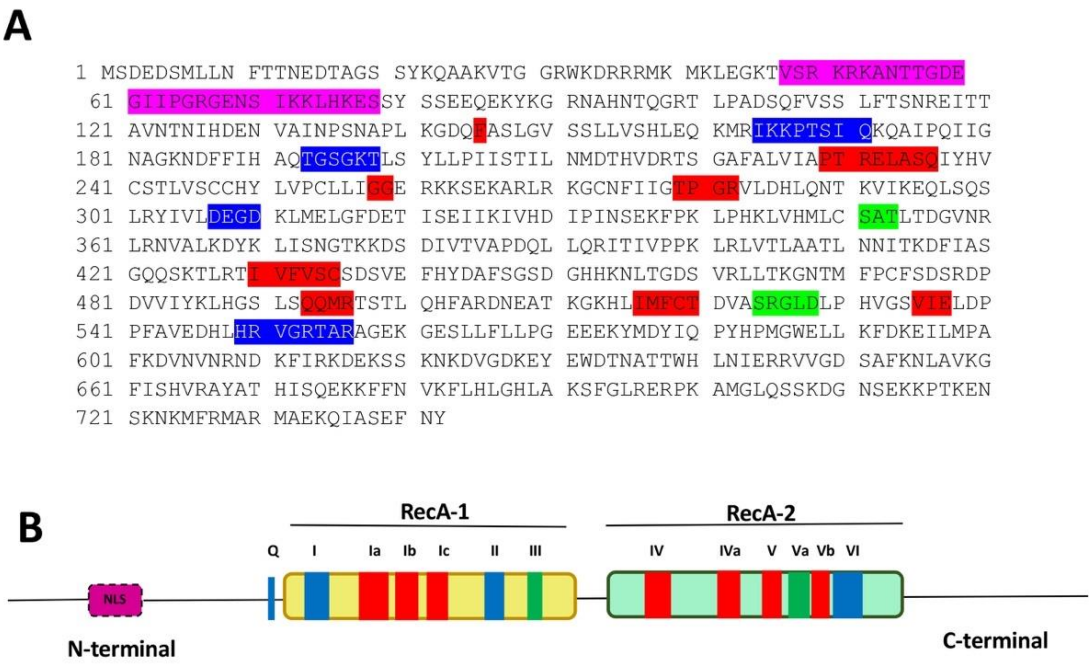

Figure 20. Sequence motifs of Dbp7 protein. (**A**) Deduced amino acid sequence of Dbp7. The conserved motifs are highlighted in different colors depending on their functions: blue, those motifs involved in ATP binding and hydrolysis; red, the motifs involved in RNA binding; and green, the motifs involved in the coordination of both functions. A putative nuclear localization signal (NLS) is also highlighted in purple. (**B**) Schematic representation of the primary structure of Dbp7. Color code of domains as above. The two RecA-like domains are represented as yellow and light green boxes. Within the domains, the conserved motifs are indicated. Note that both RecA-like domains are flanked by N- and C- terminal extensions, and that the putative NLS is located at the N- terminal one.

5.2.-Phenotypic analysis of *dbp7* point mutants

Once all the conserved motifs of Dbp7 were identified, we decided to introduce points mutations in some of them for phenotypic analyses. We first constructed the variants K197A and R553A in motifs I and VI, respectively.

These variants were performed by PCR of the ORF of *DBP7* (with the correspondent point mutation) using Ycplac22-HA-DBP7 as a template. The N-terminally HA-tagged constructs were expressed from the cognate promoter of the *DBP7* gene.

The constructs were transformed in the strain *dbp7Δ*[YCplac33-DBP7]. The transformants were selected on SD-Trp, and then the *URA3*-marked plasmid counter-selected on 5-FOA plates (plasmid shuffling). Some of the colonies growing on this media were transferred to SD-Trp plates for further use.

To assay protein expression, the steady-state levels of the respective HA-Dbp7 in the mutant strains and its wild-type counterpart were determined by western blot analyses. The protein expression levels of the wild-type HA-Dbp7 and mutant variants HA-*dbp7*[K197A], and HA-*dbp7*[R553A] were compared to the levels of a loading control protein, which corresponded to phosphoglycerate enzyme, Pgk1. As shown in **Figure 21**, all the Dpb7 variants were detected by western blot analysis using an anti-HA antibody. This identification was specific as no signal was found when the protein extract of a *dpb7Δ* strain was assayed (**Figure 21**).

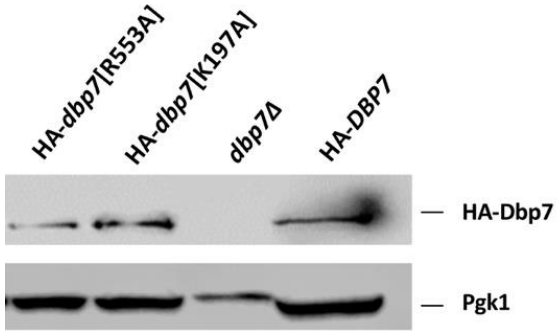

Figure 21. Immunodetection of HA-Dbp7 variant proteins. The different HA-Dbp7 variant proteins were detected with a monoclonal anti-HA antibody. Whole cell extracts were prepared from the indicated strains, grown in SD-Trp to exponential phase at 30 ^{o}C. Equivalent amounts of extracts were analysed by western blotting. As a loading control, phosphoglycerate kinase (Pgk1) protein was used. A negative *dbp7Δ* strain control was also used.

Growth was also evaluated. Firstly, this phenotype was measured by serial dilutions in solid medium. As shown in **Figure 22A**, the HA-*dbp7*[K197A] strain was slightly affected on growth, while the HA-*dbp7*[R553A] was significantly affected on this feature. Secondly, growth was also quantified in order to compare with that of isogenic wild-type HA-*DBP7*, and *dpb7Δ* strains (**Figure 22B**). The doubling times calculated for the different

strains in SD-Trp at 30 ºC were of about 140, 180 and 270 minutes for the HA-*DBP7*, HA-*dbp7*[K197A] and HA-*dbp7*[R553A] strains, respectively.

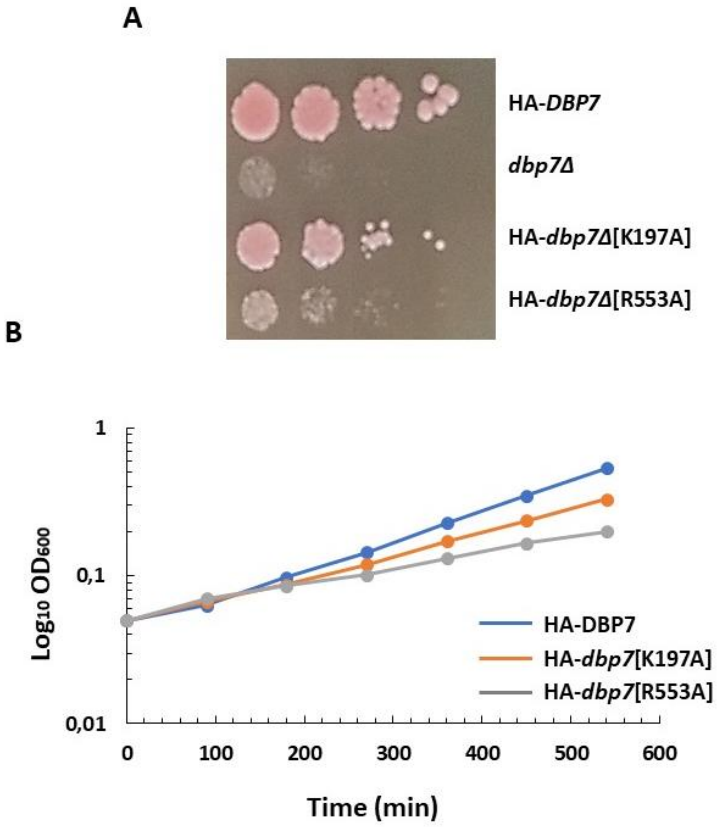

Figure 22. Growth features of the point mutant strains. The growth phenotype was measured by serial dilutions in solid medium SD-Trp medium. (**C**) Growth curves of the HA-*DBP7*, HA-*dbp7*[K197A] and HA-*dbp7*[R553A] strains. Cultures were initiated in SD-Trp liquid medium and incubated at 30 ºC. Three biological replicas were done for each strain. The curves of a representative experiment are shown. Note that only exponential growth phase is plotted.

To determine if these mutations affects ribosome biogenesis, we assayed steady-state levels of ribosomes by polysome profile analyses (**Figure 23**). Compared to wild-type HA-*DBP7* cells, the HA-*dbp7*[K197A] and HA-*dbp7*[R553A] mutant cells showed a decrease in the levels of free LSUs, an increase in the levels of free SSUs, and an overall decrease in the 80S peak and in polysomes. These defects were indicative of an LSU shortage, which in the case of the HA-*dbp7*[K197A] mutant also led to the appearance of half-mers polysomes.

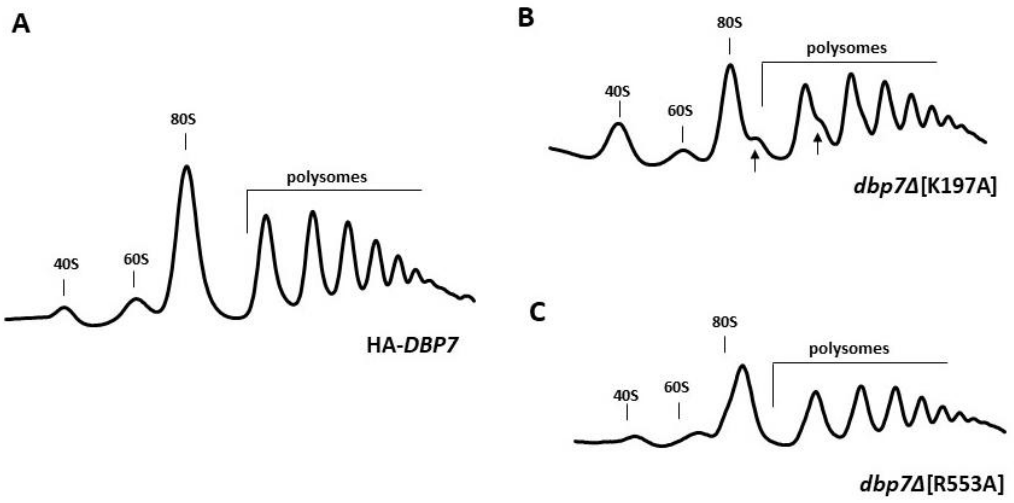

Figure 23. Polysome profile of (**A**) the HA-*DBP7*, (**B**) the HA-*dbp7Δ*[K197A] and HA-*dbp7*[R553A] strains. These strains were grown to exponential phase in liquid SD-Trp medium at 30 ºC. Cell extracts were prepared, and 10 A_{260} units resolved on 7-50% sucrose gradients. The A_{254} was continuously measured. Sedimentation comes from left to right. The absorbance peaks of free 40S, 60S r-subunits, 80S vacant ribosomes/monosomes and polysomes are indicated, and the appearance of half-mers polysomes, pointed out by arrows.

5.3.-Phenotypic analysis of truncated *dbp7* alleles in the amino- and carboxyl- terminal extensions of the Dbp7 protein

As above stated, Dbp7 harbours N- and C- terminal extension of approximately 200 amino acids. To get insight into the function of these extensions, different serial truncated *dbp7* alleles were constructed from Ycplac22-HA-DBP7 and expressed under the control of the cognate *DBP7* promoter followed by a HA epitope. Upon transformation of these constructs into the *dpb7Δ*[YCplac33-DBP7] strain, cells were subjected to plasmid shuffling on 5-FOA plates. Some of the colonies growing on this media were transferred to SD-Trp plates for further use.

The following N- and C- terminal truncations were done: (1) HA-*dbp7ΔN10,* an allele harbouring a deletion of the codons corresponding to the first 10 amino acids of the Dbp7; (2) HA-*dbp7ΔN162*, an allele harbouring a deletion of the codons corresponding

to the first 162 amino acids. (3) HA-*dbp7N693*, an allele harbouring a deletion of the codons corresponding to the last 49 amino acids, thus leading to a protein of 693 amino acids instead of 742 amino acids. (4) HA-*dbp7N635,* an allele harbouring a deletion of the codons corresponding to the last 107 amino acids of Dbp7.

To test whether mutant proteins were expressed, we first determined the steady-state level of the corresponding HA-Dbp7 proteins by western blot analyses, and compared them to that of the isogenic wild-type counterpart. As shown in **Figure 24**, the mutant as well as the wild-type full-length HA-Dbp7 proteins were detected in the western blotting using a specific antibody against the HA epitope. As expected, no signal was found when extracts of a *dpb7Δ* strain were assayed. The level of expression varied for the different HA-Dbp7 proteins. The levels of expression were very low for the HA-*dbp7N693* strain.

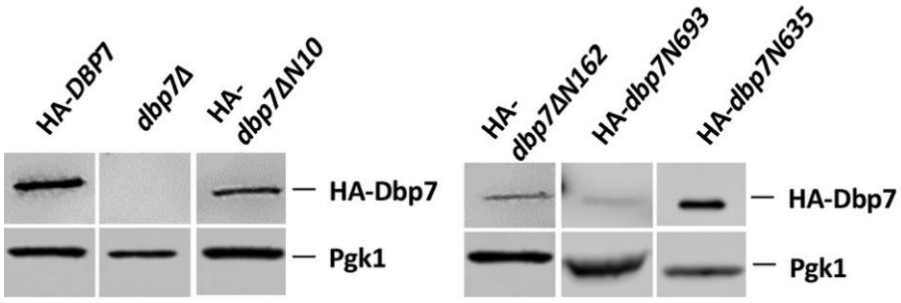

Figure 24. Immunodetection of HA-Dbp7 truncated proteins. The different HA-Dbp7 variant proteins were detected with a monoclonal anti-HA antibody. Whole cell extracts were prepared from the indicated strains, which were grown in SD-Trp to exponential phase at 30 ºC. Equivalent amounts of extracts were analysed by western blotting. As a loading control, phosphoglycerate kinase (Pgk1) protein was used. A negative *dbp7Δ* strain control was also used. Note that the levels of expression for the HA-*dbp7N693* protein were lower than for the rest of proteins.

The growth phenotype of these strains also was evaluated. First, serial dilutions were plated onto solid medium. As shown in **Figure 25**, the growth of the different mutants respect to the isogenic wild-type HA-*DBP7* strain was as follow: the HA-*dbp7ΔN162,* HA-*dbp7N693,* and HA-*dbp7N635* mutants grew significantly worse than the isogenic HA-*DBP7* strain. In fact, the growth of these mutants was very similar to that of the *dbp7Δ*

strain. Only the strain HA-*dbp7ΔN10* grew apparently similar to the HA-*DBP7* strain (**Figure 25A**). When growth curves were done, the calculated doubling time for each strain were of about 115 minutes for HA-*dbp7ΔN10*, 345 minutes for HA-*dbp7ΔN162*, 440 minutes for HA-*dbp7N693* and 400 minutes for HA-*dbp7N635.* The doubling time of the strain HA-*dbp7ΔN10* was practically identical to that of the HA-*DBP7* strain, which was of about 90 minutes. However, the doubling time of the rest of the strains were closer to the doubling time of *dbp7Δ* strain, which we calculated to be 345 minutes (**Figure 25B**).

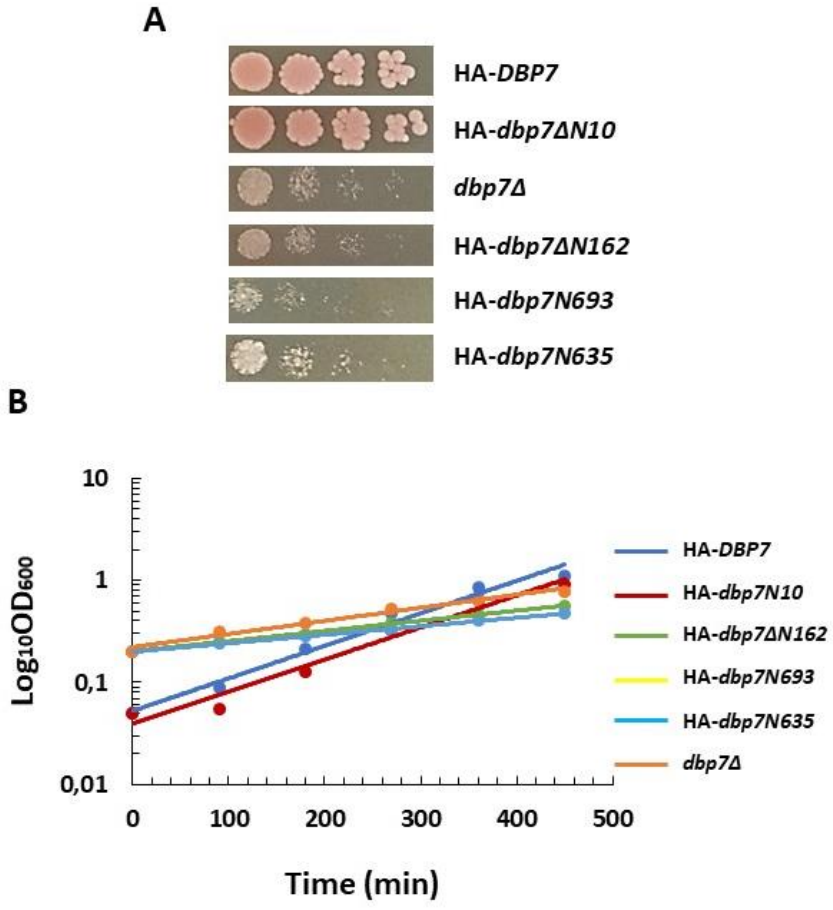

Figure 25. Phenotypic analysis of truncated mutants at the N- and C- terminal extensions of Dbp7. (**A**) The growth phenotype was measured by serial dilutions in solid medium SD-Trp medium. (**B**) Growth curves of HA-DBP7, *dbp7Δ* and truncated mutant strains. Cultures were initiated in SD-Trp liquid medium and

incubated at 30 ºC. Three biological replicas were done for each strain. The curves of a representative experiment are shown. Note that only exponential growth phase is plotted.

We also assayed the effect of these mutations on the profiles of their ribosomes. As shown in **Figure 26**, the HA-*dbp7ΔN162*, HA-*dbp7N693* and HA-*dbp7N635* strains presented polysome profiles similar to those of a *dbp7Δ* strain. Thus, these mutants showed a decrease in the free LSU peak, and a concomitant increase in the free SSU peak together with the appearance of half-mers polysomes. However, the polysome profile of the HA-*dbp7ΔN10* strain was very similar to that of the isogenic wild-type HA-*DBP7* control (**Figure 26**).

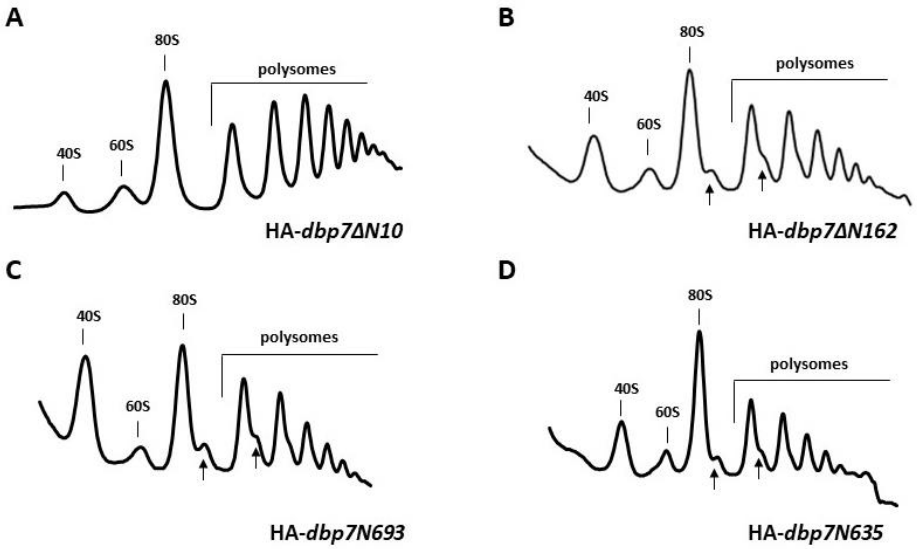

Figure 26. Polysome profiles of the truncated mutants in the N- and C- terminal extensions of the Dbp7 protein. These strains were grown to exponential phase in liquid SD-Trp medium at 30 ºC. Cell extracts were prepared, and 10 A_{260} units resolved on 7-50% sucrose gradients. The A_{254} was continuously measured. Sedimentation comes from left to right. The absorbance peaks of free 40S, 60S r-subunits, 80S vacant ribosomes/monosomes and polysomes are indicated, and the appearance of half-mers polysomes, pointed out by arrows.

The profiles obtained for most mutants suggest that the respective mutations lead to an overall deficit of LSUs. To corroborate this, we calculated for each mutant strain the 60S/40S ratio, obtained from analysis of total r-subunits by low Mg^{2+} sucrose gradients. As a result, in all the truncated mutants, the 60S/40S ratios were lower than that obtained for the isogenic HA-*DBP7* strain, except for mutant HA-*dbp7ΔN10*, whose calculated ratio was similar to that of HA-*DBP7* control strain (**Figure 27**).

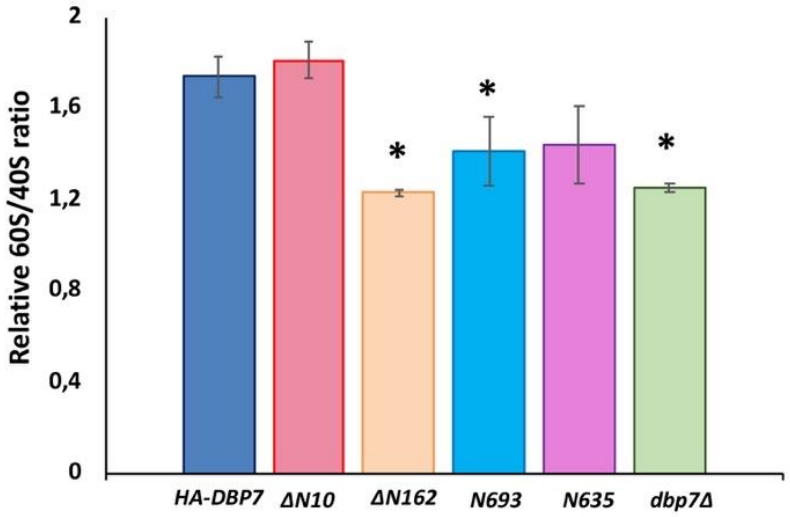

Figure 27. Quantification of the relative 60S/40S ratios of the truncated mutants in the N- and C- terminal extensions of the Dbp7 protein. The indicated strains were grown to an OD_{600} of 0.8 in liquid SD-Trp medium at 30 ^{o}C. Cell extracts were prepared for ribosome isolation, in a buffer lacking $MgCl_2$ to dissociate ribosomes in their respective subunits. Ten A_{260} units of each extract was resolved in 7-50% sucrose gradients prepared in the same buffer. The areas under the peaks were determined, and the ratio between 60S and 40S areas was calculated. At least three independent experiments were done; means and standard deviations are shown. A T-student test (independent samples) was performed using $p < 0.05$.

Next, we examined whether the respective truncated Dbp7 proteins were still being associated with pre-60S r-particles. To do so, we analysed the sedimentation behaviour or of wild-type and mutant Dbp7 proteins in sucrose gradients. For this purpose, total extracts were prepared from the strains grown in liquid SD-Trp at 30 ^{o}C and subjected to low Mg^{2+} sucrose gradient ultracentrifugation. Then, fractions were collected and

analysed by western blotting. As shown in **Figure 28**, a peak of wild-type HA-Dbp7 was associated with high-molecular mass complexes; this indicates that Dbp7 associates relatively stable to pre-ribosomal particles, as also does Erb1 (89). As additional controls, we used the proteins uL3 and eS8, which assembles in LSUs and SSUs, respectively.

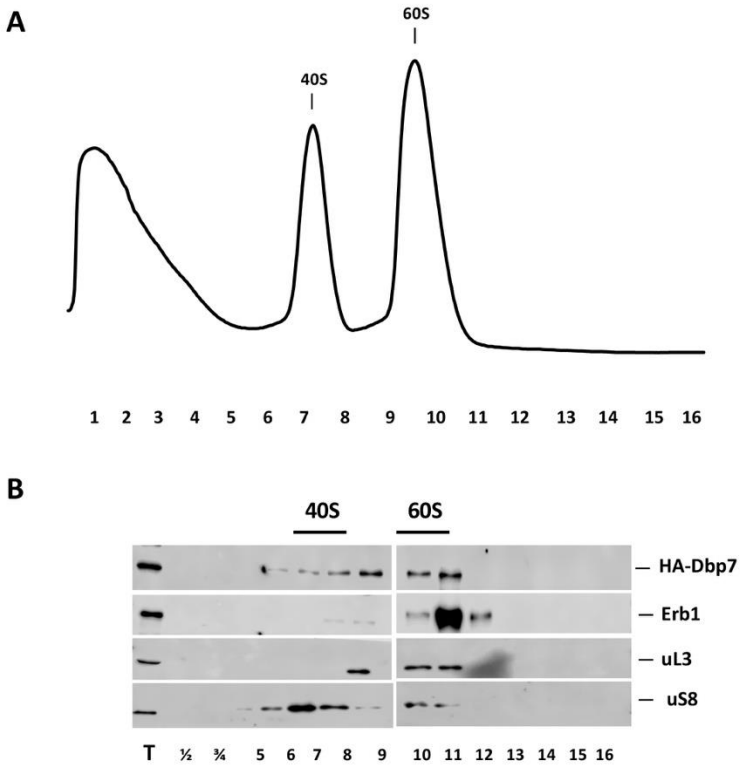

Figure 28. Immunodetection of proteins present in fractions from ribosome-enriched particle fractionation in HA-*DBP7* strain. (**A**) Profile obtained from ribosome-enriched particle fractionation in low Mg^{2+} sucrose gradients. Peaks from left to right corresponds to free fractions (low molecular weight complex and free proteins), total 40S, and total 60S subunits, respectively. Numbers at the bottom of the profile indicate the fraction. (**B**) Western blot analysis performed using the fractions collected from the above-mentioned gradient. T indicates the total extraction before particle fractionation**,** which is used as a control. The peaks corresponding to 40S and 60S subunits are indicated. Numbers at the bottom indicates the corresponding fractions. A representative profile and western blot analysis are shown from three replicates, which showed the same results.

In the case of truncated mutant strains, we could observe the same distribution as in HA-*DBP7* strain. Thus, the truncated Dbp7 variant proteins were also stably associated to pre-ribosomal particles. The only exception was that of mutant HA-*dbp7N693*, where the protein could not properly detect due to its reduced levels (**Figure 29**).

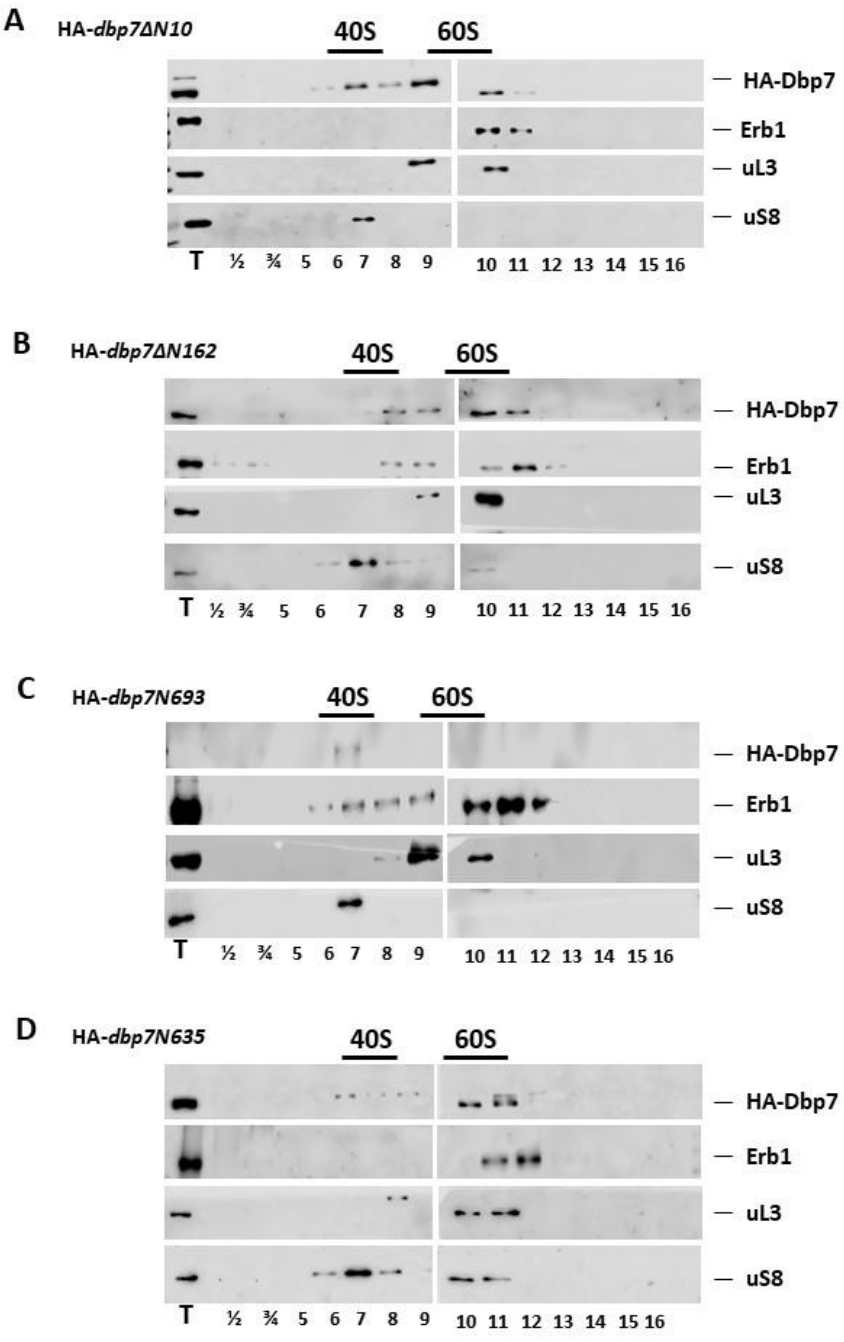
A
HA-dbp7ΔN10
40S
60S
HA-Dbp7
Erb1
uL3
uS8
T ½ ¾ 5 6 7 8 9 10 11 12 13 14 15 16
B
HA-dbp7ΔN162
40S
60S
HA-Dbp7
Erb1
uL3
uS8
T ½ ¾ 5 6 7 8 9 10 11 12 13 14 15 16
C
HA-dbp7N693
40S
60S
HA-Dbp7
Erb1
uL3
uS8
T ½ ¾ 5 6 7 8 9 10 11 12 13 14 15 16
D
HA-dbp7N635
40S
60S
HA-Dbp7
Erb1
uL3
uS8
T ½ ¾ 5 6 7 8 9 10 11 12 13 14 15 16

Figure 29. Immunodetection of proteins present in fractions from ribosome-enriched particle fractionation in Dbp7 truncated mutants. Western blot analysis performed using the fractions collected from the low Mg^{2+} sucrose gradients of (**A**) HA-*dbp7ΔN10*, (**B**) HA-*dbp7ΔN162*, (**C**) HA-*dbp7N693* and (**D**) HA-*dbp7N635* strains. T indicates the total extraction before particle fractionation**,** which is used as a control. The peaks corresponding to 40S and 60S subunits are indicated. Numbers at the bottom indicates the corresponding fractions. A representative profile and western blot analysis are shown from three replicates, which showed the same results.

5.4.-Phenotypic analysis of Dbp7 nuclear localization signal

As mentioned above, we have also identified a putative nuclear localization signal (NLS) in the N-terminal extension of the Dbp7 protein. To determine whether this putative NLS was responsible for the import of Dbp7 to the nucleus, we cloned the first 162 amino acids of Dbp7 (N-terminal extension) in phase with three tandem GFP proteins, and expressed from the strong *ADH1* promoter on a Leu2-marked pADH111 centromeric plasmid. Also, we cloned in this plasmid a variant of the N-terminal of Dbp7 lacking 31 amino acids of the NLS. As a positive control we used the NLS of the large T antigen of the SV40 virus, which was also cloned in pADH111 plasmid. Each plasmid was transformed into the YKL500 strain, which harboured a genomic functional copy of the gene coding the nucleolar reporter Nop58 tagged with the red fluorescent mCherry protein. As shown in **Figure 30**, the corresponding proteins of the constructs were detected by western blotting using a specific anti-GFP antibody.

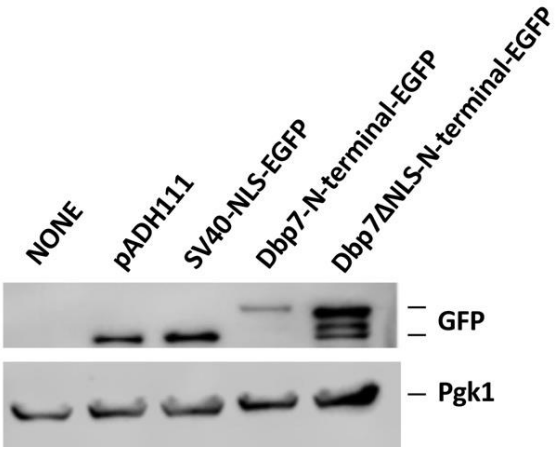

Figure 30. Immunodetection of the different GFP-tagged Dbp7 proteins. Whole cell extracts were prepared from YLK500 cells expressing the indicated constructs, which were grown to exponential phase in SD-Leu at 30 ºC. Equivalent amounts of extracts were analysed by western blotting using a specific anti-GFP antibody. As a loading control, yeast phosphoglycerate kinase (Pgk1) protein was used. As a positive control the NLS of SV40 viral protein tagged with GFP was used. As a negative control, an empty pADH111 plasmid was used.

Next, we determined the location of the different constructs by fluorescent microscopy. As shown in **Figure 31A**, the protein construction with the N-terminal of Dbp7 was observed in the nucleus, while the protein construction lacking the NLS was observed in the cytoplasm. Interestingly, in most cells, the nuclear signal was localised in the nucleoplasm, as it did not colocalised with the nucleolar Nop58 red fluorescent marker (**Figure 31B**).

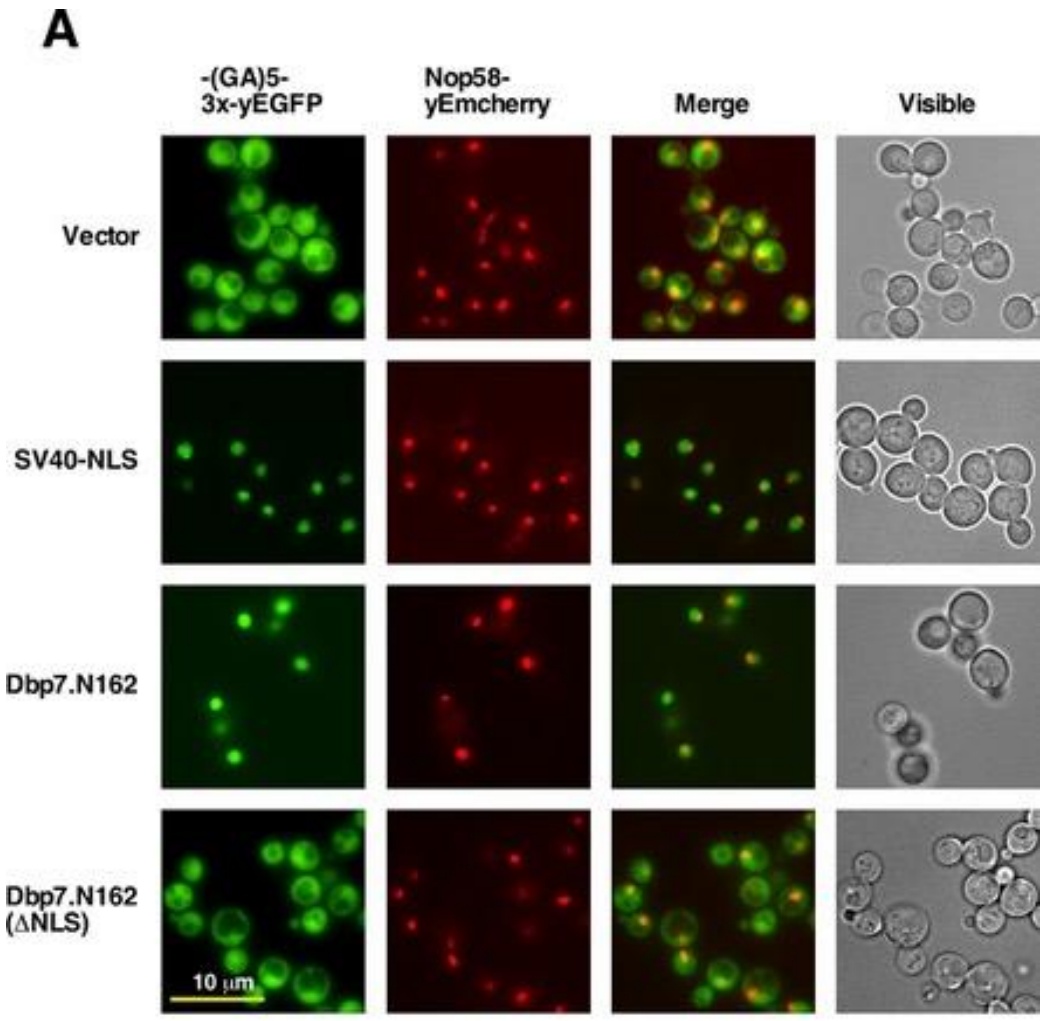
A
-(GA)5-
3x-yEGFP
Nop58-
yEmcherry
Merge
Visible
Vector
SV40-NLS
Dbp7.N162
Dbp7.N162
(ΔNLS)
10 μm

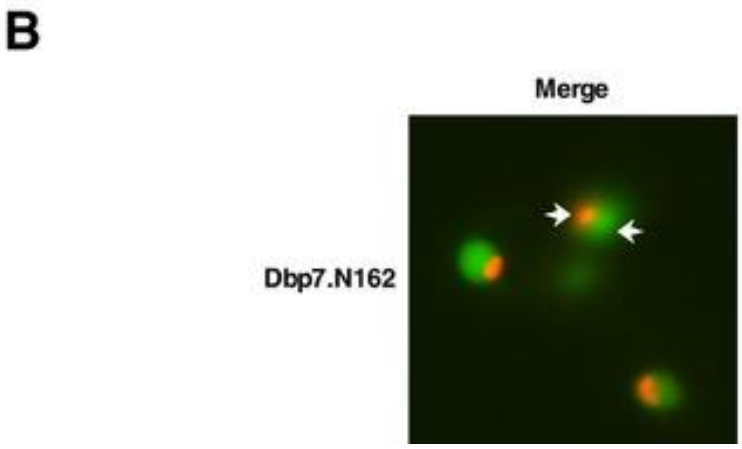
B
Merge
Dbp7.N162

Figure 31. Fluorescence microscopy analysis of the role of the N-terminal tail of Dbp7 as a functional NLS. (**A**) Strain YKL500, which expresses a yEmCherry-tagged Nop58, was transformed with plasmids: a $(GA)_5$-3xyEGFP reporter alone (Vector), the NLS sequence of the SV40 large T-antigen fused to the $(GA)_5$-3xyEGFP (SV40-NLS), the first 162 amino acids of Dbp7 fused in frame with the $(GA)_5$-3xyEGFP reporter (Dbp7.N162) and a construct of the N-terminal tail of Dbp7 lacking the amino acids comprised between positions 48 and 78 fused in frame with the (GA)5-3xyEGFP reporter (Dbp7.N162(ΔNLS)). After transformation, cells were grown in SD-Leu medium at 30 ^{o}C, and the localization of the GFP fusions was obtained by fluorescence microscopy. Nucleolus were revealed by the nucleolar marker protein Nop58-yEmCherry. Cells were identified under bright field illumination (Visible). About 200 cells were inspected for each reporter, and practically all cells gave the same results as the selected ones shown in the pictures. (**B**) Magnified picture of selected cells expressing the Dbp7.N162 construct fused in frame to the $(GA)_5$-3xyEGFP reporter. Note that the signal does not colocalized with the nucleolus, revealed by the Nop58-yEmCherry protein.

To show the physiological relevance of the NLS sequence of Dbp7, we constructed an HA-tagged Dbp7 variant lacking the 31 amino-acid corresponding to this sequence (from now on, HA-*dbp7ΔNLS* mutant). To do so, the ORF of *DBP7* lacking the codons corresponding to the NLS was obtained by PCR using Ycplac22-HA-DBP7 as a template. The construction was expressed under the control of the cognate *DBP7* promoter followed by a HA epitope. To use as a control, a full-length HA-Dbp7 protein was cloned into YCplac22. Upon transformation of these constructs into the *dpb7Δ*[YCplac33-DBP7] strain, cells were subjected to plasmid shuffling on 5-FOA plates. Some of the colonies growing on this media were transferred to SD-Trp plates for further use.

As shown in **Figure 32**, the mutant HA-*dpb7ΔNLS* protein was detected by western blot analysis using specific antibodies against the HA epitope to levels very similar to the wild-type ones.

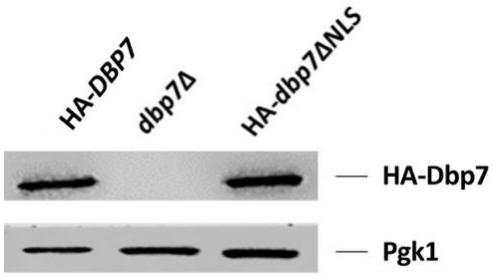

Figure 32. Immunodetection of the HA-Dbp7 variant protein lacking its putative NLS. Whole cell extracts were prepared from the indicated strains, which were grown to exponential phase in SD-Trp at 30 ºC. Equivalent amounts of extracts were analysed by western blotting. As a loading control, phosphoglycerate kinase (Pgk1) protein was used. A negative *dbp7Δ* control was also used.

We then studied the growth phenotype of the HA-*db7ΔNLS* mutant by serial dilutions in solid YPD medium at 30 ºC. As shown in **Figure 33A**, this strain grew as much as its isogenic wild-type HA-*DBP7* counterpart. Indeed, their doubling times were of about 100 and 90 minutes for HA-*dbp7ΔNLS* and *HA-DBP7,* respectively (**Figure 33B**).

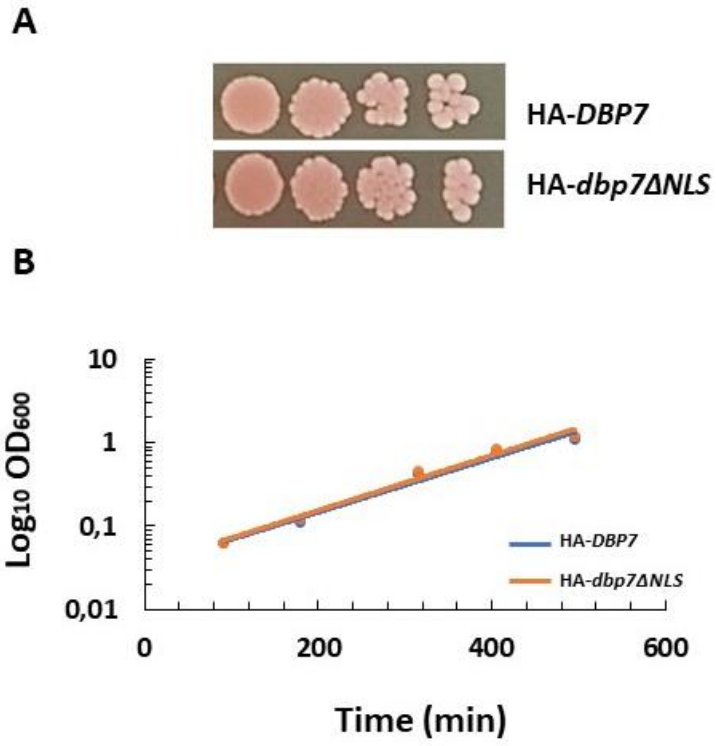

Figure 33. Growth features of *HA-dbp7ΔNLS* strain. (**A**) The growth phenotype was measured by serial dilutions in solid medium SD-Trp medium. (**B**) Growth curves of HA-*DBP7* and HA-*dbp7ΔNLS* strains. Cultures were initiated in SD-Trp liquid medium and incubated at 30 ºC. Three biological replicas were done for each strain. The curves of a representative experiment are shown. Note that only exponential growth phase is plotted.

We next analysed the polysome profile of this strain. As shown in **Figure 34**, its profile was indistinguishable from that of a wild-type profile strain.

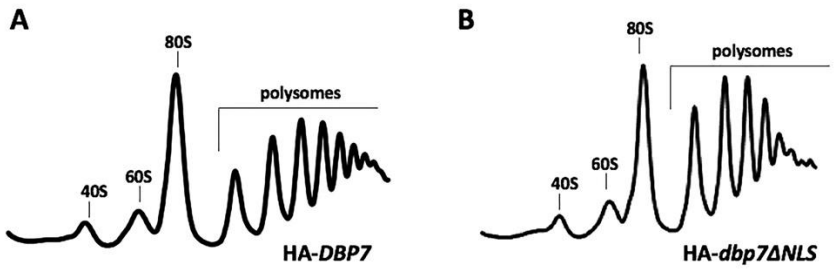

Figure 34. Polysome profile of the *HA-dbp7ΔNLS* strain. This mutant and an isogenic wild-type counterpart were grown to exponential phase in liquid SD-Trp at 30 ºC. Cell extracts were prepared, and 10 A_{260} units resolved on 7-50% sucrose gradients. The A_{254} was continuously measured. Sedimentation comes from left to right. The absorbance peaks of free 40S, 60S r-subunits, 80S vacant ribosomes/monosomes and polysomes are indicated

To confirm that Dpb7ΔNLS was indeed reaching the nucle(ol)us, Dbp7 was fused to three consecutives variant GFPs (3xyEGFP) in its C-terminus. This construct was cloned onto a YCplac111 plasmid, and expressed from the cognate DBP7 promoter. The following fusion proteins were obtained: wild-type Dbp7-$(GA)_5$-3xyEGFP, Dbp7ΔNLS-$(GA)_5$-3xyEGFP and Dbp7ΔN162-$(GA)_5$-3xyEGFP. These plasmids, were separately transformed into the YKL500 strain. Then, selected transformants were inspected by western blot analysis and fluorescent microscopy. As shown in **Figure 35**, all the constructs were properly detected by western blot analyses using specific antibodies against the GFP epitope (**Figure 35**). As expected, the full-length Dbp7-$(GA)_5$-3xyEGFP construct was localized in the nucleo(ol)us. However, the Dbp7ΔNLS-$(GA)_5$-3xyEGFP was detected in

both, the nucleus and the cytoplasm. Interestingly, the Dbp7ΔN162-$(GA)_5$-3xyEGFP was detected exclusively in the cytoplasm (**Figure 36**).

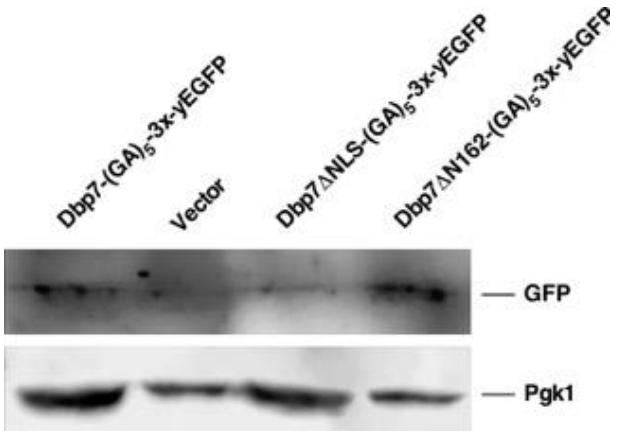

Figure 35. Immunodetection of the different GFP-tagged Dbp7 proteins. Whole cell extracts were prepared from YLK500 cells expressing the indicated constructs, which were grown to exponential phase in SD-Leu at 30 ºC. Equivalent amounts of extracts were analysed by western blotting using a specific anti-GFP antibody. As a loading control, yeast phosphoglycerate kinase (Pgk1) protein was used.

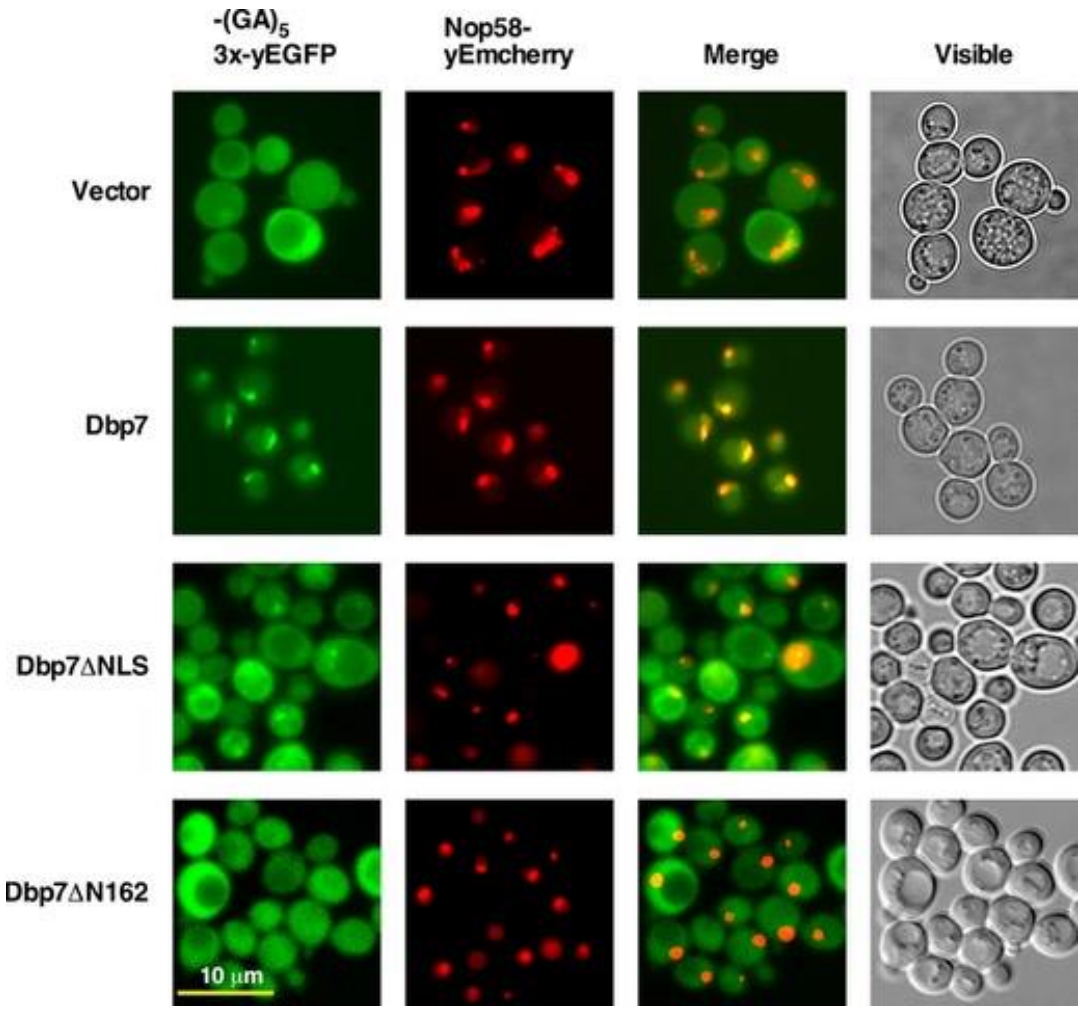

Figure 36. Subcellular localization of Dbp7. Strain YKL500, was transformed with different plasmids; a $(GA)_5$-3xyEGFP reporter alone expressed from the *ADH1* promoter (Vector), a full-length Dbp7, a Dbp7 lacking the 31 amino acids described as an NLS and a Dbp7 lacking the 162 amino acids from its N-terminal tail. All the proteins were fused to a C-terminal $(GA)_5$-3xyEGFP reporter. After transformation, cells were grown in SD-Leu medium at 30 ºC, and the localization of the GFP fusions obtained by fluorescence microscopy. Nucleolus were revealed by the nucleolar marker protein Nop58-yEmCherry. Cells were identified under bright field illumination (Visible). About 200 cells were inspected for each reporter, and practically all cells gave the same results as the selected ones shown in the pictures.

5.5.- *In vitro* properties of Dbp7

As a second aim, in addition to clarify the *in vivo* function of the N- and C- terminal extensions of Dbp7, we explored the enzymatic activities of recombinant Dbp7, making use of wild-type Dbp7,and the variants Dpb7[K197A] and Dbp7[R553A], to which *in vivo* point mutants have been discussed in 5.2 section from Results.

5.5.1.- Expression and purification of wild-type Dbp7, Dbp7[K197A], and Dbp7[R553A] proteins

A C-terminal His_6-tagged Dbp7 fusion protein was constructed by introduction of the open reading frame of *DBP7* in the plasmid pET21b, under the control of an inducible T7 promoter. We also constructed Dpb7 mutant variants, which harbour the mutation K197A or R553A in motifs I and VI, respectively. To do so, the pET21b-His_6-DPB7 plasmid was mutagenized *in vitro.* Each plasmid was transformed into the *E. coli* BL21 Codon Plus strain. Transformed cells were grown, the proteins overexpressed after IPTG induction, and, recombinant proteins purified by affinity chromatography using a nickel (Ni-NTA) agarose resin, in cases of small volume cultures, or a 5 mL HisTrap FF column (GE Healthcare) coupled to a FPLC system in cases of large volume cultures. The elution fractions from the affinity chromatography were run in a denaturing polyacrylamide gel; a prominent protein band above 75 kDa was observed (**Figure 37A and B**). This molecular mass coincides with that estimated for Dbp7 by sequence analysis (83 kDa). In the case of the purification by the FPLC system, the A_{260} profile indicated the elution profile (**Figure 37C**). The peak observed in the chromatography is coincident with the elution peak in the gel. The identity of the protein was verified by western blot analysis using anti-polyhistidine antibodies (**data not shown**).

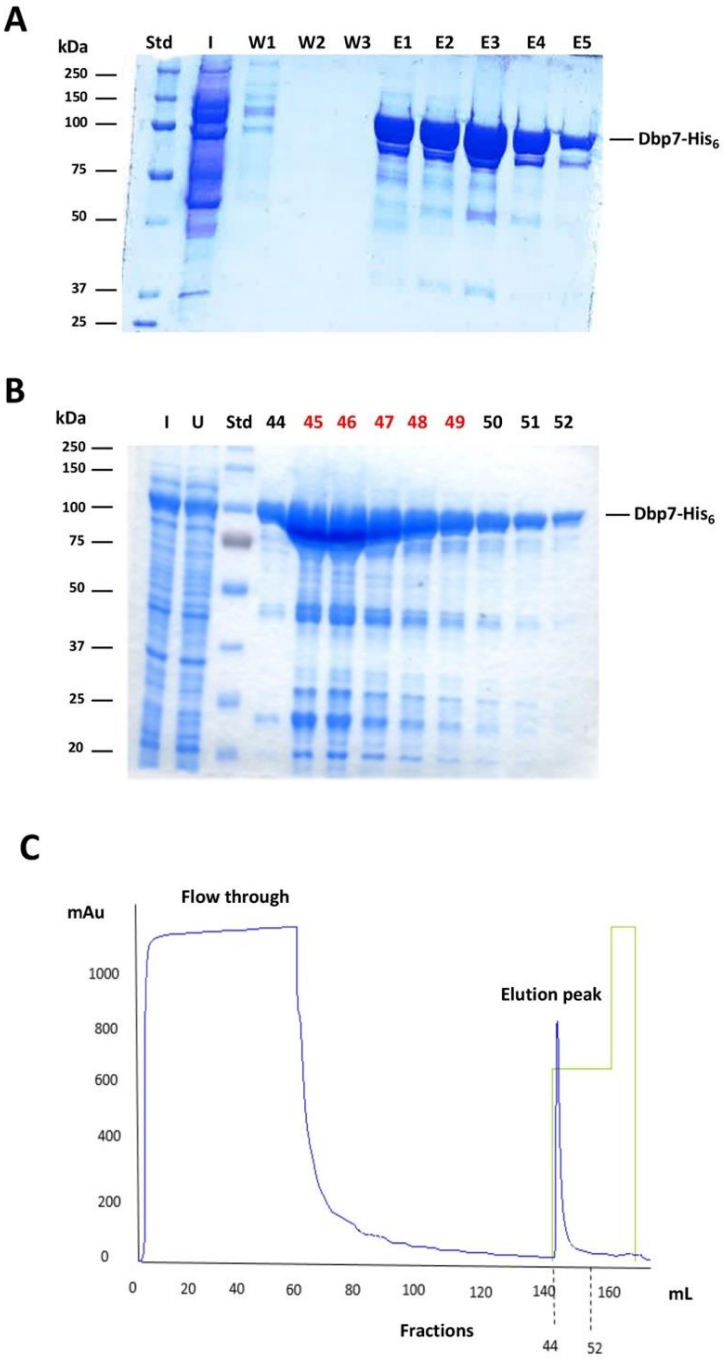

Figure 37. Purification of Dbp7 wild-type by affinity chromatography. (**A**) and (**B**) 10% SDS-PAGE gel showing the fractions obtained by affinity purification with Ni-NTA agarose resin or by a HisTrap FF column in a FPLC system, respectively. W1, W2, and W3 indicate wash volumes 1, 2 and 3. E1, E2, E3, E4, and E5 indicate elution volumes 1, 2, 3, 4 and 5, respectively. I, indicates input, Std, protein standards and U, unbound proteins. (**C**) Chromatogram of recombinant wild-type Dbp7 obtained by affinity purification in a FPLC system. Dashed lines indicate the interval of fractions in which Dbp7 protein elutes. This interval corresponds to fractions 44 to 52. Fractions 45, 46, 47, 48 and 49 (marked in red in the gel B) were pooled and injected in a Superdex 200 HiLoad 16/60 column. The flow through and elution peaks are indicated.

In order to detect multisubunit complexes, selected fractions from the affinity column (from 45 to 49 in the example of **Figure 37**) were pooled and subjected to molecular exclusion chromatography in a Superdex 200 HiLoad 16/60 column. After this purification step, it could be observed that Dbp7 was purified at a high electrophoretic homogeneity (**Figure 38A**). Surprisingly, when the molecular mass of Dbp7 wild-type was calculated by gel filtration, the protein eluted at a volume (70,59 mL) which corresponds to about 146 kDa (**Figure 38B**). Thus, these results suggest that most wild-type Dbp7 protein eluted as a dimer. A shoulder was also observed in the main peak at an elution volume of approximately 80 mL, which likely corresponded to the size of the monomer (83 kDa).

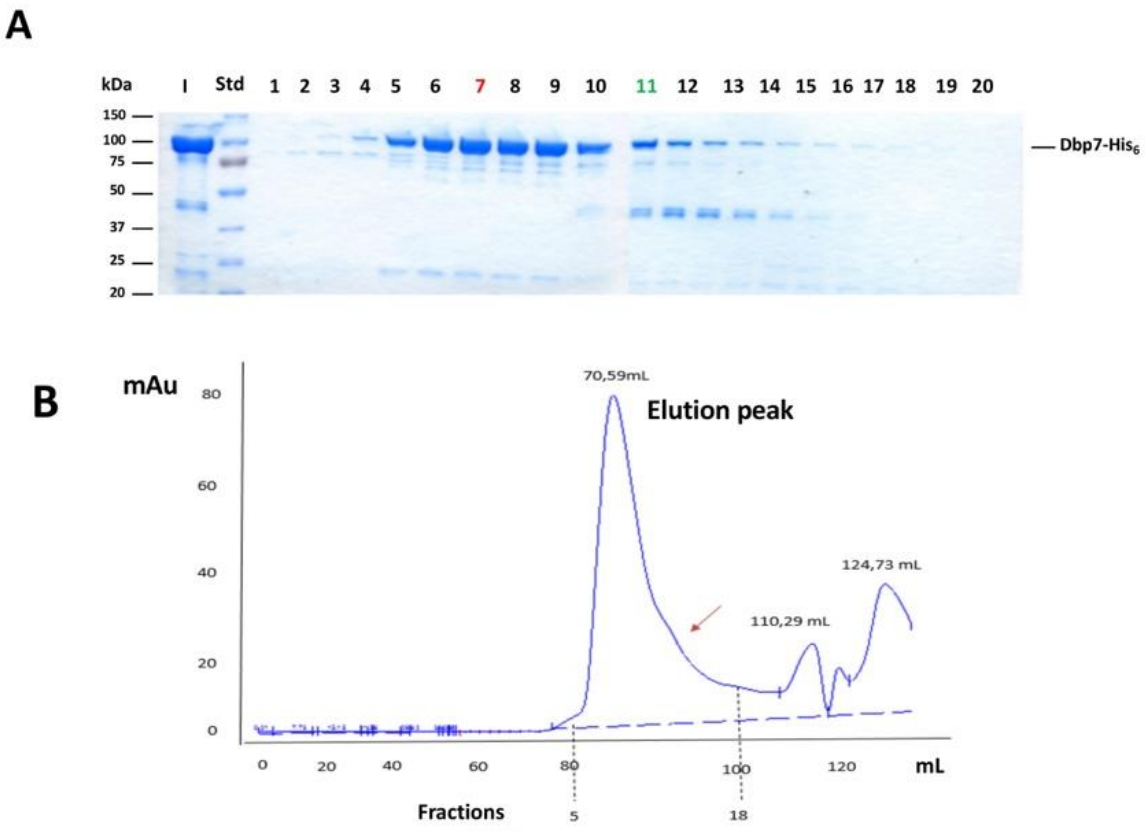

Figure 38. Purification of recombinant Dbp7 wild-type by molecular exclusion in a Superdex 200 HiLoad 16/60 column. (**A**) A 10% SDS-PAGE gel showing the fractions obtained after the chromatography. Number in red marks the fraction eluting at about 70.6 mL (dimer), and number in green fraction eluting in the shoulder of the peak (monomer). I indicates input and Std protein standards. (**B**) Chromatogram corresponding to a typical molecular exclusion chromatography of wild-type Dbp7. The shoulder of the elution peak is indicated by a red arrow.

To analyze the importance of the motifs I and VI on the enzymatic properties of the recombinant Dbp7 protein, we also overexpressed in *E. coli* and purified the Dbp7[K197A] and Dbp7[R553A] proteins. The affinity purification profile was similar to wild-type Dbp7. Thus, an apparent molecular mass above 75 kDa was estimated for Dbp7[K197A] by SDS-PAGE, which is similar to that obtained for the wild-type protein. As above, two elution peaks, one of about 110 kDa and another of about 73 kDa, were obtained after tandem affinity and molecular exclusion chromatography, suggesting again the dimeric nature of the putative RNA helicase, although none of these calculated masses exactly corresponded to the molecular masses calculated for the wild-type protein. We also purified recombinant Dbp7[R553A]. In this case, its gel filtration profile and behaviour in an SDS-PAGE gel were identical to the equivalent features of the recombinant wild-type Dbp7 protein.

5.5.2.- ATPase activity of Dbp7: the colorimetric assays

As aforementioned, Dbp7 contains motifs involved in ATP binding and hydrolysis. However, to our knowledge, whether Dbp7 hydrolyse ATP *in vitro* has not been determined so far. In order to determine whether Dbp7 has ATPase activity, reaction conditions for an enzymatic assay were set-up. First of all, the ATPase activity of Dbp7 was measured at different ATP concentrations. Afterwards, parameters such as the relationship between protein concentration and the reaction time respect the ATP hydrolysis were measured. The dependence of the cation used as a cofactor was also assessed, including assays in the presence of EDTA. In addition, we studied the relationship between the ATPase activity and the temperature or the pH in the reaction mixtures. Finally, the ATPase activity of Dbp7 was measured in presence of RNase A to

determine the RNA dependence, and using different RNA or DNA as substrates. All these assays were monitored using a standard colorimetric method, which evaluated the amount of inorganic phosphate (Pi) released during the course of the reaction. For this method, we used the semi-pure protein sample contained in the elution 1 from an experiment of affinity chromatography using the Ni-NTA agarose resin (see **Figure 37A**).

A) ATP concentration

Firstly, we evaluated the activity of Dbp7 with different concentrations of this nucleotide, ranging from 0 to 1 mM. No exogenous RNA was used in the assay. We thought that the preparation must contain co-purified RNA. As shown in the **Figure 39**, the level of hydrolyzed ATP augmented as the ATP concentration did. However, at 0.5 mM ATP, the ATP hydrolysis did not increase further, indicating the saturation of the assay. (**Figure 39**). Consequently, a concentration of 0.5 mM of ATP was thereafter used, unless otherwise stated.

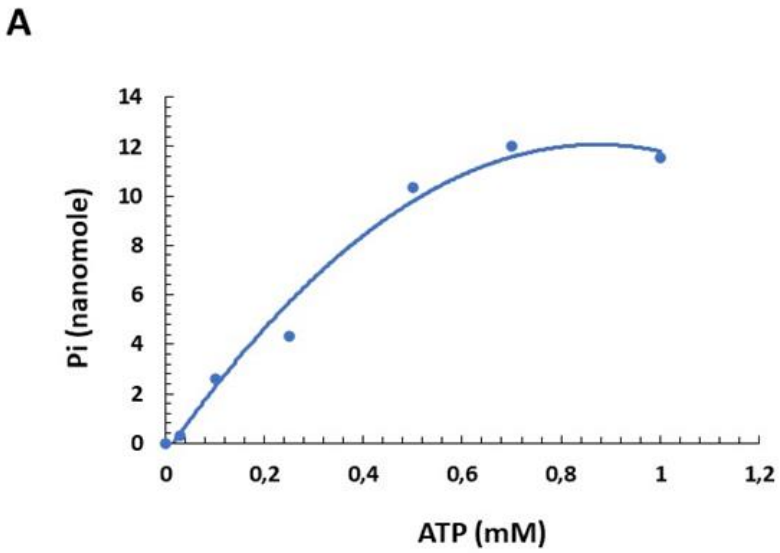

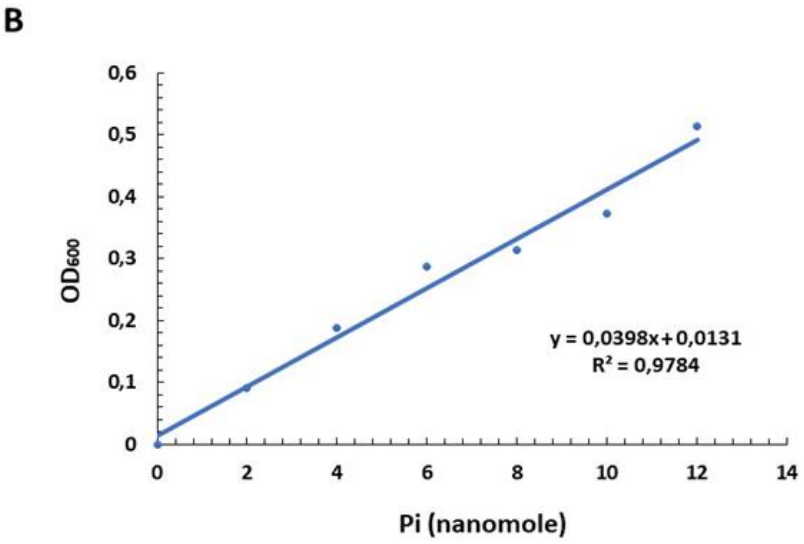

Figure 39. Plot of ATPase activity of Dbp7 wild-type with respect to ATP concentration. (**A**) A colorimetric assay was used, which measures the amount of Pi released (y-axis) at different ATP concentration (x-axis) during the assay. In all assays, 1.5 µg protein was used in a buffer containing 2 mM Mg^{2+}, pH 6.5. Note that no exogenous RNA was added. Reactions were performed at 30 °C and stopped after 10 min of incubation. (**B**) Linear regression obtained upon measuring the values given by different concentrations of NaH_2PO_4. The regression was used to calculate the amount of free Pi in the colorimetric assay.

B) Protein concentration

Secondly, we evaluated the activity of Dbp7 with different protein concentrations, ranging from 0 to 2.5 µg. As shown in **Figure 40**, we found a linear positive correlation between the protein concentration and the Pi released. We decided to use 1.5 µg of protein for further assays.

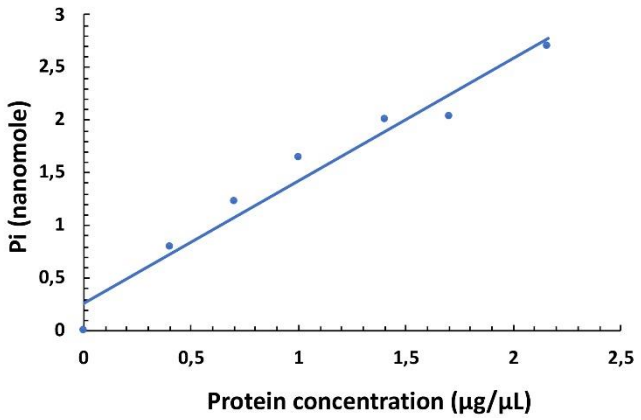

Figure 40. Plot of ATPase activity of Dbp7 wild-type with respect to protein concentration. A colorimetric assay was used, which measures the amount of Pi released (y axis) at different protein concentration (x-axis). The reaction contained 0.5 mM ATP in a buffer with 2 mM Mg^{2+}, pH 6.5. Note that no exogenous RNA was added. Reactions were performed at 30 ºC and stopped after 10 min of incubation. The amount of free Pi was calculated using the linear regression obtained upon measuring the values given by different concentrations of NaH_2PO_4 in the colorimetric assay.

C) Reaction time

We next assayed the ATPase activity of Dbp7 at different times, ranging from 0 to 50 minutes. As shown in **Figure 41**, and as expected, we obtained a saturation curve, which reached the saturation point about the 25 minutes after the reaction was started.

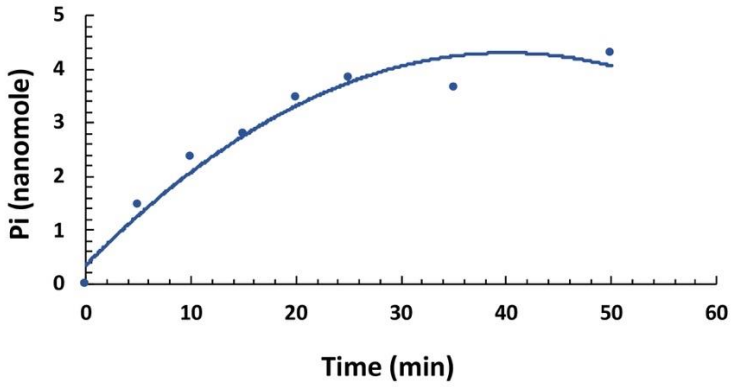

Figure 41. Plot of ATPase activity of Dbp7 wild-type along the time. A colorimetric assay was used, which measures the amount of Pi released (y-axis) at different times (x-axis). In the assays, 1.5 µg protein, and 0.5 mM ATP were used in a buffer containing 2 mM Mg^{2+}, pH 6.5. Note that no exogenous RNA was added. Reactions were performed at 30 ºC and stopped at different times of incubation. The amount of free Pi was calculated using the linear regression obtained upon measuring the values given by different concentrations of NaH_2PO_4 in the colorimetric assay.

D) Mg^{2+} dependence

Usually, ATP-dependent RNA helicases use Mg^{2+} as a cofactor to hydrolyze ATP. To study the dependence of this cation, we determined the ATPase activity of wild-type Dbp7 at different Mg^{2+} concentrations, ranging from 0.5 to 2 mM. As shown in **Figure 42**, ATP hydrolysis increased when the Mg^{2+} concentration also did it; however, at concentrations about 0.5 mM Mg^{2+}, ATP hydrolysis did not increase further.

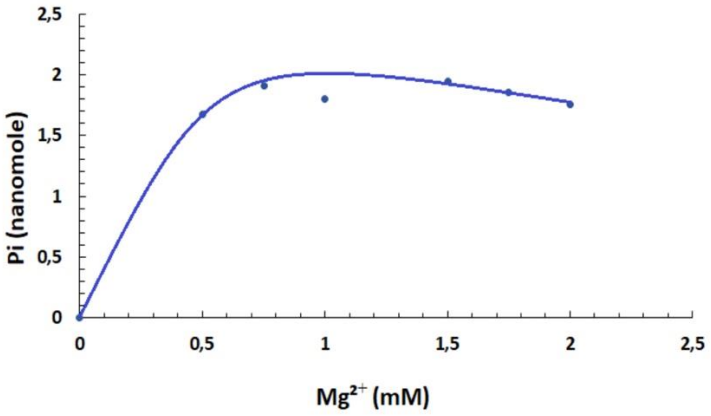

Figure 42 Plot of ATPase activity of Dbp7 wild-type with respect to Mg^{+2} concentration**.** A colorimetric assay was used, which measures the amount of Pi released (y-axis) at different Mg^{+2} concentration (x-axis). The reaction contained 1.5 µg of protein, and 0.5 mM ATP. Note that no exogenous RNA was added. Reactions were performed at 30 °C and stopped after 10 min of incubation. The amount of free Pi was calculated using the linear regression obtained upon measuring the values by different concentrations of NaH_2PO_4 given in the colorimetric assay.

E) EDTA concentration

A different approach to evaluate the dependence of Mg^{2+} on the ATPase activity of wild-type Dbp7 was performing assays at a fixed concentration of Mg^{2+} while increasing concentrations of EDTA, which is a Mg^{2+} chelating agent, are used. The EDTA concentration ranging from 15 to 200 µM. As shown in **Figure 43**, the ATPase activity of Dbp7 decreased drastically when EDTA was added at concentrations over 50 µM (**Figure 43**).

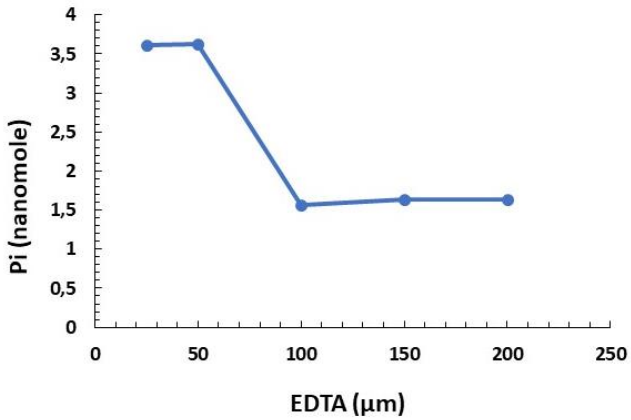

Figure 43. Plot of ATPase activity of Dbp7 wild-type with respect to EDTA concentration. A colorimetric assay was used, which measures the amount of Pi released (y-axis) respect the EDTA concentration (x-axis). Reactions contained 1.5 µg of protein, and 0.5 mM ATP in a buffer with 2 mM Mg^{2+}, pH 6.5. Note that no exogenous RNA was added. Reactions were performed at 30 ºC and stopped after 10 min of incubation. The amount of free Pi was calculated using the linear regression obtained upon measuring the values given by different concentrations of NaH_2PO_4 in the colorimetric assay.

F) Ca^{2+} dependence

We also evaluated the presence of Ca^{2+} as a cofactor, as it has been shown that some RNA helicases enhance its ATPase activity in presence of other cations different of Mg^{2+} (55). As shown in **Figure 44**, Ca^{2+} did not act as optimal as Mg^{2+} as a cofactor, when it was used at 2 mM in equivalent enzymatic assays. Thus, in presence of Mg^{2+}, ATP hydrolysis was about 2.5 times higher than in the presence of Ca^{2+} at the same concentration (**Figure 44**).

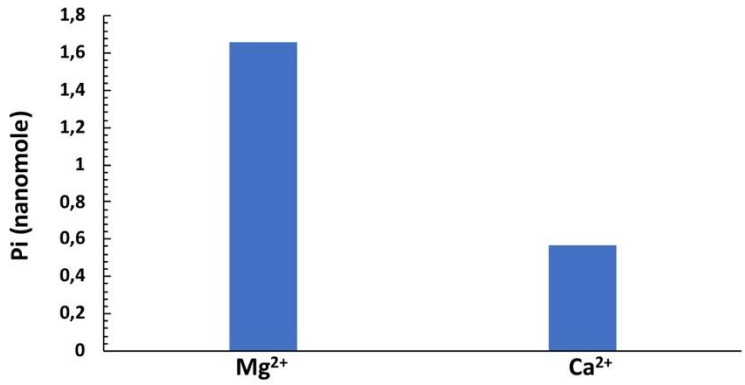

Figure 44. Bar diagram of ATPase activity of Dbp7 wild-type in the presence of Mg^{2+} or Ca^{2+} as cofactor. A colorimetric assay was used, which measures the amount of Pi released (y-axis) using Mg^{+2} or Ca^{+2} (x-axis) during the assay. Reactions contained 1.5 µg of protein, and 0.5 mM ATP in a buffer with 2 mM Mg^{2+}or 2 mM Ca^{2+}, pH 6.5. Note that no exogenous RNA was added. Reactions were performed at 30 ºC and stopped after 10 min of incubation. The amount of free Pi was calculated using the linear regression obtained upon measuring the values given by different concentrations of NaH_2PO_4 in the colorimetric assay.

G) Temperature

We also performed ATPase assays at different temperatures ranging from 22 ºC to 47 ºC. As shown in **Figure 45**, the highest level of ATPase activity was obtained at 37 ºC.

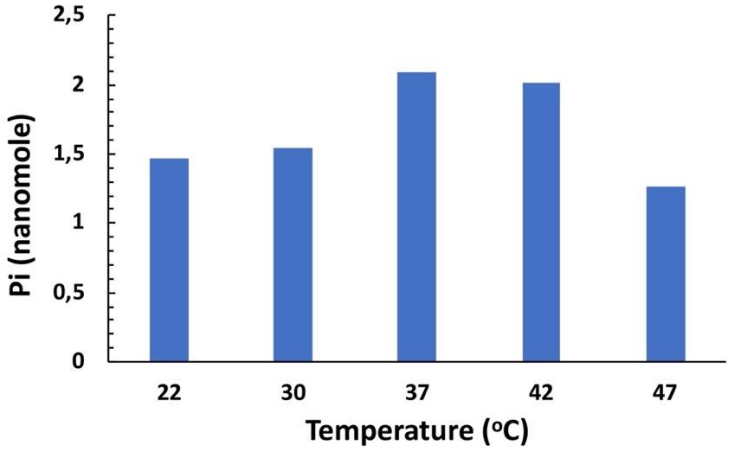

Figure 45. Bar diagram of ATPase activity of Dbp7 wild-type at different temperatures. A colorimetric assay was used, which measures the amount of Pi released (y-axis) at different temperatures (x-axis). Reactions contained 1.5 µg of protein, and 0.5 mM ATP in a buffer with 2 mM Mg^{2+}, pH 6.5. Note that no exogenous RNA was added. Reactions were incubated at the indicated temperatures and stopped after 10 min of incubation. The amount of free Pi was calculated using the linear regression obtained upon measuring the values given by different concentrations of NaH_2PO_4 in the colorimetric assay.

H) pH

ATPase assays were also performed at different pH ranging from 5 to 8.5. The highest ATPase activity was obtained at pH 6 (**Figure 46**).

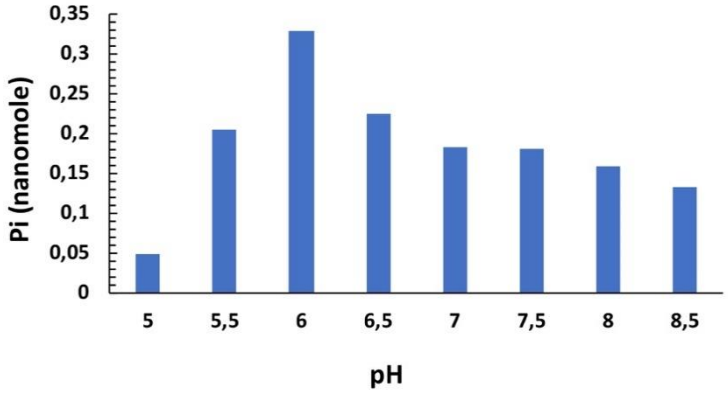

Figure 46. Bar diagram of ATPase activity of Dbp7 wild-type at different pH. A colorimetric assay was used, which measures the amount of Pi released (y-axis) at different pH (x-axis). Reactions contained 1.5 µg of protein, and 0.5 mM ATP in a buffer with 2 mM Mg^{2+}. Reactions were incubated at a buffer done at different pH and stopped after 10 min of incubation at 30 °C. The amount of free Pi was calculated using the linear regression obtained upon measuring the values given by different concentrations of NaH_2PO_4 in the colorimetric assay.

I) RNA dependence

Finally, we evaluated the dependence on RNA of the ATPase activity. To test activity in absence of RNA, we first pre-incubated the reaction mix with RNase A (0.3 mg/mL) for 10 min at 37 °C. Then, the ATPase activity was measured as usual. As shown in **Figure 47**, the RNase A treatment decreases the ATPase activity significantly. This indicated that the reactions were substantiated by certain levels of endogenous RNA likely present in the recombinant protein preparation.

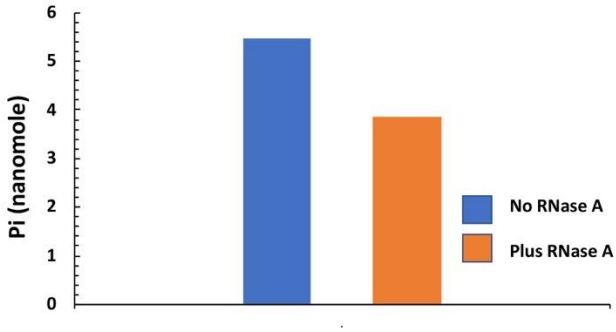

Figure 47. Bar diagram of ATPase activity of Dbp7 wild-type in presence and absence of RNAase A. A colorimetric assay was used, which measures the amount of Pi released during the assay. In all assays, 1.5 µg protein was used and no RNA was added. RNase A at 0.3 mg/mL was added to the assay for 10 minutes at 37 °C before the reactions started by the addition of 0.5 mM ATP. Reactions were performed at 30 °C and stopped after 10 min of incubation. The amount of free Pi was calculated using the linear regression obtained upon measuring the values given by different concentrations of NaH_2PO_4 in the colorimetric assay.

To further evaluate the dependence of the ATPase activity on RNA, we proceeded as follows. We first added 0.1 mg/mL of RNase A in ten mL of lysis buffer during the purification of the protein to degrade the endogenous RNA. RNase was eliminated

during the washes of the affinity resin. When no RNA was added in these types of assays, no ATPase activity was detected (**data not shown**). Thus, this indicates that Dbp7 has an RNA-dependent ATPase activity. In further assays, two sources of total RNA substrates were used: commercial total RNA from yeast (Roche) and total RNA extracted by us from a wild-type W303-1A strain of *S. cerevisiae*. However, and surprisingly, no ATPase activity was found in these conditions (**data not shown**). Thinking on the possibility that Dbp7 could be dependent of a more specific nucleic acid chain for its ATPase activity, we performed assays in the presence of several DNA oligonucleotides of different lengths. Initially, we used three different poly dT oligonucleotides of 15, 25 and 30 nucleotides long. As shown in **Figure 48**, ATPase activity was detected, the length of the oligonucleotide influencing the ATPase activity detected.

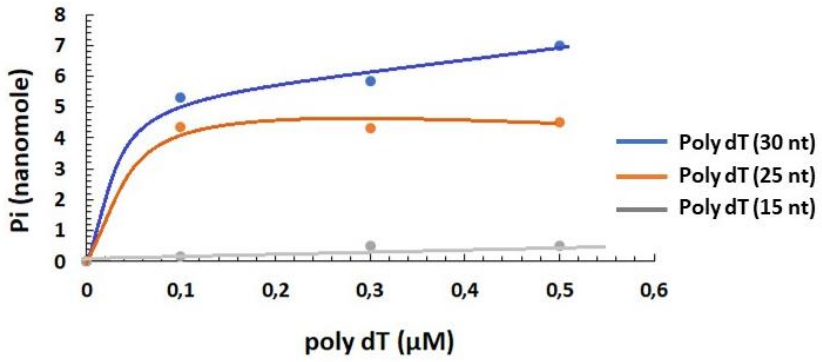

Figure 48. Plot of ATPase activity of Dbp7 wild-type in presence of DNA oligonucleotides. A colorimetric assay was used, which measures the amount of Pi released (y-axis) at different concentration of DNA oligonucleotides (x-axis) during the assay. In all assays, 1.5 µg protein, and 0.5 mM ATP were used in a buffer containing 2 mM Mg^{2+}, pH 6.0. Increasing concentrations of the different poly dT oligonucleotides were used. Reactions were performed at 30 ^{o}C and stopped after 10 min of incubation. The amount of free Pi was calculated using the linear regression obtained upon measuring the values given by different concentrations of NaH_2PO_4 in the colorimetric assay.

To test the sequence specificity of the DNA substrate, other DNA oligonucleotides were used in the assays: a poly dGC (15 nucleotides long), a poly dC (15 nucleotides long) and a poly dGA (18 nucleotides long). In these new assays, the highest ATPase activity was

observed using the poly dT (30 nt) but this activity was also detected using the poly dC (15 nt). No ATPase activity was detected using poly dGC (15 nt) or poly dGA (18 nt) (**Figure 49**).

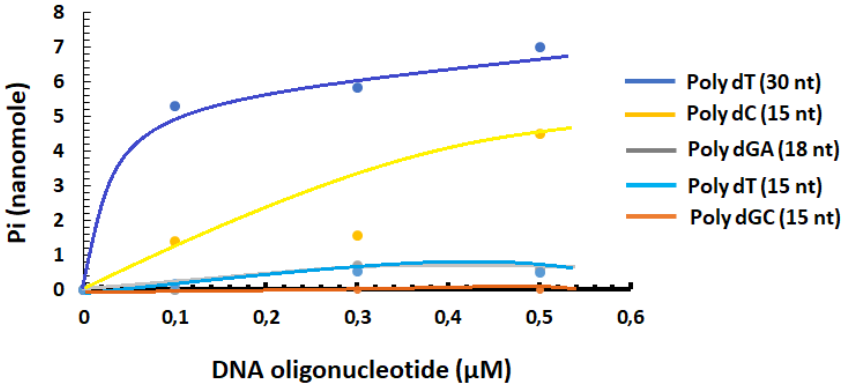

Figure 49. Plot of ATPase activity of Dbp7wild-type in presence of DNA oligonucleotides with different sequences. A colorimetric assay was used, which measures the amount of Pi released (y-axis) at different concentration of DNA oligonucleotides (x-axis) during the assay. In all assays, 1.5 µg protein, and 0.5 mM ATP were used in a buffer containing 2 mM Mg^{2+}, pH 6.0. Increasing concentration of different DNA oligonucleotides was used. Reactions were performed at 30 ^{o}C and stopped after 10 min of incubation. The amount of free Pi was calculated using the linear regression obtained upon measuring the values given by different concentrations of NaH_2PO_4 in the colorimetric assay. Practically, no ATPase activity was detected using poly dGC or poly dGA as substrates.

Once assayed the above parameters we obtained the optimal conditions for ATPase assay in Dbp7: 0.5 mM ATP, 1.5 µg of protein, 0.5 µM DNA oligo dT (30 nucleotides) in a buffer containing 2 mM Mg^{+2}, pH 6. Despite the optimised parameters, we decided to keep 30 ^{o}C as the temperature in the ATPase assays as we assumed the most similar conditions to the *in vivo* situation. Respect the reaction time, we considered 10 min the more suitable time for the course of the reaction.

Once optimized the conditions for the ATPase assay, we decided to test whether the variant Dbp7[K197A] protein was also able to hydrolyse ATP in the optimal conditions observed for the wild type protein. To do so, we first measured the Pi released at different ATP concentrations. **Figure 50** shows that the variant Dbp7[K197A] surprisingly

presented ATPase activity in the assay conditions despite its mutation in the ATP binding domain.

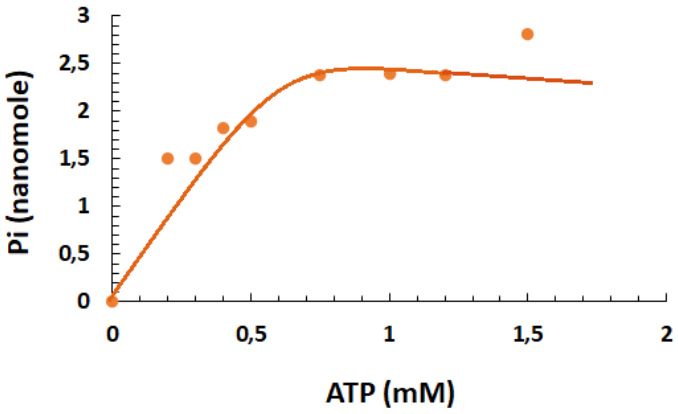

Figure 50. Plot of ATPase activity Dbp7[K197A] with respect to ATP concentration. (**A**) A colorimetric assay was used, which measures the amount of Pi released (y-axis) at different ATP concentration (x-axis) during the assay. Reactions contained 1.5 µg of protein, and 0.5 µM poly dT30 in a buffer with 2 mM Mg^{2+}, pH 6.0. Reactions were incubated with different ATP concentration and stopped after 10 min of incubation at 30 ºC. The amount of free Pi was calculated using the linear regression obtained upon measuring the values given by different concentrations of NaH_2PO_4 in the colorimetric assay.

5.5.3.- ATPase activity of Dbp7: the radioactive assay

This assay had been used previously in the laboratory of our French collaborators from Toulouse. In this kind of assays, ATP hydrolysis was measured by the calculation of the percentage of ADP released into the reaction. The reaction mixture included an amount of radioactive ATP among the whole ATP present; the conversion of ATP in ADP and Pi was followed by thin layer chromatography. In the assays, the same amount of protein was added in each reaction. As a control we used the ssRNA without protein. As substrate, a single stranded RNA (named ssRNA 1) of 58 nucleotides long was used (see Section 4.8 from Material and Methods, and **Table 3**).

We determined the ATPase activity of different fractions obtained from exclusion chromatography. The fraction arbitrarily named as number 7 corresponded likely to the maximum of the dimer peak, while the fraction arbitrarily named as number 11 corresponded to the shoulder peak, likely a Dbp7 monomer (see **Figure 38**).

As shown in **Figure 51A**, all fractions harboured ATPase activity in these conditions, being the fraction 11 the one displaying the highest activity, (**Figure 51B**). Thus, we decided to use this fraction for further assays.

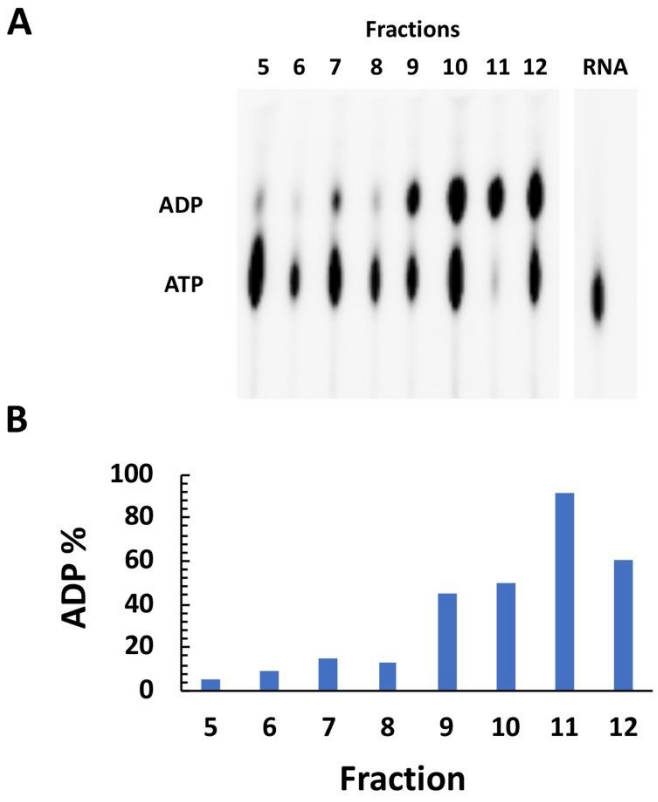

Figure 51. ATPase activity assay for Dbp7 wild-type protein. (**A**) Thin layer chromatography of the reaction products of the assay. The assay contained 0.1 µg protein, 0.1 mM non-radiactive ATP, 0.2 µM [α-^{32}P] ATP and, 3 µM ssRNA 1 in a buffer containing 10 mM Mg^{2+}, pH 8.0. The reaction time was of 1 hour at 30 ^{o}C. No RNase A was added during the protein purification. The upper spots corresponded to the amount of ADP obtained from the ATP hydrolysis and the lower spots the remained ATP, which was not hydrolyse along the duration of the assay. Different fractions of a gel exclusion column from the purification of wild-type Dbp7 (see **Figure 38**) were used. A control without protein was also loaded. (**B**) Quantification of the ATPase activities detected in A. For this, the percentage of ADP released respect the ATP remained was calculated.

To verify that the ATPase activity of Dbp7 is dependent of RNA, we performed new assays in the absence of the ssRNA 1. As shown in **Figure 52**, there was a strong decrease in the ATPase activity when the RNA molecule was excluded from the assay.

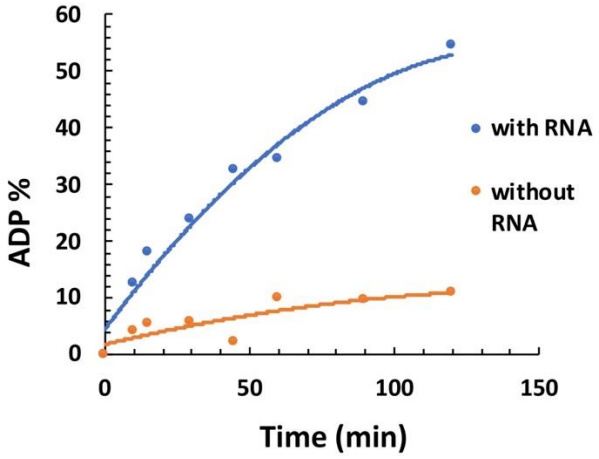

Figure 52. ATPase activity of Dbp7 wild-type in the presence or the absence of ssRNA. The figure represented the percentage of ADP released in the assay *versus* time. The assay contained 0.1 µg protein, 0.1 mM non-radiactive ATP, 0.2 µM [α-^{32}P] ATP and, 3 µM ssRNA 1 in a buffer containing 10 mM Mg^{2+}, pH 8.0. The reaction time was of 1 hour at 30 ^{o}C. No RNase A was added during the protein purification.

5.5.4.- Determination of the Michaelis-Menten kinetics parameters for recombinant Dbp7 wild-type and Dbp7[K197A] protein

We tried to calculate the Michalis-Menten kinetics parameters K_M and V_{max} for wild-type Dbp7 with the colorimetric assay, but we were unable to properly calculate them, because, at a determined ATP concentration, there was an inhibition of the reaction and the curve headed down (**Figure 53**).

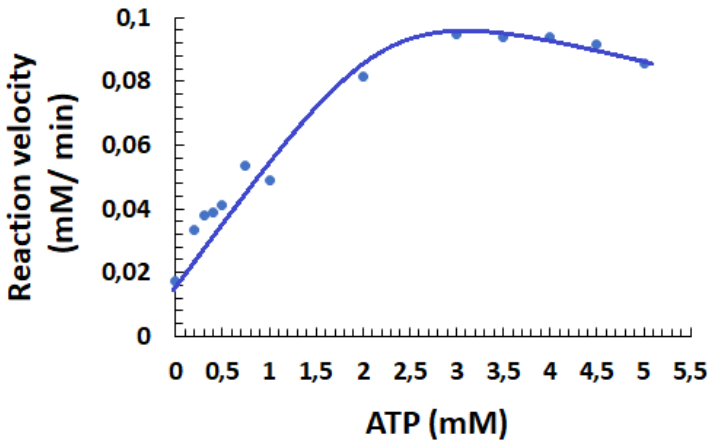

Figure 53. ATP hydrolysis velocity by Dbp7 wild-type at different concentration of ATP. The velocity increased when the ATP concentration also did it. Note that at certain concentration of ATP, the velocity decreased. Three replicas were done for this assay. Only a representative one is shown. The assay was performed with 1.5 µg protein, and 0.5 µM poly dT30 in a buffer containing 2 mM Mg^{2+}, pH 6.0. Reactions were performed at 30 ºC for 10 min of incubation. The amount of free Pi was calculated using the linear regression obtained upon measuring the values given by different concentrations of NaH2PO4 in the colorimetric assay.

To try to determine the kinetics parameter of the variant Dbp7[K197A], we proceeded as we did for the wild-type Dbp7 protein. We performed colorimetric ATPase assay at different ATP concentrations, and measured the Pi released. Unfortunately, as for the wild-type Dbp7, we observed inhibition of the ATPase activity as the ATP concentration increased (**Figure 54**).

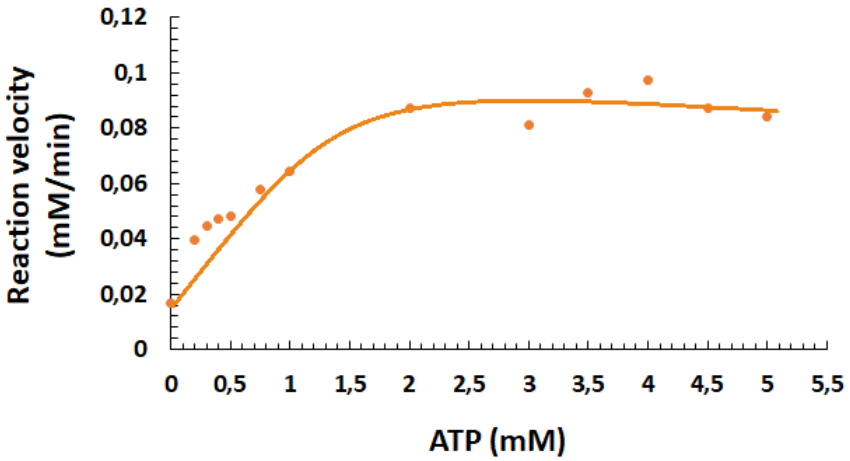

Figure 54. ATP hydrolysis velocity by Dbp7[K197A] at different concentration of ATP. The velocity increased when the ATP concentration also did it. However, note that at certain concentration of ATP, the velocity decreased. Three replicas were done for this assay. Only a representative one is shown. The assay was performed with 1.5 µg protein, and 0.5 µM poly dT30 in a buffer containing 2 mM Mg^{2+}, pH 6.0. Reactions were performed at 30 °C for 10 min. The amount of free Pi was calculated using the linear regression obtained upon measuring the values given by different concentrations of NaH_2PO_4 in the colorimetric assay.

In view of the above, we did an attempt to calculate these parameters by the radioactive assay. First, we assayed kinetically the ATPase activity at different ATP concentration and different times; then, we obtained the respective initial velocities (V_0) for each ATP concentration. One represented, the slope of each line provided the different V_0. If V_0 is represented *versus* the ATP concentration (1 µM to 300 µM), Michaelis-Menten kinetic model scenario is obtained. As shown in **Figure 55**, and strikingly, when the ATP concentration increased, the calculated V_0 of the reactions again decreased.

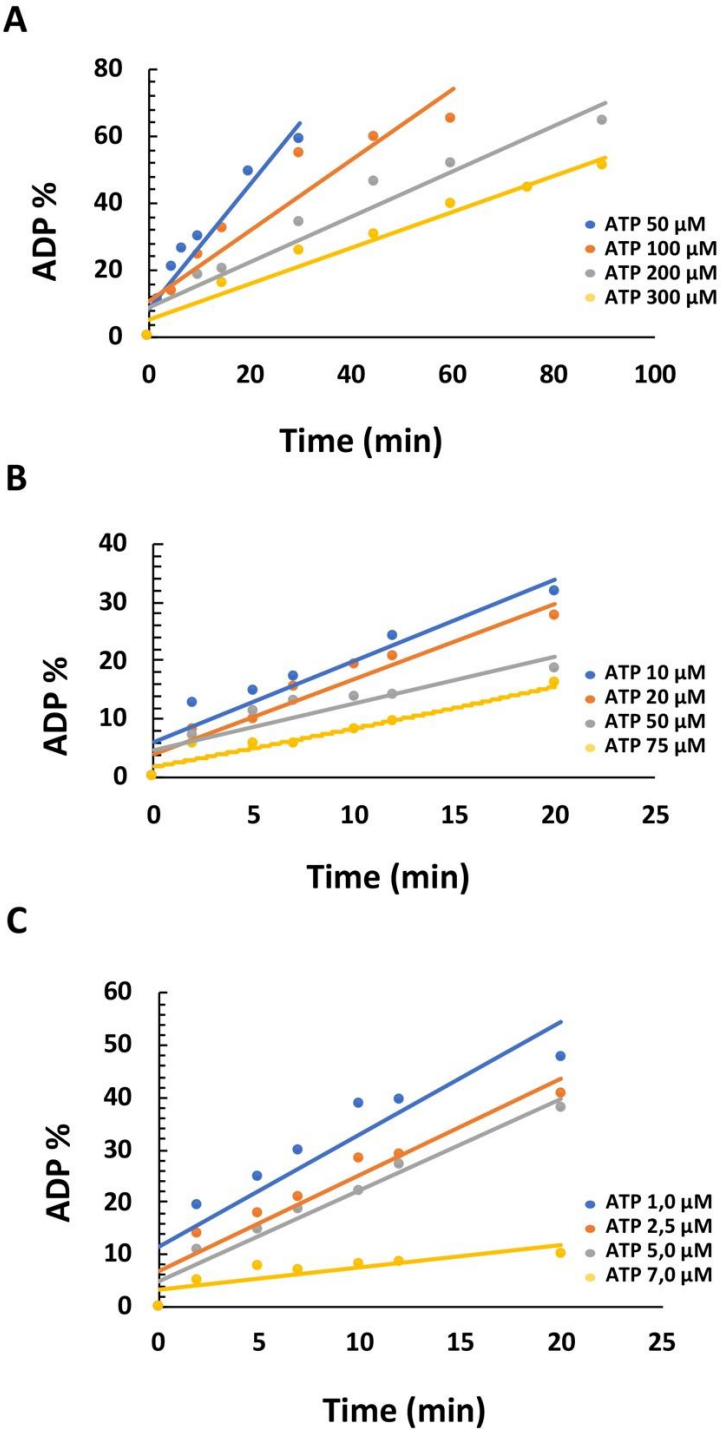

Figure 55. Representation of the ADP% along the time at different range of concentrations of ATP. Note the inhibition of the ATPase activity by increasing the ATP concentration. (**A, B, C**). The concentration of ATP used in the assays ranging from 1 µM to 300 µM. The concentration of [α-^{32}P] ATP was 0.2 µM. The concentration of protein used was 0.27 µg, and the concentration ssRNA 1 was 3 µM in a buffer containing 10 mM Mg^{2+}, pH 8.0. The reaction time was of 1 hour at 30 ^{o}C.

In this circumstance, it was impossible to calculate kinetic parameters by a standard Lineweaver-Burk representation, neither by the colorimetric nor the radioactive assay.

For this reason, in order to obtain at least an approximation of the kinetic parameters for the recombinant wild-type and mutant Dbp7 *in vitro*, we represented directly the Michaelis-Menten graphs using the data obtained after using the colorimetric assay represented in **Figures 53** and **54**. To obtain an approximation of the kinetics parameters, we eliminated from the curve the points that make the curve to head down. In this way, the curves roughly approached the model of enzymatic kinetic of Michaelis-Menten. Accordingly, the V_{max} is approximated by the maximum rate achieved by the system under substrate saturation condition. The K_M or Michaelis-Menten constant is the substrate concentration at which the reaction rate is half of V_{max}. Following this approximation, we obtained a coarse K_M of about 0.30 mM for ATP and a V_{max} of about 0.075 mM/min for wild-type Dbp7 and a coarse K_M of about 0.20 mM and a V_{max} of about 0,07 mM/min for the mutant Dbp7 (**Figure 56 and 57**).

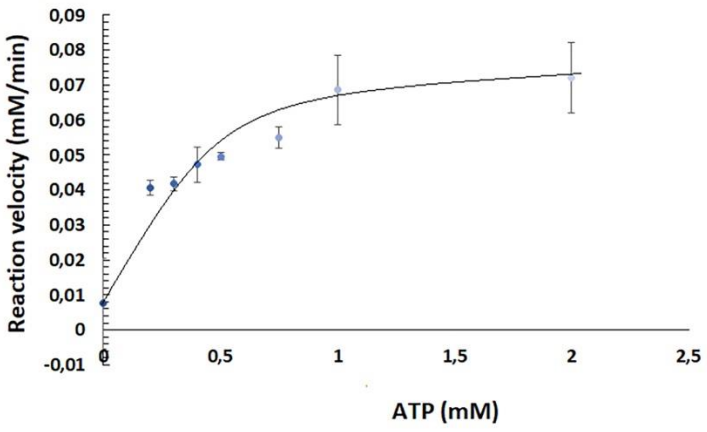

Figure 56. ATPase activity of Dbp7 wild-type with respect to ATP concentration. Only 8 values have been used to calculate the kinetic parameters. The points in which an inhibition was clearly observed (Figure 53) were eliminated from the graph. These points were the corresponding to concentrations of 2.5, 3, 3.5, 4, 4.5, 5, and 5.5 mM of ATP. Each point represented the mean and the standard deviation of at least three replicates. The coarse K_M and V_{max} were calculated using the Graph Pad Prism software.

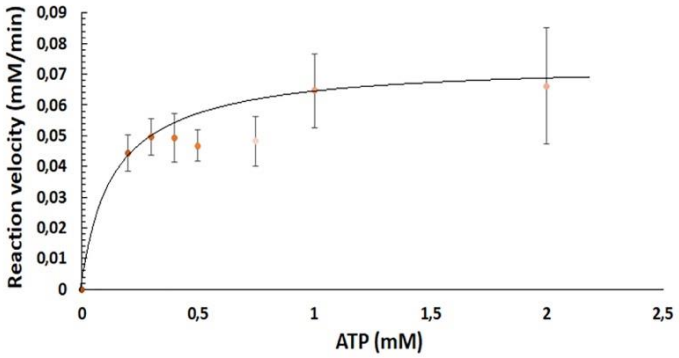

Figure 57. ATPase activity of Dbp7[K197A] with respect to ATP concentration. Only 8 values have been used to calculate the kinetic parameters. The points in which an inhibition was clearly observed (Figure 53) were eliminated from the graph. These points were the corresponding to concentrations of 2.5, 3, 3.5, 4, 4.5, 5, and 5.5 mM of ATP. Each point represented the mean and the standard deviation of at least three replicates. The coarse K_M and V_{max} were calculated using the Graph Pad Prism software.

These data suggest an inhibition of ATPase activity by substrate (ATP) or by one of the products (ADP or Pi). To get insight of a possible inhibition by product, we performed ATPase assays in the presence of ADP and ATP or in presence of ATP. Two different assays were done: in the first one, we used on one hand 50 µM of ATP and on the other hand 50 µM of ATP and 50 µM of ADP, while in the second one we used on one hand 300 µM of ATP and on the other hand 100 µM of ADP and 300 µM of ATP. In both cases, the radioactive method was used. As shown in **Figure 58**, the ATPase activity of wild-type Dbp7 was very similar in the presence or the absence of ADP independently of the ATP concentration (**Figure 58**).

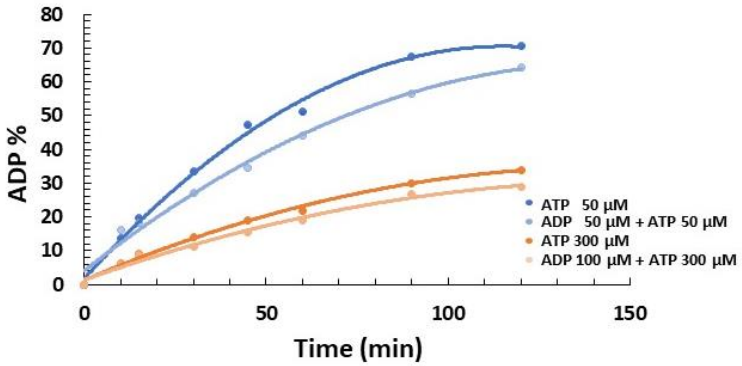

Figure 58. ATPase activity of Dbp7 wild-type protein in the presence of ADP. The assay contained 0.27 µg protein, 0.2 µM [α-^{32}P] ATP, and 3 µM ssRNA 1 in a buffer containing 10 mM Mg^{2+}, pH 8.0. The reaction time was of 1 hour at 30 °C. The amount of ATP and ADP was 50 µM in the first assay and 100 µM of ADP and 300 µM of ATP in the second assay.

5.5.5.- ATPase activity of Dbp7[R553A]

For the mutant Dbp7[R553A] variant protein, we also performed a radioactive ATPase assay to verify whether the mutant was able to hydrolyze ATP. To do the assay, we used the protein obtained after a gel filtration purification. The fraction of the mutant selected was the corresponding to a fraction equivalent to fraction number 11 in Dbp7 wild-type (see **Figure 38**). Surprisingly, this mutant protein had, as previously we also observed for the Dbp7[K197A] variant protein, ATPase activity (**Figure 59A**). When compared to the activities of the wild-type protein, the mutant Dbp7[R553A] protein had even a slightly higher ATPase activity that the wild-type Dbp7 protein (**Figure 59B**).

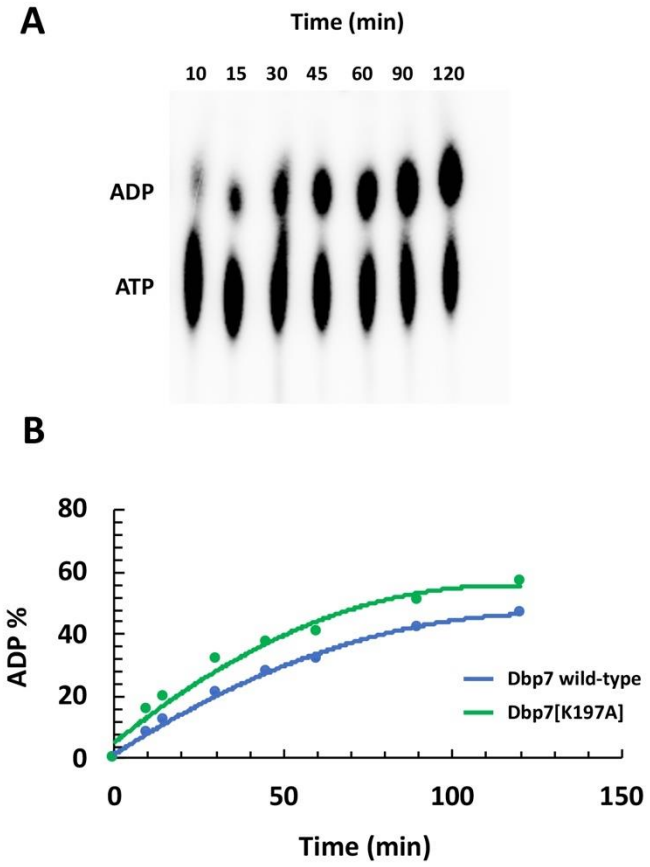

Figure 58. Radioactive ATPase activity assay for the mutant Dbp7[R553A] protein. (**A**) Thin layer chromatography of the reaction products of the assay. (**B**) Quantification of the percentage of ADP released in the assay *versus* time. The concentration of protein used in the assay was 0.1 µg, and the concentration of ssRNA 1 was 3 µM. The assay was performed with 0.3 mM of ATP as substrate and 0.2 µM [α-^{32}P] ATP in a buffer containing 10 mM Mg^{2+}, pH 8.0. The reaction time was of 1 hour at 30 ^{o}C. No RNase A was added during the protein purification. The % of ATP hydrolyzed at each time is the average between two independent experiments.

5.5.6.- RNA binding activity of the recombinant Dbp7 wild-type and Dbp7[K197A] *in vitro*

To investigate whether wild-type Dbp7 is able to bind RNA, we performed *in vitro* gel-shift assays in which the delay in the electrophoretic migration of a labelled ssRNA is interpreted as the binding capability of the protein. The substrate used for this analysis was, as for the previous radioactive enzymatic assays, the one named ssRNA1.

To set-up the assay conditions, a fix amount of RNA was incubated with increasing amounts of Dbp7 protein. In the all the cases, the gel shift assay indicated that protein-RNA complexes were formed (**Figure 60**). Two different complexes were formed. We also evaluated whether the mutant Dbp7[K197A] was able to bind RNA. Thus, similar assays as the above described were performed with the three different concentrations of Dbp7[K197A] protein. As before, two different RNA-protein complexes could be identified (**Figure 60**).

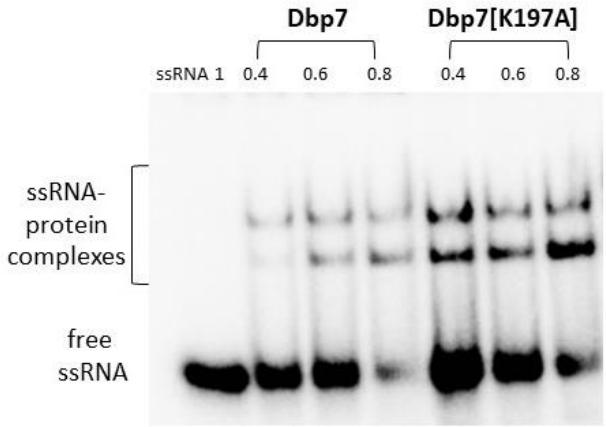

Figure 59. Gel shift assays of wild-type Dbp7 and Dbp7[K197A] protein. A ssRNA 1 at 1 nM was incubated during 15 min with increasing concentration of recombinant Dbp7 wild-type or Dbp7[K197A] protein (0.4, 0.6 and 0.8 µg). As a control, we used the ssRNA 1 substrate, which was incubated with no protein during the assay. Positions of free RNA and protein-bound to RNA forming complexes are shown at the bottom of the gel and at the top of the gel, respectively.

5.5.7.- Helicase activity of the recombinant Dbp7 wild-type and Dbp7[K197A] *in vitro*

Most of the DEAD-box RNA helicases are able to unwind RNA duplexes (dsRNA) in an ATP-dependent manner. Typically, RNA helicases need a single stranded RNA region (overhand), where the helicase binds, to open the dsRNA. Some RNA helicases have a polarity or directionality, that is defined as the direction (5´-3 or 3´-5´) of the helicase movement on the ssRNA along which it is moving. However, others are capable of bind to both ssRNA ends independently and move in both directions (5´-3 or 3´-5´) along the ssRNA. In the case of Dbp7, so far it is unknown if the enzyme is able to unwind RNA duplexes. To test the unwinding activity of Dbp7 *in vitro*, we used two potential substrates, a dsRNA with an 3´-overhand (dsRNA 3´) and dsRNA with an 5´-overhand (dsRNA 5´). Since we did not know the adequate concentration of protein to carry out the assay, we decided to first perform the assay with a range of protein concentration from 0 to 0.8 µg. The fraction of wild type protein used in the assay was the number 11 from molecular exclusion chromatography. The fraction of the mutant [K197A] selected was the fraction equivalent to fraction number 11 in Dbp7 wild-type. As shown in the **Figure 60A** and **60B,** Dbp7 wild-type and Dbp7[K197A] mutant had ATP-dependent helicase activity. Concerning to the protein concentration for the time of assay established (3 minutes), in both cases, the amount of ssRNA increased as the protein concentration increased, but at certain concentration of protein (0.7 µg), the amount of ssRNA generated did not increase even if the concentration of protein continued increasing (**Figure 60C**).

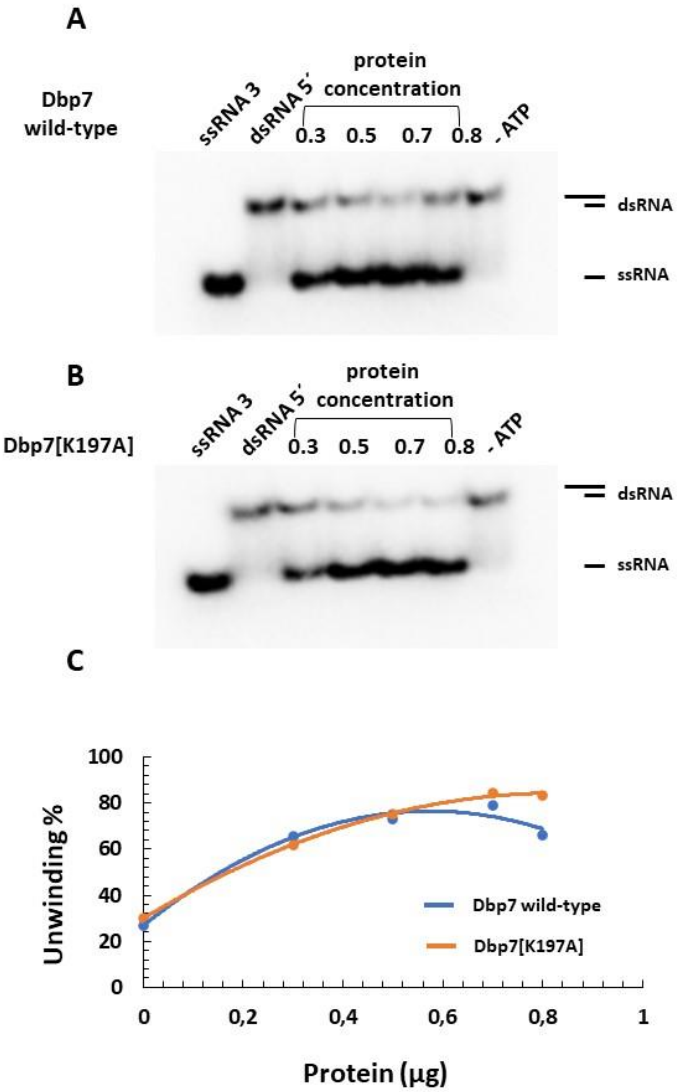

Figure 60. RNA unwinding activity of Dbp7 wild-type and Dbp7[K197A] at different protein concentrations. (**A**) and (**B**) The RNA unwinding activity of wild-type Dbp7 and Dbp7[K197A], respectively, was tested by the ability of the proteins to dissociate a partial duplex (dsRNA 5') composed of complementary oligonucleotides ssRNA4 and [γ-^{32}P] ssRNA3. The reactions contained 1 mM ATP, 1 nM dsRNA 5´, and 10 nM ssRNA complementary to displaced oligo (ssRNA comp). The reaction mixture was incubated at 30 °C for 3 minutes. The products of the reaction were separated by an 8 % non-denaturing polyacrylamide gel electrophoresis and visualised by phosphorimaging analysis. The protein concentration used were: 0, 0.3,

0.5, 0.7 and 0.8 µg. As controls, the RNAs named ssRNA 3 and the dsRNA 5´ which were incubated in the same conditions without protein were used. (**C**) Percentage of ssRNA generated during the assays.

To determine the optimal reaction time, we performed RNA unwinding assays at different times (from 0 to 15 minutes). In this case both substrates (dsRNA 3´ and dsRNA 5´) were used to simultaneously determine whether the Dbp7 recombinant protein was able to displace both 5' and 3' duplexes. As shown in **Figures 61** and **62**, Dpb7 was able to unwind both substrates with no apparent preference. Referring to the time of incubation, at the protein concentration of 0.7 µg, 5 minutes were enough to unwind all the substrate present in the assays.

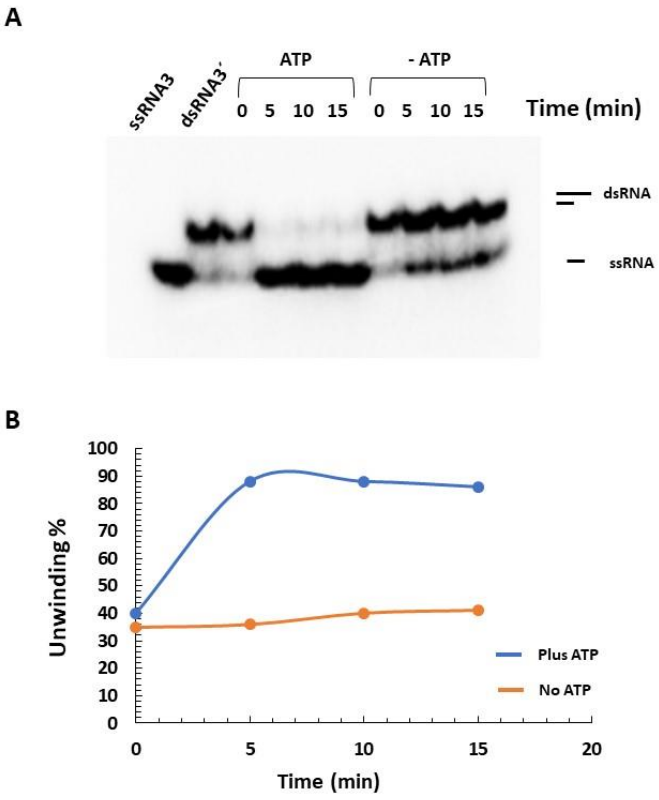

Figure 61. RNA unwinding activity of Dbp7 wild-type on a dsRNA 3' duplex at different incubation times. (**A**) The RNA unwinding activity of Dbp7 was tested by the ability of the protein to dissociate a partial duplex (dsRNA 3') composed of complementary oligonucleotides ssRNA4, and [γ-^{32}P] ssRNA3. The reactions contained 1 mM ATP, 0.7 µg protein, 1 nM dsRNA 3´ and, 10 nM ssRNA complementary to displaced oligo (ssRNA comp). The reaction mixture was incubated at 30 ^{o}C at the times indicated. The products of the reaction were separated by an 8 % non-denaturing polyacrylamide gel electrophoresis

and visualised by phosphorimaging analysis. Both the duplex components; dsRNA 3' and the ssRNA 3 were used as controls. (**B**) Percentage of ssRNA generated during the assays.

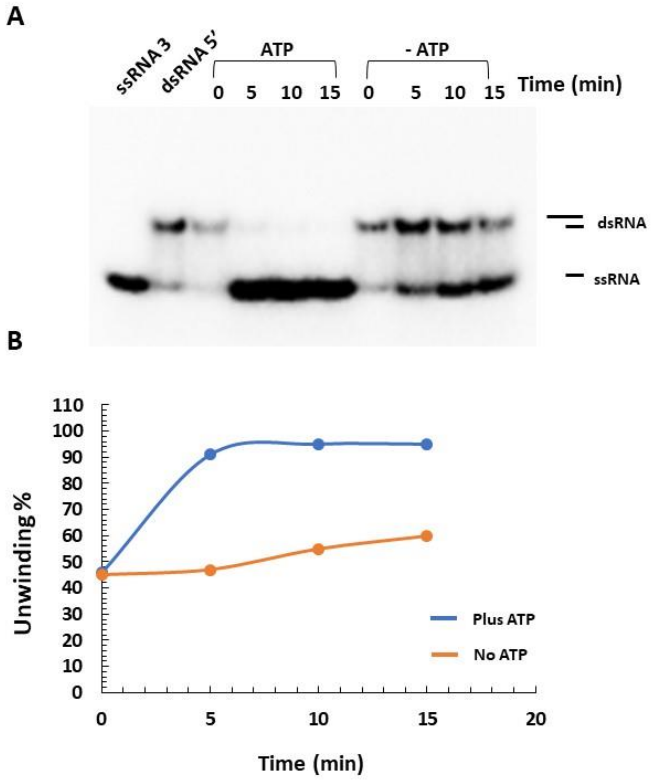

Figure 62. RNA unwinding activity of Dbp7 wild-type on a dsRNA 5' duplex at different incubation times. (**A**) The RNA unwinding activity of Dbp7 was tested by the ability of the protein to dissociate a partial duplex (dsRNA 5') composed of complementary oligonucleotides ssRNA5, and [γ-^{32}P] ssRNA3. The reactions contained 1 mM ATP, 0.7 µg protein, 1 nM dsRNA 5´, and 10 nM ssRNA complementary to displaced oligo (ssRNA comp). The reaction mixture was incubated at 30 ^{o}C at the times indicated. The products of the reaction were separated by an 8 % non-denaturing polyacrylamide gel electrophoresis and visualised by phosphorimaging analysis. Both the duplex dsRNA 5' and the ssRNA 3 were used as controls. (**B**) Percentage of ssRNA generated during the assays.

Due to the fact that after 5 minutes of assay, practically all dsRNA substrate was unwound, we repeated the experiment at shorter time interval (3 and 6 minutes). In this case, we also decided to include the Dbp7[K197A] mutant protein in the assays, as we showed previously that it was active. As shown in **Figures 63**, both Dbp7 wild-type and Dbp7[K197A] proteins rapidly unwind all the dsRNA included in the reaction after 3

minutes of incubation. Moreover, both types of substrates were apparently used at the same preference. Strikingly, we did not detect differences in the activities shown by the wild-type Dbp7 and Dbp7[K197A] variant protein.

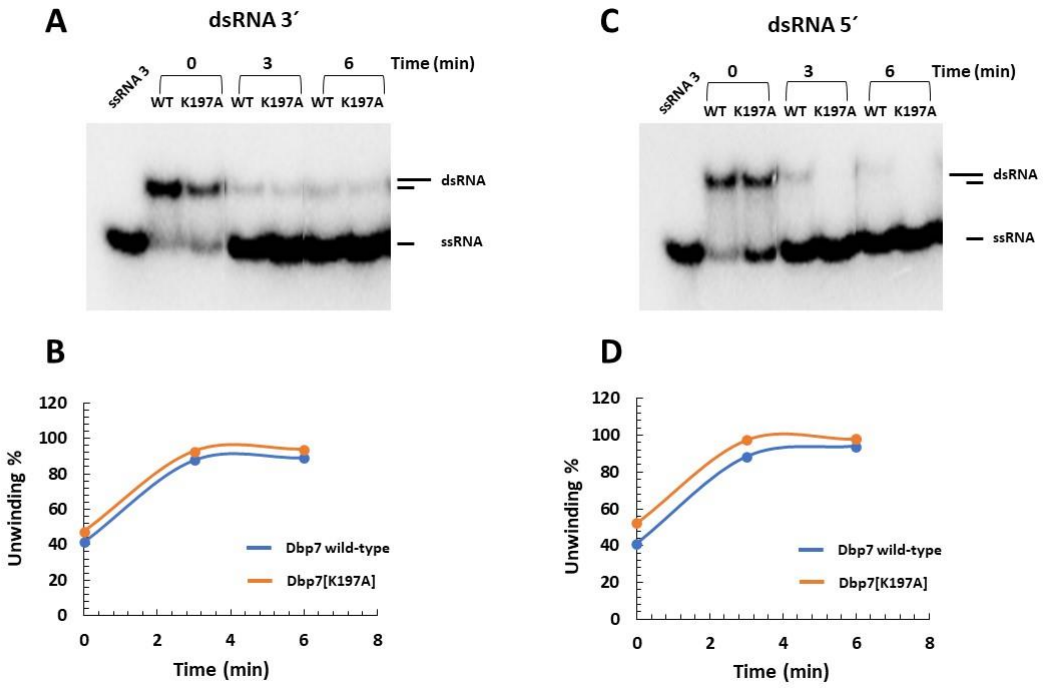

Figure 63. RNA unwinding activity of Dbp7 wild-type and Dbp7[K197A] on a dsRNA 3´and dsRNA 5´at different incubation times. (**A** and **C**) The RNA unwinding activity of Dbp7 wild-type and Dbp7[K197A] mutant protein was tested by the ability of the proteins to dissociate partial duplex 3' or 5' overhanging. The duplexes were composed of complementary oligonucleotides ssRNA4 or ssRNA5, and [γ-^{32}P] ssRNA3. The reactions contained 1 mM ATP, 0.7 µg protein, 1 nM dsRNA 5´ or dsRNA 3´, and 10 nM ssRNA complementary to displaced oligo (ssRNA comp). The reaction mixture was incubated at 30 ^{o}C at the times indicated. The products of the reaction were separated by an 8 % non-denaturing polyacrylamide gel electrophoresis and visualised by phosphorimaging analysis. The ssRNA 3 was used as control. (**B** and **D**) Percentage of ssRNA generated during the assays shown in A and C, respectively.

To determine whether is the presence of ATP or its hydrolysis the specific requirement, we performed new RNA unwinding assays in the presence of other nucleotides such as ADP or the slowly hydrolysable ATP analogs adenosine 5'-O-(3-thio)triphosphate (ATPγS) or adenosine 5’-(β, γ -imido)triphosphate (AMP-PNP). As shown in **Figure 64**, only when

ATP is used, the level of dsRNA catalytically decreased concomitantly to an ssRNA increase (**Figure 64A**). The percentage of ssRNA generated after the reaction using each nucleotide was quantified. When ATP was used, this percentage was the highest; as expected, when using ATPγS, the percentage of generated ssRNA was slightly higher than using ADP or AMP-PMP, which were similar to the background levels found in the absence of nucleotide (**Figure 64B**).

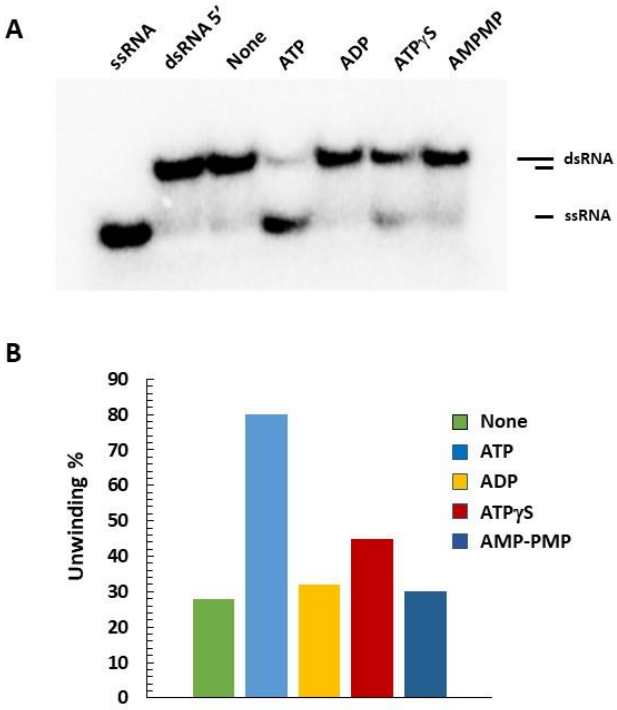

Figure 64. RNA unwinding activity of Dbp7 wild-type using different nucleotides as substrates. (**A**) The RNA unwinding activity of Dbp7 was tested by the ability of the protein to dissociate a partial duplex (dsRNA 5'). The reactions contained 0.7 µg protein, 1 nM dsRNA 5´, 10 nM ssRNA complementary to displaced oligo (ssRNA comp), and 1 mM of the indicated nucleotides. As a control we use ssRNA 3, and dsRNA 5´. The reaction mixture was incubated at 30 ºC for 3 minutes. The products of the reaction were separated by an 8 % non-denaturing polyacrylamide gel electrophoresis and visualised by phosphorimaging analysis. (**B**) Bar diagram, which represents the percentage of ssRNA generated during the assays with each nucleotide. The bars represent the average between two replicates with a standard deviation lower than 5%

5.6.- *In silico* analysis of Dbp9

In addition to Dbp7, we began to study the biochemical properties of another DEAD-box helicase, Dbp9, which is functionally related to Dbp7 (17). The biochemical characterization of this enzyme was initiated by Kikuma and co-workers years ago (39).

As for Dbp7, we first determined in Dbp9 the conserved motifs that define DEAD-box proteins. Fourteen conserved motifs were identified in the amino acid sequence of Dbp9 following the alignments from the Jankowsky's laboratory (22) (**Figure 65**, see also the Introduction section, pages 16-17).

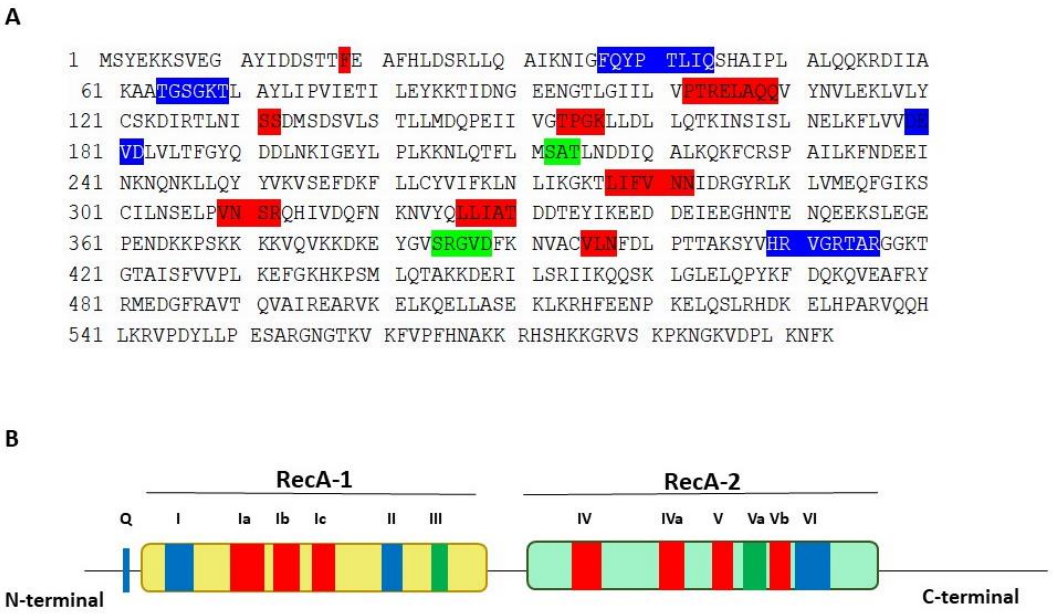

Figure 65. Sequence motifs of the yeast Dbp9. (**A**) Deduced amino acid sequence of Dbp9. The conserved motifs are highlighted in different colors depending of their functions. (**B**) Schematic representation of the primary structure of Dbp9. Color code of domains as above. The two RecA-like domains are showed in yellow and light green. Within the domains are indicated the conserved motifs. In blue, motifs involved in ATP binding and hydrolysis, in red, motifs involved in RNA binding and in green, motifs involved in the coordination of both functions. Both RecA-like motifs are flanked by N-and C-terminal extensions of different length.

5.7.- *In vitro* properties of Dbp9

5.7.1.- Expression and purification of recombinant Dbp9 wild-type and [K68A] mutant variant Dbp9

A C-terminal His_6-tagged Dbp9 fusion protein was constructed by introduction of the open reading frame of *DBP9* in the plasmid pET21b, under the control of an inducible T7 promoter. We also constructed a Dpb9 mutant variant, which harbour the point mutation K68A in motif I. To do so, the pET21b-His_6-DPB9 plasmid was mutagenized *in vitro.* Each plasmid was transformed into the *E. coli* BL21 Codon Plus. Transformed cells were grown, proteins overexpressed after IPTG induction and, recombinant proteins purified by affinity chromatography. To the affinity chromatography a nickel (Ni-NTA) agarose resin or a 5 mL HisTrap FF column (GE Healthcare) coupled to a FPLC system were used.

The elution fractions from the affinity chromatography were run in a denaturing polyacrylamide gel, in which a prominent protein band of about 70 kDa was observed (**Figure 66**). This molecular mass is similar to that estimated by sequence analysis (about 68 kDa). The band expected to be Dbp9 in the gel was confirmed by western blot using specific anti-polyhistidine antibodies (**data not shown**). Several other bands were also observed in the polyacrylamide gel. In the case of the FPLC purification, the peak observed in the chromatography was coincident with the elution peak in the gel.

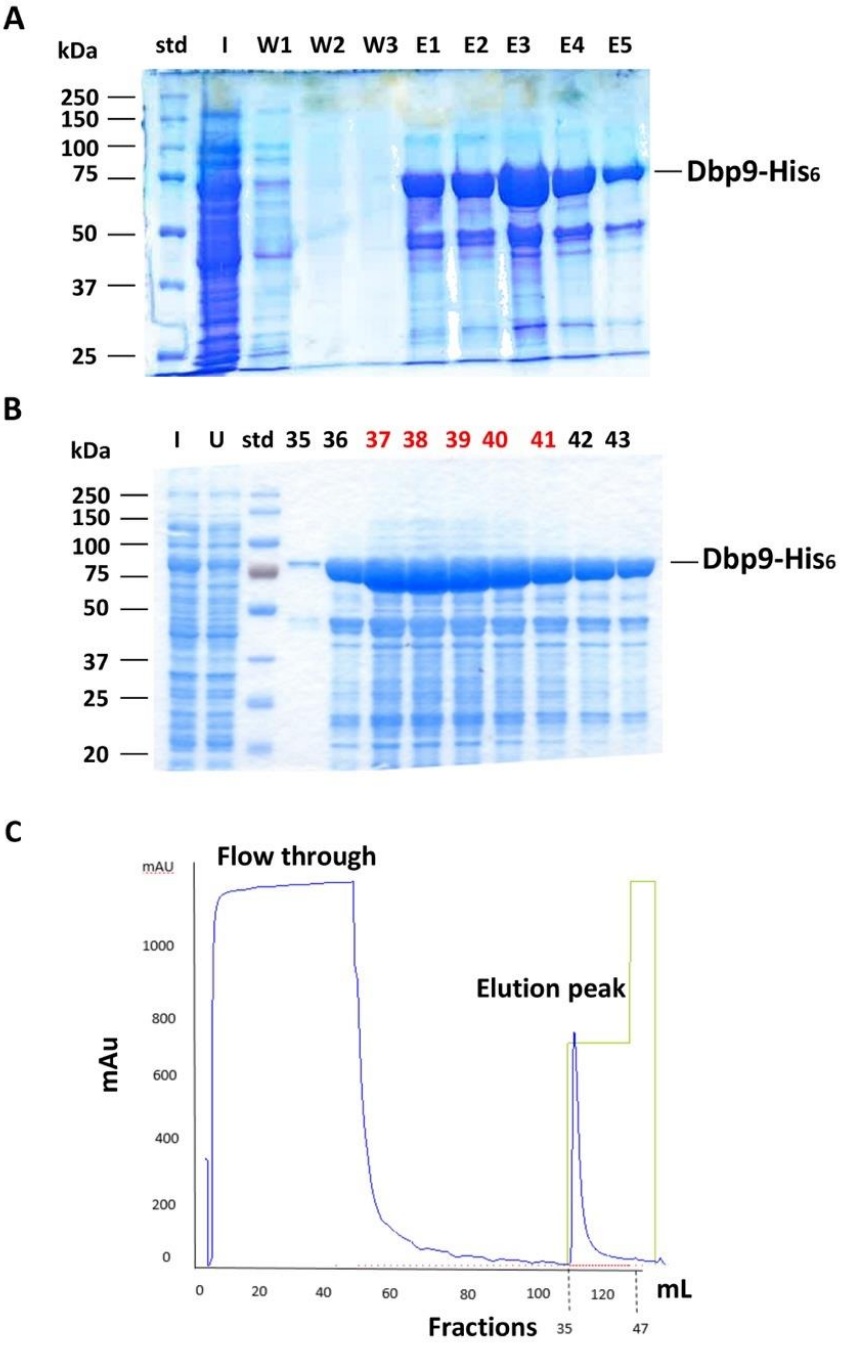

Figure 66. Purification of Dbp9 wild-type by affinity chromatography. (**A**) and (**B**) 10% SDS-PAGE gel showing the fractions obtained by affinity purification with Ni-NTA agarose resin or by a HisTrap FF column in a FPLC system, respectively. W1, W2, and W3 indicates wash volumes 1, 2 and 3. E1, E2, E3, E4, and E5 indicates elution volumes 1, 2, 3, 4 and 5 respectively. I, indicates input, std, protein standards and U, unbound proteins (**C**) Affinity purification chromatogram of recombinant Dbp9 wild-type obtained by affinity purification in a FPLC system. Dashed lines indicate the interval of fractions in which Dbp9 protein elutes. This interval corresponds to fractions 35 to 47. Fractions 37, 38, 39, 40 and 41 (marked in red in

the gel B) were pooled and injected in a Superdex 200 HiLoad 16/60 column. The flow through and elution peaks are indicated.

In order to detect multisubunit complexes, selected fractions from the affinity column from 37 to 41 in the example of **Figure 66,** were pooled and subjected to molecular exclusion chromatography. When calculated the molecular mass of the main peak of Dbp9 obtained by exclusion chromatography (fractions 16 to 29), the value was of about 77 kDa (**Figure 67B**). Thus, these results suggested that the wild-type Dbp9 protein likely eluted as a monomer. In addition, it was observed that Dbp9 was purified to electrophoretic homogeneity (**Figure 67A**). The lower band observed in SDS-PAGE gels (see red arrow) was also a product of Dbp9, as it was also revealed by anti-polyhistidine antibodies (**data not shown**).

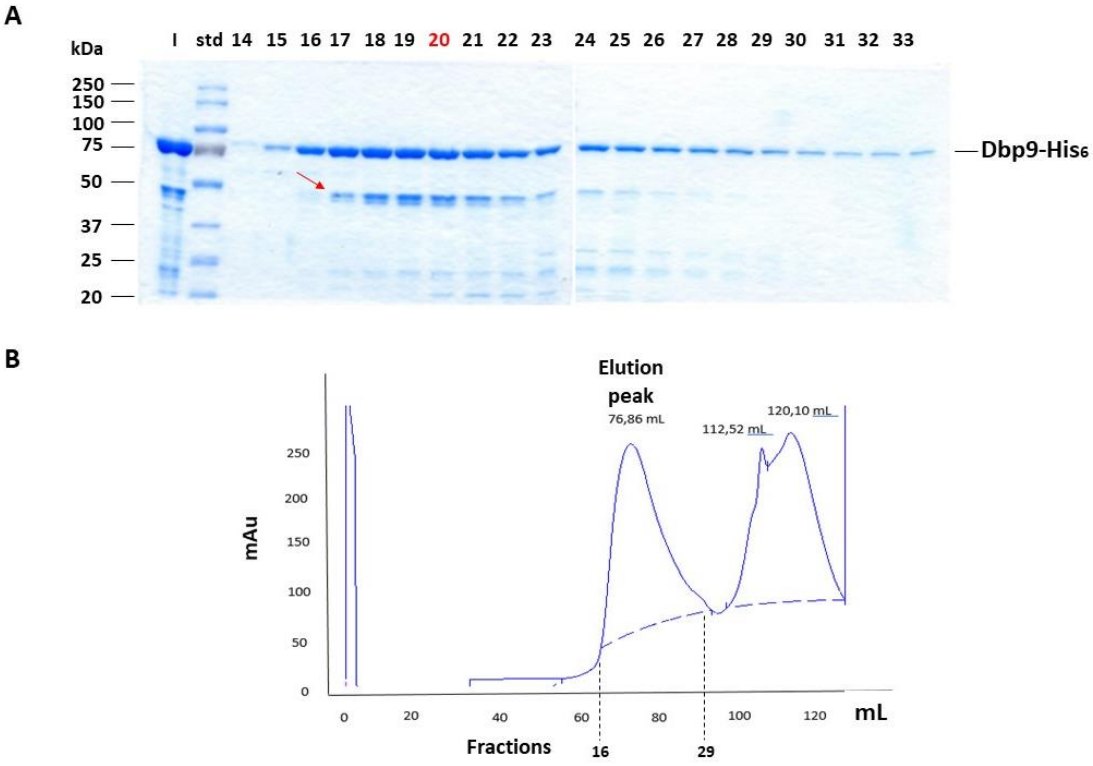

Figura 67. Purification of recombinant Dbp9 wild-type by molecular exclusion. (**A**) A 10% SDS-PAGE gel showing the fractions obtained after the chromatography. In red is marked the fraction eluting at about 77 mL. I indicates input and std protein standards (**B**) Chromatogram corresponding to a typical molecular exclusion chromatography of Dbp9 wild-type.

We also overexpressed in *E. coli* and purified the Dbp9[K68A] mutant version. The affinity purification profile by FPLC was very similar to that of wild-type Dbp9. Thus, an apparent molecular mass of about 70 kDa was calculated by SDS-PAGE for this variant, which is identical to that obtained for the Dbp9 wild-type protein. As above, the molecular exclusion profile obtained for the Dbp9[K68A] protein, and the further behaviour of the fractions obtained by SDS-PAGE gel were identical to the equivalent ones obtained for wild-type protein (**data not shown**).

5.7.2.- ATPase activity of Dbp9: colorimetric assay

In order to determine whether the DEAD-box Dbp9 protein is able to hydrolyze ATP, we performed ATPase assays following the colorimetric procedure previously used for recombinant Dbp7 protein (see Section 5.5.2 from Results), which evaluated the amount of Pi released during the course of the reaction. We also optimized some parameters of the assay, such as the reaction time or the temperature of the assay. For this section, was used the Dbp9 protein sample contained in the fraction named "elution 1" from an affinity chromatography by Ni-NTA agarose resin (see **Figure 66A**).

A) ATP concentration

We evaluated different concentrations of this nucleotide in the absence of exogenous RNA in the assay, as we suspected the presence of RNA in the preparations (see also the results obtained for recombinant Dbp7). As shown in the **Figure 68**, and as expected, the amount of ATP hydrolyzed positively correlated with the initial ATP concentration without saturation. To normalize respect the assay conditions used for recombinant Dbp7, we arbitrarily decided to use a concentration of 0.5 mM of ATP for further assays.

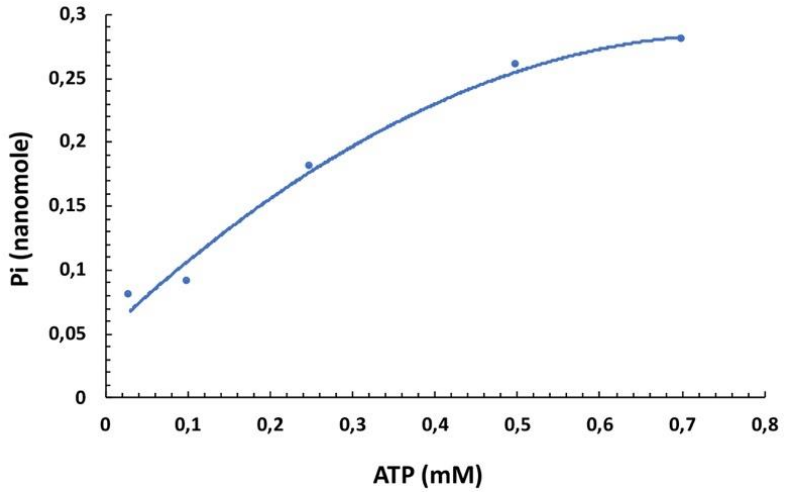

Figure 68. Plot of ATPase activity of Dbp9 wild-type with respect to ATP concentration. A colorimetric assay was used, which measures the amount of Pi released (y axis) at different ATP concentration (x-axis) during the assay. In the assays, 1.5 µg protein was used in a buffer containing 2 mM Mg^{2+}, pH 6.5. Note that no exogenous RNA was added. Reactions were performed at 30 ^{o}C and stopped after 10 min of incubation. The amount of free Pi was calculated using the linear regression obtained upon measuring the values given by different concentrations of NaH_2PO_4 in the colorimetric assay.

B) Protein concentration

As shown in the **Figure 69**, the protein concentration positive correlated with the Pi released. In other words, the higher concentration of protein, the higher ATP hydrolysis was also detected. For further analysis, 3.5 µg of protein were employed per assay.

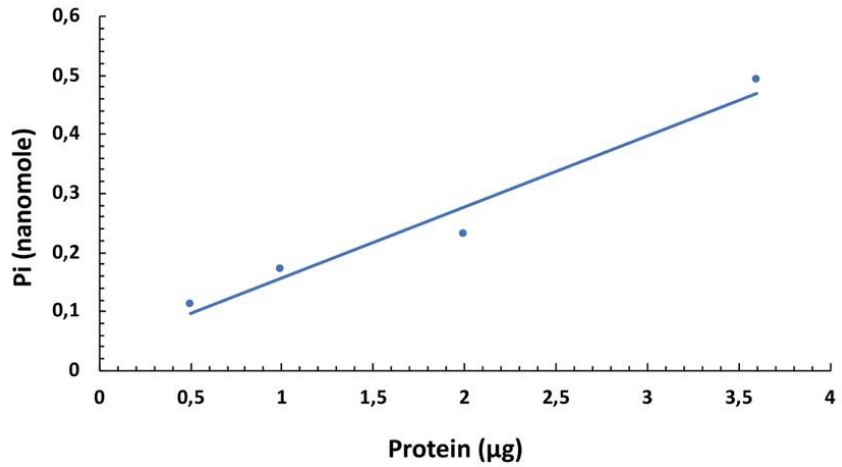

Figure 69. Plot of ATPase activity of Dbp9 wild-type with respect to protein concentration. A colorimetric assay was used, which measures the amount of Pi released (y axis) at different protein concentration (x-axis). The indicated amounts of protein were added to the reaction mixture; 0.5 mM ATP was used in a buffer containing 2 mM Mg^{2+}, pH 6.5. Note that no exogenous RNA was added. Reactions were performed at 30 ºC and stopped after 10 min of incubation. The amount of free Pi was calculated using the linear regression obtained upon measuring the values given by different concentrations of NaH_2PO_4 in the colorimetric assay.

C) Reaction time

We next assayed the relation between time and ATPase activity. As shown in **Figure 70**, and as expected, we obtained a positive correlation between the incubation time and the concentration of Pi released.

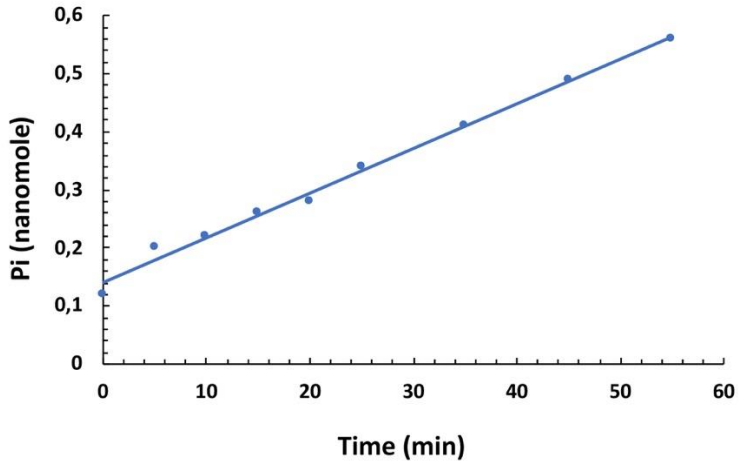

Figure 70. Plot of ATPase activity of Dbp9 wild-type along the time. A colorimetric assay was used, which measures the amount of Pi released (y-axis) at different times (x-axis). In the assays, 3.5 µg protein, and 0.5 mM ATP were used in a buffer containing 2 mM Mg^{2+}, pH 6.5. Note that no exogenous RNA was added. Reactions were performed at 30 ºC and stopped at the indicated times. The amount of free Pi was calculated using the linear regression obtained upon measuring the values given by different concentrations of NaH_2PO_4 in the colorimetric assay.

D) Temperature

We also performed ATPase assays at a range of different temperatures from 22 °C to 47 °C. As shown in **Figure 71**, all the temperatures assayed gave rise to the similar level of ATP hydrolysis

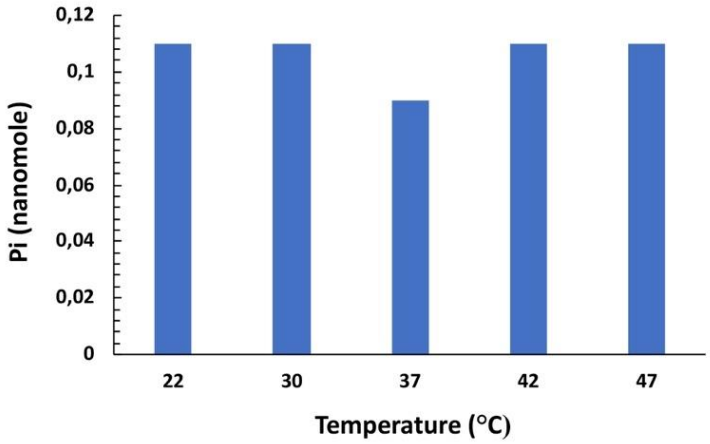

Figure 71. Bar diagram of ATPase activity of Dbp9 wild-type at different temperatures. A colorimetric assay was used, which measures the amount of Pi released (y-axis) at different temperatures (x-axis). Reactions contained 3.5 µg of protein, and 0.5 mM ATP in a buffer containing 2 mM Mg^{2+}, pH 6.5. Note that no exogenous RNA was added. Reactions were incubated at the indicated temperatures and stopped after 10 min of incubation. The amount of free Pi was calculated using the linear regression obtained upon measuring the values given by different concentrations of NaH_2PO_4 in the colorimetric assay.

5.7.3.- ATPase activity of Dbp9 wild-type and Dbp9[K68A] proteins: radioactive assays

To evaluate the dependence on RNA by the ATPase activity, we performed radioactive assays, which were previously used for the biochemical characterization of Dbp7 wild-type and the mutant variant Dbp7[K197A]. To this aim, we used fractions obtained after exclusion chromatography of Dbp9 and Dbp9[K68A] protein (i.e. from 16 to fraction 22). As RNA substrate, we used the single stranded RNA (ssRNA 1) of 58 nucleotides long that was previously used for the equivalent assays for Dbp7 (see Section 4.8 from Material and Methods, and **Table 3**). **Figure 72** shows the results obtained. Dbp9 did not present ATPase activity in the presence of ssRNA 1 as substrate (**Figure 72A**). Similar results were obtained for the Dbp9[K68A] protein (**Figure 72B**).

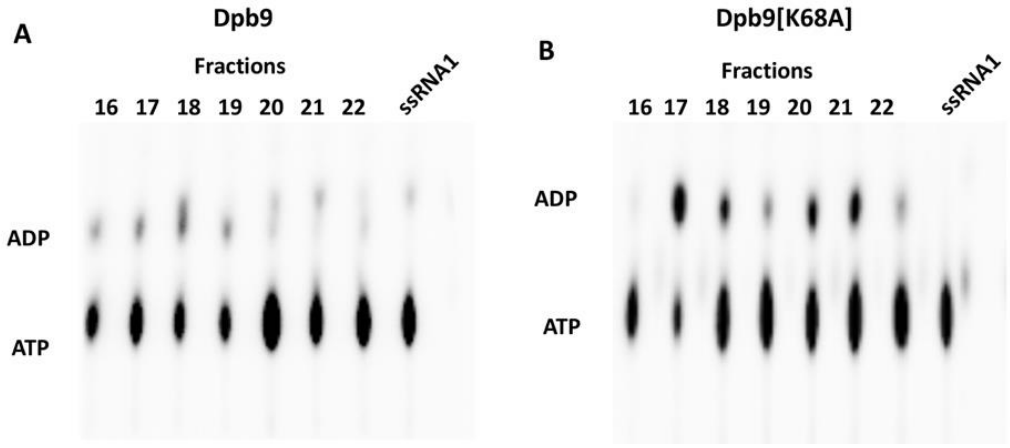

Figure 72. ATPase activity assay for Dbp9 wild-type and Dbp9[K68A] proteins. (**A**) and (**B)** Thin layer chromatography of the reaction products of the assays for Dbp9 wild-type and Dbp9[K68A] proteins, respectively. The assay contained 0.1 µg protein, 0.1 mM non-radioactive ATP, 0.2 µM [α-^{32}P] ATP and, 3 µM ssRNA 1 in a buffer containing 10 mM Mg^{2+}, pH 8.0. The reaction time was of 1 hour at 30 ^{o}C. No RNase A was added during the protein purification. The upper spots corresponded to the amount of ADP obtained from the ATP hydrolysis and the lower spots the remained ATP, which was not hydrolyze along the duration of the assay.

As a discrete ATPase activity was measured, assays in the presence of a different substrate were performed, in particular we made use of the DNA oligonucleotide previously used in the Dbp7 characterization, the oligonucleotide poly dT30. With this substrate, a more robust ATPase activity was detected using the same fractions used above (**Figure 73 A** and **B**). As shown in the quantification panel, no differences at the level of activity could be detected among the wild-type and the mutant Dbp9 (**Figure 73C**).

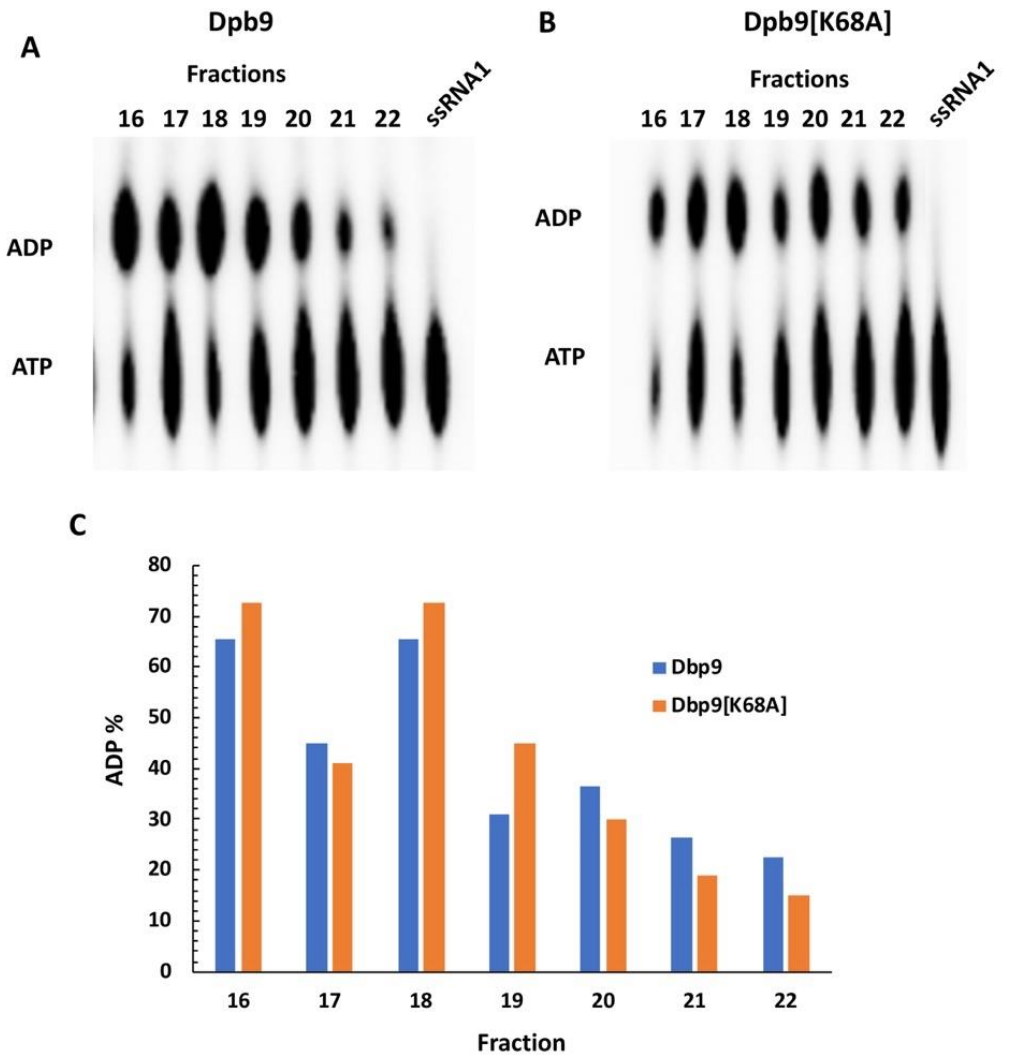

Figure 73. ATPase activity assay for Dbp9 wild-type and Dbp9[K68A] proteins using DNA oligonucleotide. (**A**) and (**B)** Thin layer chromatography of the reaction products of the assay for Dbp9 wild-type and Dbp9[K68A], respectively. The assay contained 0.1 µg protein, 0.1 mM ATP, 0.2 µM [α-^{32}P] ATP, and 0.5 µM poly dT30 in a buffer containing 10 mM Mg^{2+}, pH 8.0. The reaction time was of 1 hour at 30 ^{o}C. No RNase A was added during the protein purification. The upper spots corresponded to the amount of ADP obtained from the ATP hydrolysis and the lower spots the remained ATP, which was not hydrolyse along the duration of the assay. (**C)** Quantification of the ATPase activities detected in A and B. For this, the percentage of ADP released respect the ATP remained was calculated.

5.7.4.- RNA binding and unwinding activities of the recombinant Dbp9 wild-type protein *in vitro*

We only performed preliminary experiments regarding these activities using the same parameters previously established for the characterization of Dbp7 wild-type.

The capacity to bind to RNA of the fractions 17, 18 and 19 of Dbp9 wild-type was measured *in vitro* using the ssRNA1 as substrate. However, in contrast to Dbp7, Dbp9 did not form RNA-protein complexes in any of the fraction assayed (**data not shown**).

Concerning to the helicase activity, there were previous evidences that Dbp9 was able to unwind duplexes of nucleic acids even in absence of NTP. Interestingly, it was also reported that recombinant Dbp9 protein presented unwinding activity dependent of ATP hydrolysis on duplexes of DNA or of DNA-RNA (39). To test *in vitro* the unwinding activity of our Dbp9 wild-type protein preparation, we used the fraction 18 of the wild-type Dbp9 protein sample. As a substrate, we used a dsRNA with an overhand in the 3´ end (dsRNA 3´). However, Dbp9 did not present unwinding activity in the assay conditions (**data not shown**).

5.8.- Role of Dbp7 in the proper interaction with pre-ribosomal particles of a subset of snoRNAs

In addition to protein trans-acting factors, about 80 smalls nucleolar RNAs are required to facilitate the accurate progression of ribosome biogenesis. To perform their activity, snoRNAs perform imperfect base pairing with the pre-rRNAs. Indeed, snoRNAs can be detected in stable association with pre-ribosomal particles upon immunoprecipitation or on sucrose density gradients (72, 80) .

Our group has uncovered via synthetic lethal analysis a defined functional network involving the DEAD-box proteins Dbp6, Dbp7 and Dbp9, as well as the ribosomal protein uL3 and protein *trans*-acting factors Rsa3, Nop8, Rsa1, Npa1 and Npa2, all of them involved in early steps during the maturation of pre-60S ribosomal particles (18, 20, 73,

74). Some of these factors form a physical subcomplex that it has been referred to as Npa1 complex (37, 73). More recently, it has been shown that Npa1 bind to important rRNA elements in the $27SA_2$ pre-rRNA of early pre-60S ribosomal complexes, more specifically to distinct helices of rRNA domain I and VI (20, 37). In the neighborhood of the binding site of the Npa1 complex in early pre-60S precursors, it is found the binding site of different snoRNPs. Indeed, CRAC-analysis has shown that Npa1 crosslinks to a subset of these snoRNAs, including snR5, snR10, snR42, and snR190.

Interestingly, our group has reported that mutations in the 25S rRNA domain VI where snR190 binds are able to suppress the severe slow growth of the *dbp7Δ* mutant (21).

To assess whether Dbp7 has a relevant functional role that involve the supposed compactation reaction of the central core of 25S rRNA, we have performed different experiments. Thus, we first combined the null *dpb7* mutation with a mutation on the snR190 expected to impair the binding to its targeted site in 25S rRNA (Anthony Henras, unpublished results). We generated this combination by performing genetic crosses and sporulation of selected diploid strains. Double *dbp7Δ snr190* mutants were obtained as spore clones of different tetratype tetrads. The presence of the different mutations was confirmed by DNA sequencing. When the phenotype of tetratypes was inspected, we observed that the growth of the single *snr190* mutant was very similar to that of the wild-type (**Figure 74**). In turn, the growth defect of the single *dpb7Δ* spore clone was, as expected, very severe. Importantly, the growth defect of the *dbp7Δ* mutation was partially suppressed by the *snr190* mutation at 37 ^{o}C, both by drop tests and growth curves (**Figure 74**). Thus, specially at 37 ^{o}C, the *snr190* mutation led to a mild improvement in the growth of the *dbp7Δ* mutant (from 280 to 200 min), aspect that it is also observed at 30 ^{o}C (from 300 to 220 minutes).

A

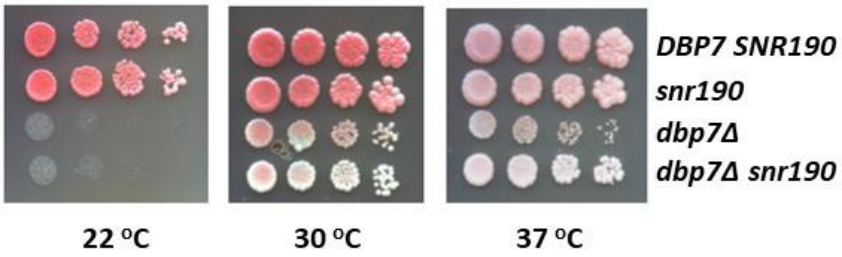
DBP7 SNR190
snr190
dbp7Δ
dbp7Δ snr190
22 °C
30 °C
37 °C

B

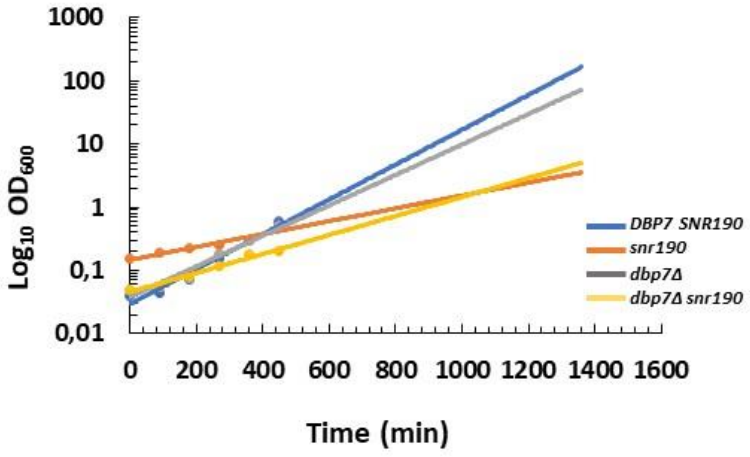
Log10 OD600
1000
100
10
1
0,1
0,01
0
200
400
600
800
1000
1200
1400
1600
Time (min)
DBP7 SNR190
snr190
dbp7Δ
dbp7Δ snr190

C

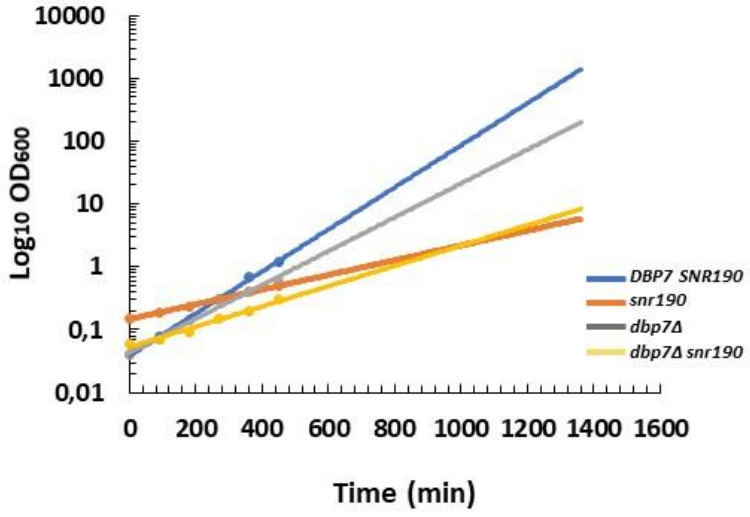
Log10 OD600
10000
1000
100
10
1
0,1
0,01
0
200
400
600
800
1000
1200
1400
1600
Time (min)
DBP7 SNR190
snr190
dbp7Δ
dbp7Δ snr190

Figure 73. Growth features of the *dbp7Δ-snR190* strain (**A**) The indicated strains, result of a representative tetratype after crossing single *dbp7Δ* and *snr190* mutants, were grown in YPD medium to an OD_{600} of 0.8. The cultures were diluted to an OD_{600} of 0.05 and then spotted in 10-fold serial dilutions onto YPD plates that were incubated at 22, 30 or 37 ºC. (**B** and **C**) Growth curves of the same strains. Cultures were initiated in liquid YPD medium and incubated at 30 or 37 ºC, respectively. Three biological replicates were done for each strain. The curves that correspond to a representative experiment of such ones are shown.

To further analyse the functional relationship of Dbp7 with snR190, we tested whether the absence of Dbp7 altered the association status of this and other neighbor snoRNAs with pre-ribosomal particles. Thus, we performed cell extracts from wild-type and *dbp7Δ* cells grown at 30 ºC, which were fractionated by centrifugation thorough low Mg^{+2} sucrose gradients. RNA was prepared from each fraction and analysed by northern blot following electrophoresis. The blots were then hybridized with specific probes directed against a set of different snoRNAs. Preliminary results showed that in *dpb7Δ* cells, there is an accumulation of snR190 in the fractions correspondent to pre-60S or 60S r-particles. Nevertheless, in the W303-1A strain the distribution of snR190 is homogeneous in all the fractions. The distribution of snR10, snR42, whose are snoRNAs located in the same area as snR190 was the same in both strains. Finally, snoRNAs control as snR5, which are located in other domain far away of snR190 area of 25S rRNA maintain also the same position in both strains (**Figure 74 A, B, C**).

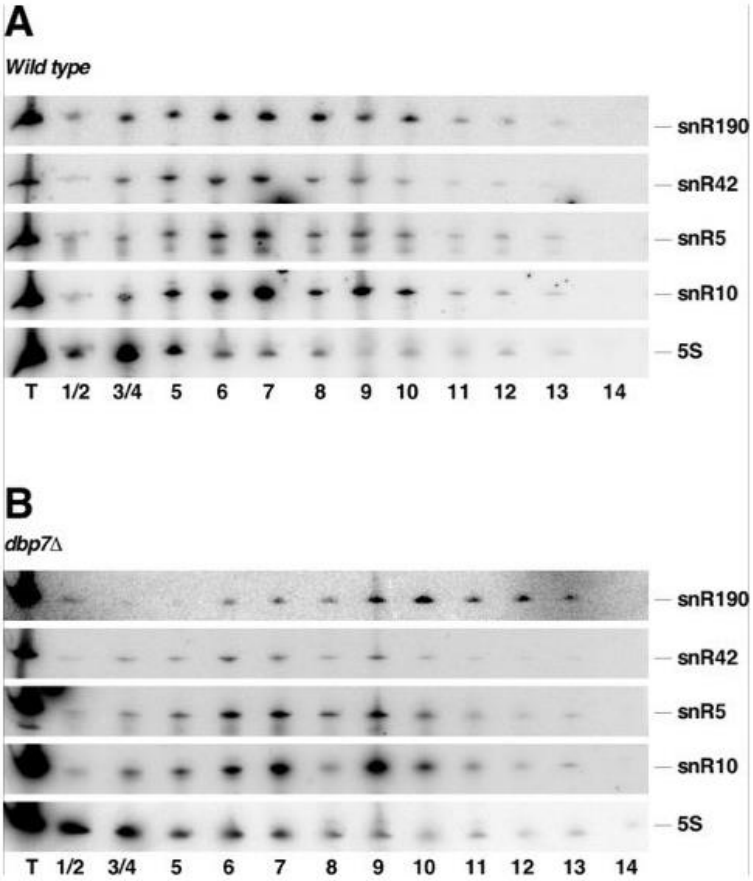
A
Wild type
snR190
snR42
snR5
snR10
5S
T 1/2 3/4 5 6 7 8 9 10 11 12 13 14
B
dbp7Δ
snR190
snR42
snR5
snR10
5S
T 1/2 3/4 5 6 7 8 9 10 11 12 13 14

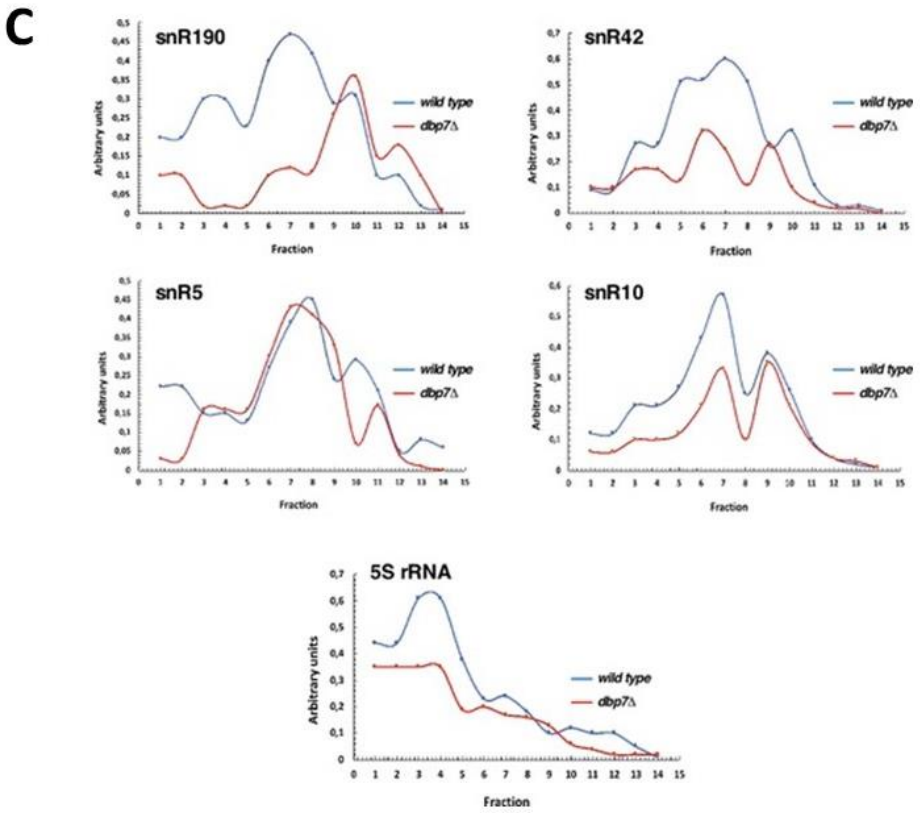

Figure 74. RNA hybridisation with specific probes directed against a set of different snoRNAs. (**A**) and (**B**) Nylon membrane showing the RNA hybridisation with snR190, snR42, snR10, snR5 and 5S RNA in W303 1-A and *dbp7Δ* strains, respectively. The RNA was obtained from the fractions collected from low Mg^{2+} sucrose gradients. At the bottom of the membranes are indicated the number of the fractions. T indicates the total extraction before particle fractionation, which is used as a control (**C**) Graphic representation of the accumulation of each snoRNA in W303 1-A (blue) and *dbp7Δ* (red) strains. In the x axis are indicated the fractions and in the y axis the level of snoRNA accumulation in arbitrary units. The level of accumulation of each snoRNA was normalised dividing the value of the snoRNA in each fraction between the total value of each snoRNA.

6. DISCUSSION

6.-DISCUSSION

The yeast Dbp7 protein is classified as a DEAD-box ATP-dependent RNA helicase according to its amino acid sequence. To date, the knowledge about Dbp7 is scarce; only a few papers have been published containing information about this protein (17, 18, 22, 71).

In 1998, Daugeron *et al.*, showed that Dbp7 was a nucleolar protein and that its absence resulted in slow-growing cells with reduced amounts of LSUs and accumulation of 80S and polysome half-mers. Thus, they, therefore, concluded that Dbp7 is involved in LSU biogenesis (17). In order to recapitulate some of the experiments by these researchers, we constructed a null haploid mutant strain lacking Dbp7 (*dbp7Δ*). This mutant strain was obtained by sporulation of the same heterozygous diploid strain (*dbp7Δ*/DBP7) used in above mentioned study (17). The phenotypes of *dbp7Δ* and *dbp7-1* strains were fully comparable. Additionally, we have generated a Dbp7-$(GA)_5$-3xyEGFP construct that confirms that Dbp7 localises in the nucleolus.

In growth experiments, *dbp7-1* and *dbp7Δ* showed, as expected, very similar phenotypical behaviour. Thus, both strains showed a slow growth in YPD medium, being this phenotype more pronounced at high (37 ^{o}C) or low (22 or 18 ^{o}C) temperatures than at 30 ^{o}C. The *dbp7Δ* strain showed aberrant polysome profiles, which displayed a decrease in the peak corresponding to the free LSU, and half-mers in the 80S peak and polysomes peaks. This aberrant profile was indistinguishable to that previously reported by Daugeron *et al.* with their *dbp7-1* strain. Therefore, our results confirm the fact, drawn by Daugeron *et al*., that nucleolar Dbp7 is a quasi-essential protein involved in LSU synthesis.

DEAD-box helicases usually contain the N- and C- terminal extensions that constitute protein or RNA binding platforms (19), providing the respective binders the specificity that the RNA helicases must harbour *in vivo*. In some cases, these extensions may also contain sequences to target the proteins to their functional location. Dbp7 contains two long N- and C- terminal extensions flanking the RecA-like domains. Although Dbp7 was

previously shown to be localized in the nucleolus (17), the mechanism that allow Dbp7 to travel to this subcellular compartment is still unknown. In our work, we have demonstrated the presence of an NLS in the N-terminal extension of Dbp7; this sequence allowed Dbp7 to reach the nucleus but not the nucleolus. Thus, another determinant must be present in the primary sequence of the protein to target Dbp7 to the nucleolus. Moreover, working with constructions of full length Dbp7, we concluded that this NLS is only necessary but not essential for the optimal transport of Dbp7 to the nucleus. Indeed, a Dbp7 construct lacking this NLS was still detected in the nucleus, although was also enriched in the cytoplasm, indicating that Dbp7 may contain additional sequences able to optimally bring the protein into the nucleus. These additional sequences must also map in the N-terminal tail of the protein, as a Dbp7 construct lacking the complete N-terminal extension of the protein is fully retained into the cytoplasm.

The fluorescent microscopy data are complemented by the phenotype of a strain lacking the NLS sequence (HA-*dbp7ΔNLS*), which showed an apparent wild-type growth phenotype and no LSU shortage at the level of polysome profiles. We assumed that, therefore, the herein identified NLS must be complemented by a second NLS present in the N-terminal end of the Dbp7 sequence to target it to the nucleus. Alternatively, Dbp7 can be redundantly imported to the nucleus bound to a second protein, a phenomenon known as piggy-backing.

The deletion of the complete N-terminal extension, or deletions of different size in the C-terminal extension of Dbp7 led to slow growth phenotype, decrease in free LSUs, and 80S and polysome half-mers. However, the truncated Dbp7 proteins showed the same sedimentation behaviour in low Mg^{2+} sucrose gradients than the full length Dbp7 protein. Therefore, the terminal extensions of Dbp7 seems not to be involved in the association of Dbp7 with pre-60S particles, but instead, provide other roles to the *in vivo* function of the protein, as indicated by the slow growth and ribosome biogenesis defects of the mutants in the N- and C- terminal extensions. These roles might consist on the

recruitment of other factors to execute whatever restructuring reaction might exert Dbp7 *in vivo* or the optimisation of the enzymatic catalytic activities of the protein.

We have also analysed the role of some of the conserved motifs within the two RecA-like domains of Dbp7. The amino acid residues that belong to the conserved motifs vary in importance. It is known that some of them carry out specific functions in ATP binding and hydrolysis, nucleic acid binding and unwinding or coordination between the ATP hydrolysis and the unwinding functions (7, 15, 80). For other RNA helicases, it has been reported that mutations in motif I, either in the first alanine residue, in the conserved lysine, or in the last threonine, reduce the affinity towards ATP and its hydrolysis (15). In motif VI, the first and second arginine residues could bind the γ-phosphate of the ATP, therefore, mutations in these residues affect ATP binding and hydrolysis (15). The functions that carry out the different residues (ATP binding and hydrolysis, and nucleic acid binding, and unwinding) are possible due to the interactions established between the different conserved motives (15).

To analyse the importance of the lysine of the motif I and the second arginine of the motif VI, we constructed the mutant strains HA-*dbp7*[K197A] and HA-*dbp7*[R553A] by site-directed mutagenesis. Usually, the equivalent changes of amino acids in the motifs I and VI of others DEAD-box helicases seriously affect the functionality of the respective proteins *in vivo*, and the binding and hydrolysis of ATP activities *in vitro*. Thus, DEAD-box helicases mutated in equivalent residues in motif I such as K92A in Has1, K52A in Dbp8, and K52R in Dbp8 were unable to complement the corresponding null mutants (30, 70). In motif VI, the mutation R376A in Has1 also showed a lethal phenotype (70). In our series of experiments, the growth of the HA-*dbp7*[K197A] and HA-*dbp7*[R553A] strains was significantly slower than that of the wild-type strain at 30 ^{o}C, although not as drastically affected as a complete loss-of-function mutation does. In agreement, the HA-*dbp7*[K197A] and HA-*dbp7*[R553A] showed a decrease in the peak of the free LSU subunits, with the appearance of half-mers polysomes only in HA-*dbp7*[K197A] strain.

We have purified recombinant Dbp7 protein to electrophoretical homogeneity. Our *in vitro* experiments showed that wild-type Dbp7 had ATPase activity dependent of ssRNA.

Strikingly, Dbp7 showed ATPase activity when using a ssDNA substrate, a poly dT of 30 nucleotides. Dbp7 is not the only DEAD-box protein that has been described to use DNA as a substrate since a similar case was observed for yeast Dbp9, whose ATPase activity was stimulated by DNA (39). Another examples of protein that use DNA in ATP hydrolysis are *Drosophila* Vasa or HCV CAP-Rf proteins and *S. cerevisiae* Mer3 (39).

We have also evaluated the ATPase activity of the Dbp7[K197A] mutant protein and surprisingly, it showed similar rates of ATPase as the wild-type protein. This fact could explain why the HA-*dbp7*[K197A] mutant strain has a very slight growth defect as its catalytically activities seems not to be impaired.

The K_M of Dbp7 wild-type measured using the deoxynucleotide poly dT of 30 nucleotides was about 300 µM. This K_M is in the range of the constant calculated for others DEAD-box helicases purified from *E. coli* as Has1 (440 µM), Ded1 (300 µM), Prp5 (438 µM), or eIF4A (470 µM) (15, 34, 70). The K_M of Dbp7[K197A] protein for the same DNA substrate was about200 µM, even lower than that of the wild-type protein. In contrast, mutations in the equivalent amino acid in others ATP-dependent RNA helicases generate an increase in the K_M values, and a decrease in the ATPase activity. Such is the case of Has1[K92A], which showed ~2-5% of the wild-type activity and almost 20 times higher K_M for ATP, or Dbp8, whose mutants Dbp8[K52A] and, Dbp8[K52R] showed a decrease ~ 10-fold in ATPase activity respect the wild-type protein (30, 70).

The function of this lysine of the motif I is coordinating the β-phosphate of the ATP, stabilizing the binding of ATP-Mg^{2+} during the catalysis (80). It is known that not only motif I but other motifs as F, II, V and VI participate in ATP binding and hydrolysis (7, 15, 80). Thus, we speculate, as the most parsimonious explanation, Dbp7[K197A] protein did not display a decreased ATPase activity, because the change K by A does not distort the motif of the enzyme and therefore its activity. Another plausible explanation is that Dbp7[K197A] could have a redundant motif with motif I, which could be the one promoting ATPase activity. Finally, we could not discard that other residues can replace the function of K197; K184, A181 or T188 are alternative residues able to conform a functional non-orthodox motif I. It is known that the two last residues are also involved

in ATP binding and hydrolysis. In fact, in some enzymes the last threonine of the motif I is found in the vicinity of the Mg^{2+} ion, being able to also stabilize the binding ATP-Mg^{2+} (15).

Motif VI plays an important role in ATPase and helicase activities through the communication with the motif II. Mutants in the second arginine of the motif VI in Dbp7 (Dbp7[R553A]) showed slightly higher ATPase activity than the wild-type protein. However, in other DEAD-box helicases such as eIF4A, equivalent mutations of the conserved arginine residues of this motif (R359Q, R362Q, R365Q) impair ATP hydrolysis, RNA binding, and helicase activity, likely due to the loss of the coordination between motif VI and motif II (15, 63). Schneider and Schwer in 2001, showed that the mutation of the second arginine of motif VI in Prp22 drastically reduced the ATPase activity of the protein (77). Additionally, Dbp9 mutants in the second arginine of motif VI (R414I, R414T and R414K) did not have ATPase activity (39). Maybe the increase of the ATPase activity of the Dbp7[R553A] protein is caused by a communication breakdown between motifs VI and II. In this regard, it is worth to note that the amino acid sequence of the motif II of Dbp7 deviates (DE**G**D) respect with the canonical sequence (DE**A**D).

The ATPase activity of Dbp7 had a particular behaviour, since the increase in the substrate concentration generates a decrease in the ATP hydrolysis velocity. It is possible that this behaviour relates to the non-processive helicases mechanism. The non-processive enzymes only unwind about 6-10 base pairs of RNA duplex in each ATP hydrolysis cycle (13, 19, 35). When the short duplex is opened the enzyme can inhibit the reaction if the unwinding activity is not required yet. Nonetheless, it is more probably that this behaviour, although unclear for us, could be due to product inhibition. Upon ATP hydrolysis, two products are generated: ADP and Pi. In this scenario, the ADP could bind to the ATP binding pocket of the enzyme and inhibit the reaction. This is apparently the case for the inhibition exerted by the recombinant Has1 protein (70). However, we were unable to detect inhibition by ADP at the concentration used. We cannot discard a possible inhibition by Pi. It is possible that the Pi could bind to a second site in the enzyme and act as an allosteric inhibitor. This mechanism could avoid the

unnecessary use of the substrate and the products accumulation. An inhibition by substrate (ATP) is also possible, but in this case, it may exist a negative cooperative relationship between protein and substrate; when the substrate binds to the protein the affinity of the protein by the substrate decreases. In this regard, the DEAD-box helicase Has1 contains a consensus sequence of the motif I localised downstream of the motif VI (^{383}GTKGKGKS^{390}), which is probably also involved in ATP binding. It was demonstrated that mutation K389A in this second Walker A motif increased the ATP hydrolysis rate of the Has1 mutant enzyme. Interestingly, an *in vivo* K389A mutant had no effect on cell growth. This fact suggests that Has1 has two putative motifs for ATP binding; one of high and a second of low ATP affinity. According to this possibility, ATP can be accommodated in two ATP binding sites: the site in the motif I (high ATP affinity) or the site in the motif downstream of the motif VI (low ATP affinity). It has been suggested that when the lysine in the second Walker A motif is mutated (K389A), ATP could only bind in the high affinity site and the hydrolysis occur faster (70). Despite this possibility, we cannot find a possible second ATP binding motif with a sequence consensus of motif I in Dbp7. In contrast, Dbp9 contains downstream of motif VI a possible consensus sequence of the motif I (^{415}ARGGKT^{420}). Therefore, the presence of a putative second ATP binding motif could be a characteristic shared by different members of the DEAD-box family of proteins.

According to our *in vitro* experiments, Dbp7 had also the ability to bind RNA. We detected two different bands corresponding to different Dbp7-RNA complexes in gel shifts assays. Similar results were obtained with the recombinant Dbp7[K197A] mutant protein. This result suggests that Dbp7 could bind the RNA substrate in form of a monomer or a multiprotein complex. In fact, our molecular exclusion chromatography data suggest that Dbp7 could have a tendency to form dimers.

ATP dependent RNA helicases are able to open RNA duplexes following different mechanism. Usually, RNA helicases need a single stranded RNA region (overhand), where the helicase binds, to open the dsRNA but in other cases, these enzymes are able to open blunt ends RNA duplexes. Moreover, some RNA helicases can show polarity or

directionality, that is defined as the direction (5´-3 or 3´-5´) of the helicase movement on the ssRNA along which it is moving. Our *in vitro* experiments also demonstrated that wild-type Dbp7 and Dbp7[K197A] proteins are able to unwind RNA duplexes in both 5´-3´and 3´-5´directions. The RNA helicase activity of Dbp7 is comparable to that of others DEAD-box RNA helicases, such as Ded1, which is able to unwind blunt ends duplexes (34). Similarly, Has1 unwinds RNA/DNA duplexes in both directions, showing higher extend of unwinding with the 5´ RNA/DNA duplexes (70).

In light of the *in vitro* results, Dbp7 has ATPase activity, it is able to bind RNA, and displays helicase activity, as several others DEAD-box RNA helicases do. However, our results show some Dbp7 features that make it special. Such features are related with the conserved residues that contain the DEAD-box proteins. Firstly, the residue K197 of motif I seems to be no essential for ATP binding and hydrolysis, while in others DEAD-box RNA helicases this motif is strictly essential for ATPase activity; secondly, the conserved motif II, which is DEAD in the most of DEAD-box helicases, is deviated to DEGD in Dbp7.

To better understand why the mutation K197A in Dbp7 did not affect the ATPase activity of the protein *in vitro*, we decided to study the equivalent mutation in a Dbp7-related DEAD-box helicase. The DEAD-box helicase chosen was Dbp9 because i) the sequence of the motif II of Dbp9 (DE**V**D) is also deviated respect the canonical sequence (DE**A**D), as it occurs in Dbp7 (DE**G**D); ii) both proteins are involved in LSU biogenesis, most likely, in the same early step of this process; and iii) Dbp7 and Dbp9 genetically interact, as the null *dbp7* allele synthetically enhances the slow growth phenotype of distinct *dbp9* alleles (16, 17, 18). The enzymatic activities of Dbp9 were previously studied by Kikuma *et al*. in 2004. They determined that the ATPase activity of Dbp9 is stimulated by DNA and inhibited by RNA, Dbp9 presents RNA/DNA helicase activity dependent of ATP, and mutations in the second arginine residue in the motif VI abolish this helicase activity (39). In consonance, our results showed that Dbp9 does not display ATPase activity in presence of a ssRNA, unlike Dbp7. As it occurs for Dbp7, ATPase activity could be detected for recombinant Dbp9 when a DNA poly dT oligonucleotide is included in the

reaction mix. Surprisingly, as it also occurs for Dbp7, no differences could be detected for the ATPase activity of Dbp9 wild-type and mutant Dbp9[K68A] protein, which harbours a mutation in motif I.

Dbp7 and Dbp9 show similar features that could led us to understand why the mutants in the lysine of the motif I have ATPase activity at the same level as the wild-type proteins. However, it is necessary to perform more *in vitro* and *in vivo* assays to decipher the action mechanism of these enzymes.

In the last part of this thesis, we have explored the precise *in vivo* role of Dbp7 in LSU biogenesis. Dbp7 is part of a functional interaction network that also includes Dbp6, Dpb9, Npa1, Npa2, Nop8, Rsa3, Rsa1, and the ribosomal protein uL3 (18). Among these factors, Npa1, Npa2, Rsa3, Nop8 and Dbp6 form the Npa1 complex. (74). Dbp7 is not part of this physical complex, but it could interact with it through the binding to Dbp6 or Dbp9, as a part of a helicase heterodimer. The function of the Npa1 complex has been related to the control of snoRNA/pre-RNA interactions; it has been shown to be important for the structural rearrangement of rRNA domains I and II during the earliest reaction of formation of LSU precursor particles (37). It is known that Npa1 interact with several snoRNAs involved in the decoding centre and the peptidyl transferase centre modifications in the environment of the binding sites of these snoRNAS on 25S rRNA (37). Thus, Dbp6, Dbp9, and Dbp7 would be the responsible for the establishment of the binding or dissociation of these snoRNAs from 25S rRNA (37). We determined that mutations in the 25S rRNA region, where snR190 binds, are able to suppress the severe slow growth of the *dbp7Δ* mutant (21). Apparently, these mutations will relax or impede the interaction of snR190 with the 25S rRNA, suggesting that the *in vivo* function of Dbp7 must be related to the dissociation of distinct snoRNAs from early pre-60S ribosomal particles. To explore this view, a mutant lacking Dbp7 and harbouring a snR190, apparently unable to base pair to its binding site in 25S rRNA, was constructed. When we analysed the growth of this double mutant, a clear suppression of the growth defect phenotype of the *dbp7Δ* mutation was observed. This result suggests that in the absence of Dbp7, snR190 exert a negative role in ribosome biogenesis, and therefore in growth.

To test the association status of different snoRNAs with pre-ribosomal particles in the presence or absence of Dbp7, we obtained cell extracts of isogenic wild type and *dbp7Δ*, which were fractionated through low Mg^{+2} sucrose gradients. RNA was prepared from the fractions and analysed by northern blotting with specific probes against a set of snoRNAs included snR190. Interestingly, this analysis showed a clear and specific accumulation of snR190 in the fractions corresponding to pre-60S and 60S r-particles in the *dbp7Δ* strain, compared to the wild-type strain. These data strongly suggest that Dbp7 is required for snR190 dissociation from pre-60S ribosomal particles. Therefore, we envisage a scenario where the loss-of-function of Dbp7 impairs snR190 dissociation from early pre-60S ribosomal particles leading to formation of aberrant particles that are unable to progress in their maturation, and consequently being subjected to degradation. In this scenario, the simultaneous absence of a productive interaction of snR190 with these particles might partially alleviate the conformational constraints in their maturation. Further experiments are required to demonstrate this view.

7. CONCLUSIONS

7.-CONCLUSIONS

1.- Dbp7 and Dbp9 are two members of the *DEAD-box* protein subfamily of RNA helicases that contain RecA-like conserved cores flanked by N- and C- terminal extensions. The extensions from Dbp7 contribute to growth and ribosome biogenesis.

2.- Dbp7 contains a nuclear localization signal (NLS) in its N- terminal extension. This NLS serves for transporting the protein into the nucleus, but not to the nucleolus. The identified NLS may not be the sole sequence responsible for the nuclear transport of Dbp7.

3.- Strains containing point mutations either in the domain I (K197A) or in the domain VI (R553A) of Dbp7 show growth and ribosome biogenesis defects *in vivo*, though these defects are not as severe as those displayed by the null *dbp7* strain.

4.- *In vitro*, recombinant Dbp7 possesses RNA- and DNA-dependent ATPase activity, binds single-stranded RNA, and unwinds double-stranded RNA in an ATPase-dependent manner.

5.- *In vitro*, recombinant Dbp7[K197A] and Dbp7[R553A] also possess RNA-dependent ATPase activity. Dbp7[K197A] binds single-stranded RNA, and unwinds double-stranded RNA in an ATPase-dependent manner. These activities are apparently similar to those of recombinant wild-type Dbp7.

6.- *In vitro*, recombinant wild-type Dbp9 possesses DNA-dependent ATPase activity.

7.- *In vivo*, Dbp7 is required for the release of snR190 from pre-ribosomal particles.

8. BIBLIOGRAPHY

8.- BIBLIOGRAPHY

1. Alberts B, Johnson A, Lewis J, Raff M, Roberts K, Walter P. (2008). Molecular biology of the cell. The RNA message is decoded by ribosomes, 374-378.
2. Andreou AZ, Klostermeier D. (2013). The DEAD-box helicase eIF4A: paradigm or the odd one out? RNA Biol 10: 19-32.
3. Aregger R, Klostermeier D. (2009). The DEAD box helicase YxiN maintains a closed conformation during ATP hydrolysis. Biochemistry 48: 10679-10681.
4. Barrio-Garcia C *et al*. (2016). Architecture of the Rix1-Rea1 checkpoint machinery during pre-60S-ribosome remodeling. Nat Struct Mol Biol 23: 37-44.
5. Bassler J, Kallas M, Hurt E. (2006). The NUG1 GTPase reveals and N-terminal RNA-binding domain that is essential for association with 60 S pre-ribosomal particles. J Biol Chem 281: 24737-24744.
6. Ben-Shem A, Garreau de Loubresse N, Melnikov S, Jenner L, Yusupova G, Yusupov M. (2011). The structure of the eukaryotic ribosome at 3.0 Å resolution. Science 334: 1524-1529.
7. Bernstein K.A, Granneman S, Lee A.V, Manickam S, Baserga S.J. (2006). Comprehensive mutational analysis of yeast DEXD/H box RNA helicases involved in large ribosomal subunit biogenesis. Mol Cell Biol 26: 1195-1208.
8. Calviño FR *et al*. (2015). Symportin 1 chaperones 5S RNP assembly during ribosome biogenesis by occupying an essential rRNA-binding site. Nat Commun 6: 6510.
9. Caruthers JM, Johnson ER, McKay DB. (2000). Crystal structure of yeast initiation factor 4A, a DEAD-box RNA helicase. Proc Natl Acad Sci U S A 97: 13080-13085.
10. Cerezo E *et al*. (2019). Maturation of pre-40S particles in yeast and humans. Wiley Interdiscip Rev RNA 10: e1516.
11. Chaker-Margot M, Barandun J, Hunziker M, Klinge S. (2017). Architecture of the yeast small subunit processome. Science 355: eaal1880.

12. Chaker-Margot M, Hunziker M, Barandun J, Dill BD, Klinge S. (2015). Stage-specific assembly events of the 6-MDa small-subunit processome initiate eukaryotic ribosome biogenesis. Nat Struct Mol Biol 22: 920-923.
13. Chen Y, Potratz JP, Tijerina P, Del Campo M, Lambowitz AM, Russell R. (2008). DEAD-box proteins can completely separate an RNA duplex using a single ATP. Proc Natl Acad Sci U S A 105: 20203-20208.
14. Ciganda M, Williams N. (2011). Eukaryotic 5S rRNA biogenesis. Wiley Interdiscip Rev RNA 2: 523-533.
15. Cordin O, Banroques J, Tanner N.K, Linder P. (2006). The DEAD-box protein family of RNA helicases. Gene 367: 17-37.
16. Daugeron M.C, Kressler D, Linder P. (2001). Dbp9p, a putative ATP-dependent RNA helicase involved in 60S-ribosomal-subunit biogenesis, functionally interacts with Dbp6p. RNA 7: 1317-1334.
17. Daugeron M.C, Linder P. (1998). Dbp7p, a putative ATP-dependent RNA helicase from Saccharomyces cerevisiae, is required for 60S ribosomal subunit assembly. RNA 4: 566-561.
18. de la Cruz J, Lacombe T, Deloche O, Linder P, Kressler D. (2004). The putative RNA helicase Dbp6p functionally interacts with Rpl3p, Nop8p and the novel trans-acting Factor Rsa3p during biogenesis of 60S ribosomal subunits in Saccharomyces cerevisiae. Genetics 166: 1687-1699.
19. de la Cruz J, Kressler D, Linder P. (1999). Unwinding RNA in *Saccharomyces cerevisiae*: DEAD-box proteins and related families. Trends Biochem Sci 24: 192-198.
20. Dez C, Froment C, Noaillac-Depeyre J, Monsarrat B, Caizergues-Ferrer M, Henry Y. (2004). Npa1p, a component of very early pre-60S ribosomal particles, associates with
a subset of small nucleolar RNPs required for peptidyl transferase center modifi cation. Mol Cell Biol 24: 6324-6337.

21. Domínguez H. (2014). Análisis genético y molecular de helicasas de RNA implicadas en la síntesis de la subunidad 60S del ribosoma de *Saccharomyces cerevisiae.* Thesis master.

22. Fairman-Williams M.E, Guenther U.P, Jankowsky E. (2010). SF1 and SF2 helicases: family matters. Curr Opin Struct Biol 20: 313-324.

23. Fatica A, Oeffinger M, Dlakić M, Tollervey D. (2003). Nob1p Is Required for Cleavage of the 3' End of 18S rRNA. Mol Cell Biol 23: 1798-1807.

24. Fernández-Pevida A, Kressler D, de la Cruz J. (2015). Processing of Preribosomal RNA in *Saccharomyces cerevisiae*. Wiley Interdiscip Rev RNA 6: 191-209.

25. Frank J, Agrawal RK. (2000). A ratchet-like inter-subunit reorganization of the ribosome during translocation. Nature 406: 318-322.

26. Gasse L, Flemming D, Hurt E. Coordinated Ribosomal ITS2 RNA Processing by the Las1 Complex Integrating Endonuclease, Polynucleotide Kinase, and Exonuclease Activities. (2015). Mol Cell 60: 808-815.

27. Gerhardy S, Menet A.M, Peña C, Petkowski J.J, Panse V.G. (2014). Assembly and nuclear export of pre-ribosomal particles in budding yeast. Chromosoma 123: 327-344.

28. Gilman B, Tijerina P, Russell R. (2017). Distinct RNA-unwinding mechanisms of DEAD-box and DEAH-box RNA helicase proteins in remodeling structured RNAs and RNPs. Biochem Soc Trans 45: 1313-1321.

29. Gorbalenya A.E, Koonin E.V. (1998). Helicases: amino acid sequence comparisons and structure-function relationships. Curr opin struc biol 3: 419-429.

30. Granneman S, Lin CY, Champion EA, Nandineni MR, Zorca C, Baserga SJ. (2006). The Nucleolar Protein Esf2 Interacts Directly With the DExD/H Box RNA Helicase, Dbp8, to Stimulate ATP Hydrolysis. Nucleic Acids Res 34: 3189-3199.

31. Henry Y, Wood H, Morrissey JP, Petfalski E, Kearsey S, Tollervey D. (1994). The 5' end of yeast 5.8S rRNA is generated by exonucleases from an upstream cleavage site. EMBO J 13: 2452-2463.
32. Hughes JM, Ares M Jr. (1991). Depletion of U3 small nucleolar RNA inhibits cleavage in the 5' external transcribed spacer of yeast pre-ribosomal RNA and impairs formation of 18S ribosomal RNA. EMBO J 10: 4231-4239.
33. Hunziker M*el al*. (2016). UtpA and UtpB chaperone nascent pre-ribosomal RNA and U3 snoRNA to initiate eukaryotic ribosome assembly. Nat Commun 7: 1-10.
34. Iost I, Dreyfus M, Linder P. (1999). Ded1p, a DEAD-box protein required for translation initiation in Saccharomyces cerevisiae, is an RNA helicase.J Biol Chem 274: 17677-17683.
35. Jacewicz A, Schwer B, Smith P, Shuman S. (2014). Crystal structure, mutational analysis and RNA-dependent ATPase activity of the yeast DEAD-box pre-mRNA splicing factor Prp28. Nucleic Acids Res 42: 12885-12898.
36. Jarmoskaite I, Russell R. (2011). DEAD-box proteins as RNA helicases and chaperones. Wiley Interdiscip Rev RNA 2: 135-152.
37. Joret C *et al*. (2018). The Npa1p complex chaperones the assembly of the earliest eukaryotic large ribosomal subunit precursor. PLoS Genet 14: e1007597.
38. Kater L *et al*. (2017). Visualizing the Assembly Pathway of Nucleolar Pre-60S Ribosomes. Cell 171: 1599-1610.
39. Kikuma T *et al*. (2004). Dbp9p, a member of the DEAD box protein family, exhibits DNA helicase activity. J Biol Chem 279: 20692-20698.
40. Klinge S, Woolford J.L Jr. (2019). Ribosome assembly coming into focus. Nat Rev Mol Cell Biol 20: 116-131.
41. Konikkat S, Woolford J.L Jr. (2017). Principles of 60S ribosomal subunit assembly emerging from recent studies in yeast. Biochem J 474: 195-214.
42. Kornprobst M *et al*. (2016). Architecture of the 90S Pre-ribosome: A Structural View on the Birth of the Eukaryotic Ribosome. Cell 166: 380-393.

43. Kos M, Tollervey D. (2010). Yeast pre-rRNA processing and modification occur cotranscriptionally. Mol Cell 37: 809-820.
44. Kressler D, Hurt E, Baßler J. (2017). A Puzzle of Life: Crafting Ribosomal Subunits. Trends Biochem Sci 42: 640-654.
45. Kressler D, de la Cruz J, Linder P. (1998). Dbp6p Is an Essential Putative ATP-dependent RNA Helicase Required for 60S-ribosomal-subunit Assembly in *Saccharomyces Cerevisiae.* Mol Cell Biol 18: 1855-1865.
46. Kressler D. (2012). Synchronizing nuclear import of ribosomal proteins with ribosome assembly. Science 338: 666-671.
47. Lebaron S *et al*. (2012). Proofreading of pre-40S ribosome maturation by a translation initiation factor and 60S subunits. Nat Struct Mol Biol 19: 744-753.
48. Leidig C *et al*. (2014). 60S ribosome biogenesis requires rotation of the 5S ribonucleoprotein particle. Nat Commun 5: 3491.
49. Leitão A.L, Costa M.C, Enguita F.J. (2015). Unzippers, resolvers and sensors: a structural and functional biochemistry tale of RNA helicases. Int J Mol Sci 16: 2269-2293.
50. Linder P, Jankowsky E. (2011). From unwinding to clamping - the DEAD box RNA helicase family. Nat Rev Mol Cell Biol 12: 505-516.
51. Liu F, Putnam A, Jankowsky E. (2008). ATP hydrolysis is required for DEAD-box protein recycling but not for duplex unwinding. Proc Natl Acad Sci U S A 105: 20209-20214.
52. Liu F, Putnam AA, Jankowsky E. (2014). DEAD-box helicases form nucleotide-dependent, long-lived complexes with RNA. Biochemistry 53: 423-433.
53. Ma C *et al*. (2017). Structural snapshot of cytoplasmic pre-60S ribosomal particles bound by Nmd3, Lsg1, Tif6 and Reh1.Nat Struct Mol Biol 24: 214-220.
54. Mallam A.L, Sidote D.J, Lambowitz A.M. (2014). Molecular insights into RNA and DNA helicase evolution from the determinants of specificity for a DEAD-box RNA helicase. Elife 3: e04630.
55. Manikas R.G, Thomson E, Thoms M, Hurt E. (2016). The K^+-dependent GTPase Nug1 is implicated in the association of the helicase Dbp10 to the immature

peptidyl transferase centre during ribosome maturation. Nucleic Acids Res 44: 1800-1812.

56. Martin R, Straub AU, Doebele C, Bohnsack MT. (2013). DExD/H-box RNA helicases in ribosome biogenesis. RNA Biol 10: 4-18.

57. Matsuo Y, Granneman S, Thoms M, Manikas RG, Tollervey D, Hurt E. (2014). Coupled GTPase and remodelling ATPase activities form a checkpoint for ribosome export. Nature 505: 112-116.

58. McCaughan UM, Jayachandran U, Shchepachev V, Chen ZA, Rappsilber J, Tollervey D, Cook AG. (2016). Pre-40S ribosome biogenesis factor Tsr1 is an inactive structural mimic of translational GTPases. Nat Commun 7: 11789.

59. Melnikov S, Ben-Shem A, Garreau de Loubresse N, Jenner L, Yusupova G, Yusupov M. (2012). One core, two shells: bacterial and eukaryotic ribosomes. (2012). One core, two shells: bacterial and eukaryotic ribosomes. Nat Struct Mol Biol 19: 560-567.

60. Nomura M, Nogi Y, Oakes M. (2004). Transcription of rDNA in the yeast *Saccharomyces cerevisiae*. Madame Curie Bioscience Database. Austin (TX): Landes Bioscience. Oncology.

61. Oh JY, Kim J. (1999). ATP hydrolysis activity of the DEAD box protein Rok1p is required for in vivo ROK1 function. Nucleic Acids Res 27: 2753-2759.

62. Osheim Y.N *et al*. (2004). Pre-18S ribosomal RNA is structurally compacted into the SSU processome prior to being cleaved from nascent transcripts in Saccharomyces cerevisiae. Mol Cell 16: 943-954.

63. Pause A, Méthot N, Sonenberg N. (1993). The HRIGRXXR Region of the DEAD Box RNA Helicase Eukaryotic Translation Initiation Factor 4A Is Required for RNA Binding and ATP Hydrolysis. Mol Cell Biol 13: 6789-6798.

64. Peña C, Hurt E, Panse V.G. (2017). Eukaryotic ribosome assembly, transport and quality control. Nat Struct Mol Biol 24:689-699.

65. Pérez-Fernández J, Martín-Marcos P, Dosil M. (2011). Elucidation of the assembly events required for the recruitment of Utp20, Imp4 and Bms1 onto nascent pre-ribosomes. Nucleic Acids Res 39: 8105-8121.
66. Pérez-Fernández J, Román A, De Las Rivas J, Bustelo X.R, Dosil M. (2007).The 90S preribosome is a multimodular structure that is assembled through a hierarchical mechanism. Mol Cell Biol 27: 5414-5429.
67. Planta RJ, Mager WH. (1998). The list of cytoplasmic ribosomal proteins of Saccharomyces cerevisiae. Yeast 14: 471-477.
68. Putnam A.A, Jankowsky E. (2013). DEAD-box helicases as integrators of RNA, nucleotide and protein binding. Biochim Biophys Acta 1829: 884-893.
69. Ramakrishnan V, White SW. (1998). Ribosomal protein structures: insights into the architecture, machinery and evolution of the ribosome. Trends Biochem Sci 23: 208-212.
70. Rocak S, Emery B, Tanner N.K, Linder P. (2005). Characterization of the ATPase and unwinding activities of the yeast DEAD-box protein Has1p and the analysis of the roles of the conserved motifs. Nucleic Acids Res 33: 999-1009.
71. Rodríguez-Galán O, García -Gómez J.J, de la Cruz J. (2013). Yeast and human RNA helicases involved in ribosome biogenesis: Current status and perspectives. Biochim Biophys Acta 1829: 775-790.
72. Rosado IV, Dez C, Lebaron S, Caizergues-Ferrer M, Henry Y, de la Cruz J. (2007). Characterization of Saccharomyces cerevisiae Npa2p (Urb2p) reveals a low-molecular-mass complex containing Dbp6p, Npa1p (Urb1p), Nop8p, and Rsa3p involved in early steps of 60S ribosomal subunit biogenesis. Mol Cell Biol 27: 1207-1221.
73. Rosado IV, de la Cruz J. (2004). Npa1p is an essential trans-acting factor required for an early step in the assembly of 60S ribosomal subunits in *Saccharomyces cerevisiae*. RNA 10: 1073-1083.
74. Scaiola A *et al*. (2018). Structure of a eukaryotic cytoplasmic pre-40S ribosomal subunit. EMBO J 37: e98499.

75. Schluenzen F*el al*. (2000). Structure of functionally activated small ribosomal subunit at 3.3 angstroms resolution. Cell 102: 615-623.

76. Schmeing TM, Ramakrishnan V. (2009). What recent ribosome structures have revealed about the mechanism of translation. Nature 461: 1234-1242.

77. Schneider S, Schwer B. (2001). Functional domains of the yeast splicing factor Prp22p. J Biol Chem 4: 566-581.

78. Schütz P *et al*. (2010). Comparative structural analysis of human DEAD-box RNA helicases. PLoS One 5: e12791.

79. Sharma S, Lafontaine DLJ. (2015). 'View From A Bridge': A New Perspective on Eukaryotic rRNA Base Modification. Trends Biochem Sci 40: 560-575.

80. Sloan K.E, Bohnsack M.T. (2018). Unravelling the Mechanisms of RNA Helicase Regulation. Trends Biochem Sci 43: 235-250.

81. Strunk BS, Novak M.N, Young C.L, Karbstein K. (2012). A translation-like cycle is a quality control checkpoint for maturing 40S ribosome subunits. Cell 150: 111-121.

82. Thomson E, Tollervey D. (2010). The final step in 5.8S rRNA processing is cytoplasmic in Saccharomyces cerevisiae. Mol Cell Biol 30: 976-984.

83. Trabuco L.G *et al*. (2010). The role of L1 stalk-tRNA interaction in the ribosome elongation cycle. J Mol Biol 402: 741-760.

84. van Hoof A, Lennertz P, Parker R. (2000). Three conserved members of the RNase D family have unique and overlapping functions in the processing of 5S, 5.8S, U4, U5, RNase MRP and RNase P RNAs in yeast. EMBO J 19: 1357-1365.

85. Veldman GM, Brand RC, Klootwijk J, Planta R. (1980). Some characteristics of processing sites in ribosomal precursor RNA of yeast. Nucleic Acids Res 8: 2907-2920.

86. Veldman GM, Klootwijk J, van Heerikhuizen H, Planta RJ. (1981). The nucleotide sequence of the intergenic region between the 5.8S and 26S rRNA genes of the yeast ribosomal RNA operon. Possible implications for the interaction between

5.8S and 26S rRNA and the processing of the primary transcript. Nucleic Acids Res 9: 4847-4862.

87. Wegrecki M, Rodríguez-Galán O, de la Cruz J, Bravo J. (2015). The Structure of Erb1-Ytm1 Complex Reveals the Functional Importance of a High-Affinity Binding Between Two β-Propellers During the Assembly of Large Ribosomal Subunits in Eukaryotes. Nucleic Acids Res 43: 11017-11030.
88. Wells GR *et al*. (2016). The PIN domain endonuclease Utp24 cleaves pre-ribosomal RNA at two coupled sites in yeast and humans. Nucleic Acids Res 44: 5399-5409.
89. Woolford J.L Jr, Baserga S.J. (2013). Ribosome biogenesis in the yeast Saccharomyces cerevisiae. Genetics 195: 643-681.
90. Young C, Khoshnevis S, Karbstein K. (2013). Cofactor-dependent Specificity of a DEAD-box Protein. Proc Natl Acad Sci U S A 110: 2668-2676.
91. Zhang J *el al*. (2007). Assembly factors Rpf2 and Rrs1 recruit 5S rRNA and ribosomal proteins rpL5 and rpL11 into nascent ribosomes. Genes Dev 21: 2580-2592.
92. Zhang L, Wu C, Cai G, Chen S, Ye K. (2016). Stepwise and dynamic assembly of the earliest precursors of small ribosomal subunits in yeast. Genes Dev 30: 718-732.